HOT-WIRE CHEMICAL VAPOUR DEPOSITION OF SILICON CARBIDE THIN FILMS FROM PURE SILANE AND METHANE GASES

FATEMEH SHARIATMADAR TEHRANI

FACULTY OF SCIENCE
UNIVERSITY OF MALAYA
KUALA LUMPUR

2013

HOT-WIRE CHEMICAL VAPOUR DEPOSITION OF SILICON CARBIDE THIN FILMS FROM PURE SILANE AND METHANE GASES

FATEMEH SHARIATMADAR TEHRANI

THESIS SUBMITTED IN FULFILLMENT OF THE REQUIREMENT FOR THE DEGREE OF DOCTOR OF PHILOSOPHY

DEPARTMENT OF PHYSICS
FACULTY OF SCIENCE
UNIVERSITY OF MALAYA
KUALA LUMPUR

2013

ABSTRACT

A hot-wire chemical vapour deposition (HWCVD) system is a simple and cost-effective technique for deposition of Si-based films. Silicon carbide (SiC) on the other hand is a very interesting material with many unique properties. This work is directed towards understanding how the structural properties of the SiC films affect the opto-electronic properties of the films. This is important for application of this wide band gap semiconductor as a window material in photovoltaic solar cells.

In this work, an HWCVD system built in the laboratory is successfully utilized to grow multi-phased SiC films from silane (SiH_4) and methane (CH_4) gases without hydrogen dilution. In the first part of this work, the influence of precursor gas concentration on chemical bonding, crystallinity and elemental composition of the films is studied. The precursor gas concentration is changed by depositing films at different CH_4 flow-rates with the SiH_4 flow-rate fixed at SiH_4 starving condition and at different total gas partial pressures with the fixed ratio of SiH_4 to CH_4 flow-rate. In the second part of this work, the effects of deposition pressure and substrate-to-filament distance on the structural and optical properties of films are investigated. The deposition pressure controls the residence time of precursor molecules in the reactor and the filament-to-substrate distance determines the energy of the radicals reaching the growth sites. Then, the structural properties of the films are studied with respect to the optical energy gap (E_g), refractive index (n), and photoluminescence properties of the SiC films. The final part of this work focuses on the growth mechanism of SiC films.

In this work, high quality SiC films have been successfully grown in the HWCVD system. The highest growth rate of the SiC films achieved in this work is higher than reported values for films grown by conventional deposition techniques. It is established that the formation of SiC nano-crystals can be manipulated by controlling the CH_4 to SiH_4 flow-rate ratio in SiH_4 starving condition. It is also shown that an optimum total gas partial pressure is required for the formation of SiC nano-crystalline phases in the films. The decrease in filament-to-substrate distance is shown to promote the formation of nano-crystalline SiC phases and hydrogenated amorphous carbon (a-C:H) clusters in the film structure. It is verified that the structure of SiC films grown is independent of the substrate used for the films. Also, It is shown that the E_g and n values are strongly affected by the structural properties of the films such as the Si-C bond density and the presence of a-C:H clusters. Compositional analysis showed that the carbon content controls both the E_g and n values of the films. Photoluminescence emission from the SiC films is the result of band-to-band transition and radiative recombination processes in the band tail states. The precursor gases concentration in the reactor, residence time of the precursor gas molecules, growth radicals in the reactor, and the flux of energetic growth radicals determine the growth mechanism involved in the growth process of the SiC thin films by HWCVD technique.

ABSTRAK

Sistem pemendapan wap kimia dawai panas (HWCVD) adalah teknik yang mudah dan kos efektif untuk pemendapan filem berasaskan silikon. Silikon karbaid (SiC) pula adalah suatu bahan yang sangat menarik yang mempunyai banyak ciri-ciri yang unik. Hala tuju kerja ini adalah untuk memahami kesan sifat struktur filem SiC ke atas sifat opto-elektronik filem. Ini adalah penting untuk aplikasi bahan semikonduktor jurang jalur lebar ini sebagai bahan tetingkap dalam sel-sel solar fotovoltan.

Di dalam kerja ini, sistem HWCVD yang dibina di makmal berjaya digunakan untuk pemendapan filem SiC pelbagai fasa dari gas silan (SiH_4) dan metana (CH_4) tanpa pencairan gas hidrogen. Di dalam bahagian pertama kerja ini, pengaruh kepekatan gas pelopor ke atas ikatan kimia, penghabluran dan komposisi elemen di dalam filem dikaji. Kepekatan gas pelopor diubah dengan memendapkan filem dengan kadar aliran gas CH_4 yang bebeza pada kadar aliran SiH_4 yang ditetapkan pada tahap keadaan ketandusan SiH_4 dan jumlah tekanan separa gas yang berbeza dengan nisbah kadar aliran SiH_4 kepada CH_4 yang tetap. Dalam bahagian kedua kerja ini, kesan tekanan di masa pemendapan dan jarak filamen-ke-substrat ke atas sifat-sifat struktur dan optik filem dikaji. Tekanan pemendapan mengawal masa mastautin molekul pelopor dalam reaktor dan jarak filamen-ke-substrat menentukan tenaga radikal yang sampai di kawasan pemendapan. Sifat struktur filem pula dikaji merujuk kepada jurang tenaga optik (E_g), indeks biasan (n) dan pemancaran fotoluminesen filem SiC. Bahagian akhir kerja ini memberi tumpuan kepada mekanisme pertumbuhan filem SiC.

Di dalam kerja ini, filem SiC berkualiti tinggi telah berjaya dimendapkan dengan kadar pemendapan yang tinggi di dalam sistem HWCVD ini. Kadar pertumbuhan tertinggi filem SiC yang dicapai dalam kerja adalah lebih tinggi daripada yang dilaporkan bagi filem-filem yang dimendapkan dengan kaedah konvensional. Pembentukan nano-hablur SiC boleh dimanipulasi dengan mengawal nisbah kadar aliran CH_4 kepada SiH_4 dalam keadaan ketandusan SiH_4 telah dimantapkan. Ia juga menunjukkan bahawa jumlah tekanan separa gas optimum diperlukan untuk pembentukan fasa SiC nano-kristal ke dalam filem. Penurunan jarak filamen-ke-substrat menggalakkan pembentukan fasa SiC nano-kristal dan kelompok amorfus karbon berhidrogen (a-C: H) dalam struktur filem. Telah disahkan juga di dalam kerja ini bahawa struktur filem SiC yang dimendapkan tidak bergantung pada substrat yang digunakan untuk filem. Perubahan struktur dalam filem seperti ketumpatan ikatan Si-C dan kehadiran kelompok a-C:H dalam struktur filem telah ditunjukkan mempengaruhi nilai E_g dan n dengan ketara. Analisis komposisi menunjukkan bahawa kandungan karbon mengawal kedua-dua nilai E_g dan dan n bagi filem. Pemancaran fotoluminesen daripada filem SiC adalah hasil peralihan jalur-ke-jalur dan proses penggabungan semula radiatif yang berlaku di keadaan jalur ekor. Kepekatan gas pelopor di dalam reaktor, masa mastautin molekul gas pelopor dan radikal pertumbuhan dalam reaktor dan fluks radikal pertumbuhan bertenaga menentukan mekanisme pertumbuhan yang terlibat dalam proses pertumbuhan filem nipis SiC dengan kaedah HWCVD.

ACKNOWLEDGEMENTS

First and foremost, I would like to thank God for giving me health, strength, and excellent supporters who really encouraged me during this research.

I owe my deepest gratitude to my supervisor, Prof. Datin Saadah Abdul Rahman, who has greatly supported me throughout my Ph.D. research for her patience, motivation, valuable and friendly guidance and giving me the benefit of her immense knowledge.

I would like to thank the Head of the Physics Department, for providing a well-equipped and conducive working environment.

I would like to express my gratitude to the members of the Low Dimensional Material Research Centre (LDMRC) especially, Prof. Dato Muhamad Rasat Mohamad, Laboratory assistants Mrs. Norlela Mohd Shahardin, Mr. Mohamad Aruf, and Mrs Zurina Marzuki. I would not forget the kind assistances and constructive comments from my friends in LDMRC, especially Dr. Goh Boon Tong, Dr. Richard Ritikos, Ragib Bararuddin, Chong Su Kong, Chan Kee Wah and others who I worked with directly or indirectly throughout my Ph.D. work.

I would like to extend my appreciation to Dr. Reza Rahbari for his helpful and valuable discussions, support and encouragement.

To University of Malaya, I am grateful for the financial support of my research through research grants PS221-2009A and PS475-2010B.

My heart-felt gratitude and love go to my entire family, especially my dear parents for their continuous love, support, encouragements and prayers. I would also like to thank my in-lows parents and my sister-in-low, Fatemeh, for their unbelievable help and support.

I would like to specially thank my grandparents, who always prayed for me; even though I lost three of them during these years. May God bless them.

Last but certainly not least and most importantly, I can find no words to adequately express my gratitude to my very kind husband, Dr. Ali Ashrafi and my cute daughter, Viyana. I would never have been able to finish this project without his compassionate assistance and supports and his love in the difficult days. This thesis is dedicated to both of you.

TABLE OF CONTENTS

LIST OF FIGURES

LIST OF TABLES

CHAPTER 1

Introduction

1.1 Introduction

Silicon carbide (SiC) was discovered by an American inventor, Edward G. Acheson in 1891 while attempting to produce artificial diamonds. It is a wide band gap semiconductor long known to have potential for high temperature, high power, high frequency and radiation hardened applications. SiC has been used as an industrial material since the last century because of its unique properties, such as high thermal conductivity (3.2 W cm^{-1} K^{-1}), high breakdown electric field (2.2 × 10^6 Vcm^{-1}), high forward current density, high saturated electron drift velocity, high electronic mobility, high blocking voltage, excellent oxidation resistance, strength retention to high temperature (above 600°C), high wear resistance and so on. The scientific interest in SiC is driven by the existence of a diversity of different polytypes of SiC. SiC is the only IV-IV compound that forms stable long-range ordered structures. Over 200 crystallographic modifications of SiC have been reported originating from differences in the stacking sequence of Si-C double layers along the [111] or [0001] direction. The most common polytypes of SiC crystals include 3C (zinc blend), 6H, 4H, and 2H (wurtzite) (Z.C. Feng, 2004; Friedrichs, Kimoto, Ley, & Pensl, 2011; Harris, 1995; Y. S. Park, 1998).

Hydrogenated amorphous SiC (a-$Si_{1-x}C_x$:H) is also of considerable current interest both fundamentally, as a typical amorphous system with variable disorder and microstructure, and technologically, with regard to its applications in electronics and optoelectronics. Wide applications of this material are due to the fact that its optical gap can be significantly tailored by varying the compositional ratio of its constituent elements. In addition, a-SiC:H film is known to be chemically and mechanically stronger than hydrogenated amorphous silicon (a-Si) films and recently has been recognized to be compatible for applications in biomedical devices (Saddow, 2012; Will

et al., 2010). SiC in its crystalline and amorphous form has also become attractive as an important wide band-gap semiconductor material for applications in optoelectronic devices, such as window layer in silicon solar cells (G. Ambrosone et al., 2002; Chang et al., 2012; Klein, Finger, Carius, & Stutzmann, 2005; Mao et al., 2012; S. Miyajima, Irikawa, Yamada, & Konagai, 2010; Ogawa et al., 2008). Window layer is a transparent film that allows full penetration of solar spectrum into the active part of the solar cell.

It is well known that the growth of crystalline SiC thin films requires high temperatures (above 1000°C) that exceed the melting point of available and cheap substrates. Therefore, for applications such as in thin film solar cells on cheap glass substrates, low-temperature deposition of SiC is necessary. Amorphous SiC films can be easily deposited by glow discharge technique at low substrate temperatures. Nevertheless, for such applications, a material with high electron mobility is desired. Later studies showed that nano-crystalline SiC, which contains SiC nano-crystallites embedded in an amorphous SiC matrix, is more suitable than amorphous SiC for applications in solar cells. Many researchers have attempted to produce this kind of SiC thin films, which is expected to exhibit excellent properties due to the quantum confinement effect (Chang, et al., 2012; Q. Cheng, Xu, S. , 2007; Y. Hoshide, Tabata, A., Kitagawa, A., Kondo, A., 2009; Jha et al., 2012; A. Tabata, Komura, Hoshide, Narita, & Kondo, 2008).

Amorphous and nanocrystalline SiC thin films have been conventionally grown by plasma enhanced chemical vapour deposition (PECVD) technique, which allows low substrate temperature growth at temperatures below 300°C. However, it has some disadvantages such as low deposition rate and degradation of SiC optical properties induced by the surface damage due to ion bombardment effect.

Hot-wire chemical vapour deposition (HWCVD) technique, invented for deposition of Si films at high deposition rate, has been realized to be a promising method to grow high quality SiC films at low substrate temperature compared to those prepared by conventional PECVD method (A. A. Kumbhar, Dusane, Bauer, & Schröder, 1998; A. S. Kumbhar, Bhusari, & Kshirsagar, 1995; Mahan, Nelson, Salamon, & Crandall, 1991). The presence of neutral radicals and molecules instead of ionized plasma in this system during the growth process makes it a more attractive process for thin film growth. This technique involves an efficient decomposition of the source gas catalytically in the presence of a resistively heated filament (usually tungsten). The generated species are transported to the substrate for film growth at low temperatures in the range of 150°C – 400°C, making the process suitable for film growth on low-cost glass substrates. Also, a HWCVD system is simple to develop and can be built in any research laboratory at low-cost without complications. This technique emphasizes gentle reactions on the growing surface and is free from ion bombardment damage. The deposition area could be expanded arbitrarily by enlarging the spanning area of the catalyser filaments. In HWCVD, the gas utilization efficiency is 5 to 10 times higher than in PECVD, thus contributing to higher growth rate of the material. The HWCVD thus provides enormous promise for better technological feasibility in the commercial production of large area semiconductor devices (Chakraborty & Das, 2006; Matsumura, Umemoto, Izumi, & Masuda, 2003). Therefore, there has been a growing interest in the last decade among researchers to produce SiC films for optoelectronic applications using HWCVD technique. It has been generally accepted that HWCVD generates H radicals at a higher density than plasma processes by 1 or 2 order of magnitude (Umemoto, 2002). It is commonly believed that H radicals play an important role in the low-temperature growth of nanocrystalline Si-based thin films (Matsuda, 2004). Thus, for deposition of nanocrystalline SiC films, usually the source gases are

diluted by hydrogen gas. However, this significantly reduces the growth rate of the films, which is a disadvantage from the view point of cost reduction. In addition, it should be noted that a PECVD system is comparatively more expensive and less economical to run than a HWCVD system. A home-built HWCVD system has the added advantage of flexibility for design modification to suit the needs of research for enhancing the properties of the films produced for relevant applications.

In spite of the abundance of published works on the deposition of silicon films by HWCVD with detailed investigations on its optical and structural properties, similar research aspects done on SiC films are still lacking. Many aspects on the growth mechanism of SiC films by HWCVD technique particularly and studies on the dependence of its properties on the deposition conditions have yet to be understood.

In this work, a home-built HWCVD system in the Low Dimensional Materials Research Centre (LDMRC), University of Malaya was utilized to grow SiC thin films. This system was designed and built by Aniszawati Azis, a former PhD student in the centre for her PhD research. She has shown in her work that this system has the ability to produce SiC films (Azis, 2012). However, the films were mostly Si-rich and amorphous and the density of Si-C bonds in the films was low. Moreover, very little investigation was done on the properties of the films deposited using this system since the focus of her research was mainly to design and build the HWCVD system and to test it for the production of SiC films. In the present work, this system has been slightly modified to improve the efficiency of the system and selected deposition parameters have been chosen as the variable parameters studied to be optimized for production of good quality SiC films. Various important characterization techniques will be utilized to study the films' properties with respect to the deposition parameters. In addition, the growth mechanism of SiC films produced by this system will be studied from analysis

done on the structural properties of the films with respect to the deposition parameters studied.

Some neglected aspects of SiC films deposited by HWCVD, specifically from pure silane and methane gases without hydrogen dilution will be explored in this work. The deposition parameters are known to significantly influence the growth mechanism and the film properties. However, investigations on the effect of some important deposition parameters on the film properties is still needed to understand the growth mechanism of the films by HWCVD, especially in the absence of hydrogen dilution which has been established to be necessary to produce nano-crystalline SiC films. The effect of deposition parameters such as filament-to-substrate distance, methane gas flow-rate and total gas partial pressure on the SiC deposition mechanism and film properties have occasionally been reported (A. Tabata & Komura, 2007) but more studies are still needed to fully justify the reported effects. Also, studies on the correlation of the structural properties with respect to the important optical parameters like optical energy gap and refractive index of SiC films have not been reported much in literature. In this work, the above mentioned issues will be investigated comprehensively.

1.2 Objectives of Research

In order to address the issues much needed to understand the properties and deposition mechanisms of SiC films grown by HWCVD as mentioned above, this PhD thesis will present the work done to achieve the following objectives:

1. To produce SiC film involving high Si-C bond density with wide-band gap using a home-built HWCVD system at high deposition rate from a mixture of pure silane and methane gases without hydrogen dilution.

2. To determine the influence of critical deposition parameters on the structural and optical properties of SiC films deposited. The important deposition parameters include methane gas flow-rate, total gas partial pressure, deposition pressure and filament-to-substrate distance.
3. To determine that the structural properties of SiC films are not dependent on the substrate used and correlate the structural properties to the optical properties of the films.
4. To determine the growth mechanisms of these SiC thin films grown by HWCVD technique from the discharge of pure silane (SiH_4) and methane (CH_4) without hydrogen dilution.

In order to achieve these main objectives, the results in this work are presented, discussed and analyzed in two main chapters with specific objectives detailed in each of these chapters.

1.3 Organization of the Thesis

This thesis is organized into six chapters. Chapter 2 provides a brief literature review related to this research. This chapter provides some information on SiC material and its various structures, properties and applications. Subsequently, description on the HWCVD technique is provided with information on the advantages of this technique and its development in the deposition of SiC.

Chapter 3 presents the experimental and analytical methods involved in this research. This chapter consists of two main parts and the first part includes a description of the home-built HWCVD deposition system and all the procedures required for deposition of SiC film including substrate cleaning, filament pre-heating and the film

deposition procedures. The second part of this chapter presents various characterization techniques utilized in this work. This part gives a description of each characterization method, instrumentation and theoretical calculation involved.

The results and discussions are presented in Chapters 4 and 5. Chapter 4 presents the study on the effects of methane gas flow-rate at silane starving condition and the total gas partial pressure on the crystallinity, elemental composition and chemical bonding properties of films grown on crystal silicon substrates. Chapter 5 presents the study on the influence of deposition pressure and filament-to-substrate distance, two important deposition parameters in HWCVD on the structural, elemental composition, morphology and optical properties of films deposited on both glass and crystal silicon substrates. Correlation between the structural and optical properties of the films is presented and discussed in this chapter. Finally, the growth mechanisms of SiC films are formulated and presented based on the all the results obtained. This thesis is concluded in Chapter 6 along with suggestions for future works on the SiC films deposited using the home-built HWCVD system.

CHAPTER 2

Literature Review

2.1 Introduction

This chapter presents a literature review related to this research, which contains three parts. The first part provides general information about silicon carbide material, its structural properties and potential applications. The second part involves most conventional deposition techniques used for preparation of SiC thin films and their advantages and disadvantages. The last part of this chapter will introduce hot-wire chemical vapour deposition as a technique used in this work and give a brief history of its development, its advantages over other techniques, and some proposed chemical reactions involved during the deposition process.

2.2 General Properties of Silicon Carbide

Silicon carbide (SiC) is a binary compound, which is well known as an important wide band gap semiconductor. It is the only chemically stable form of Si and C atoms. Since Si and C are both group IV atoms, they are covalently bonded. Nevertheless, because of the difference in electronegativity of Si and C, this compound has 12% ionicity (Yoshida et al., 2007).

SiC is a part of a family of materials called polytypism that is a one-dimensional polymorphism. An almost infinite number of SiC polytypes are possible, and approximately 250 polytypes have been already discovered (Fissel, 2003; Karch, Bechstedt, Pavone, & Strauch, 1996; Wang, Ma, & Zupan, 2006; Willander, Friesel, Wahab, & Straumal, 2006). Different polytypes arise from the different stacking sequences of the Si-C bilayer producing crystals with different unit cell dimensions along the [0001] or c-axis. The reason for the stability of so many polytypes in SiC is not well understood yet. It is noticeable that each polytypes differs from the others in

terms of band gap, and other fundamental properties. Therefore, SiC can be considered as a family of a large number of semiconductors. The most dominant polytypes are 3C (cubic), 2H, 4H and 6H (hexagonal), and 15 R (rhombohedral). The number represents the number of double layers in the stacking sequence and the letter represents crystal structure. Figure 2.1 illustrates the three most common SiC polytypes.

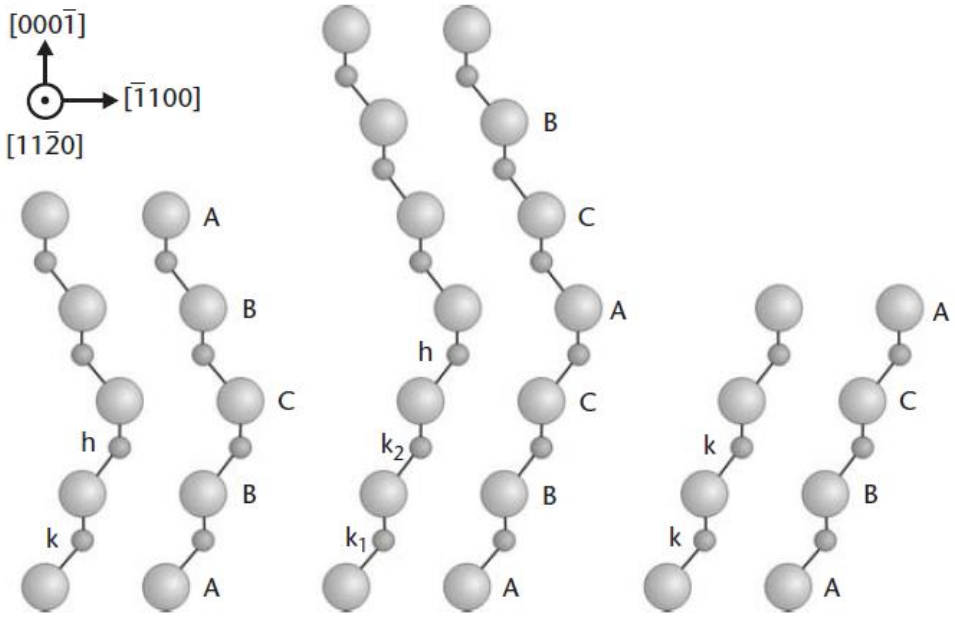

Figure 2.1: The three most common polytypes in SiC viewed in the [1120] plane. From left to right, 4H-SiC, 6H-SiC, and 3C-SiC; k and h denote crystal symmetry points that are cubic and hexagonal, respectively.

It is well known that among the different SiC polytypes, the cubic SiC (3C-SiC) exhibits the highest electron mobility and is more stable than hexagonal system. Meanwhile, it is the only one that can be grown on low-cost Si substrates to merge into the well-developed Si-bases integration technology (Zhe Chuan Feng, 2006; Hiromasa, Takahiro, Tetsuya, Hiroaki, & Kiyoshi, 2011; Komiyama, Abe, Suzuki, Kita, & Nakanishi, 2005).

Physical properties of crystalline SiC, such as high thermal conductivity, high-saturated drift velocity, and high breakdown field make it attractive for many

applications including high temperature, high power and high frequency devices that are not possible using Si or GaAs. SiC is also resistant to high radiation doses and thus suitable for nuclear power applications (Harris, 1995; Y. S. Park, 1998). However, because of difficulties in production of good quality SiC single crystals with low cost, the SiC technology has faced major limitation yet.

Beside crystalline SiC, its amorphous form (a-SiC) has attracted much attention due to its magnificent properties such as high stability, tuneable band gap and refractive index by varying the chemical composition and so on. Si-rich a-SiC is usually employed as a transparent layer in solar cells and photo-detectors, while C-rich a-SiC films are a good candidate as an active layer in electroluminescent devices (Q. Cheng & et al., 2008; Vasin, 2008). In addition, due to coexistence of topological, structural and compositional disorder, it is a representative material for fundamental studies of an amorphous system with variable disorder (Compagnini, Foti, & Makhtari, 1998; El Khakani, Guay, Chaker, & Feng, 1995; Rovira & Alvarez, 1997; Solomon, 2001; Tersoff, 1994). This complexity of a-SiC films has led to long time study on this material which has been deposited by various deposition techniques.

It should be mentioned that there are other structures than crystalline and amorphous SiC that have been obtained by several researchers that are microcrystalline and nano-crystalline SiC. These structures involve crystalline SiC or Si grains that embedded in the amorphous SiC matrix. These kinds of systems usually exhibit unique and interesting properties such as strong room temperature PL, wide band gap and high electron mobility as reported in the literature (G. Ambrosone et al., 2006; Coscia, Ambrosone, & Basa, 2008; Klein, Dasgupta, Finger, Carius, & Bronger, 2008; Xu, Yu, Rusli, Yoon, & Che, 2000; M. B. Yu, Rusli, Yoon, Xu, et al., 2000; W. Yu, Wang, X., Lu, W., Wang, S., Bian, Y., Fu, G., 2010). It should be mentioned that these unique properties have been attributed to the quantum confinement of nano-crystallites.

The structural model of amorphous and nano-crystalline SiC is not unique. This is because of the capability of carbon to have twofold, threefold and fourfold coordination adds a degree of freedom in local structure arrangement which is absent in the other amorphous semiconductor alloys. However, there have been some suggested models of chemical ordering in amorphous silicon carbon alloys according to what have been obtained from various theoretical and experimental techniques. (Bhusari & Kshirsagar, 1993; King, et al., 2011; Lee & Bent, 2000; Pascarelli, Boscherini, Mobilio, & Evangelisti, 1992; Rovira & Alvarez, 1997; Tersoff, 1994). Here, some of these models are demonstrated for clarity. Figure 2.2 (a) and (b) show the a-SiC :H with so called polymethylsilane and polycarbosilane structures, respectively. These structures have been proposed by M.-S. Lee et al. from analysis of a-SiC:H films deposited by HWCVD technique from mono- and trimethylsilane gases (Lee & Bent, 2000). They have also suggested microcrystalline structure for the films containing SiC crystallites in the a-SiC matrix, which were deposited under higher substrate temperature (See Figure 2.3).

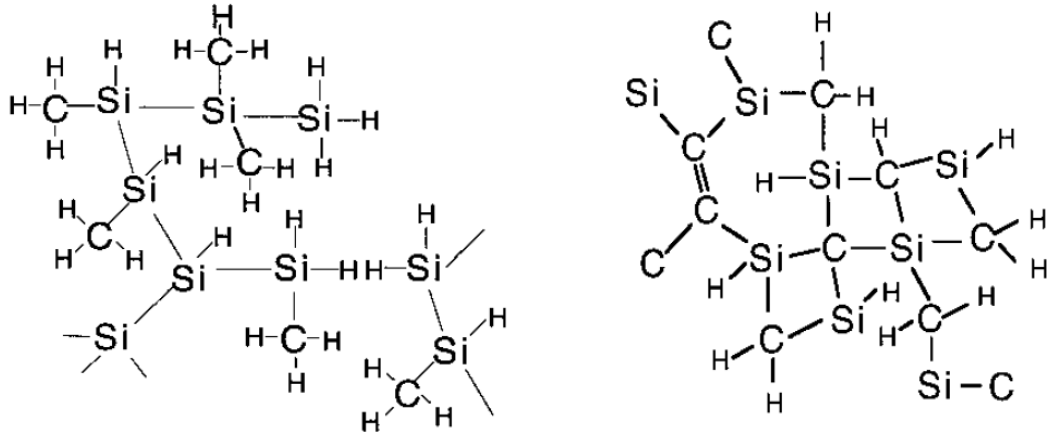

(a) (b)

Figure 2.2: Schematic illustration of a-SiC:H proposed by Lee et al. (a) polymethylsilane structure and (b) polycarbosilane structure (Lee & Bent, 2000).

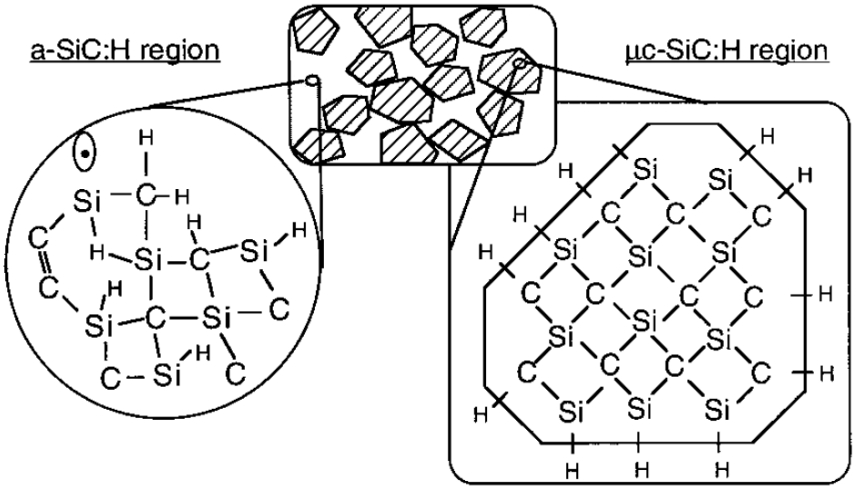

Figure 2.3: Proposed microcrystalline SiC structure by Lee et al.

There are other structural models for a-SiC which have been proposed recently by S.W. King et al. (King, et al., 2011) as shown in Figure 2.4. They suggested various models of the atomic bonding/network structure for the a-SiC:H films by detail analysis of Fourier transform infrared (FTIR) spectra. Figure 2.4 (a) shows an amorphous SiC structure with a random orientation of the SiC_4 tetrahedra and the formation of vacancies and dangling bonds. In addition, the incorporation of hydrogen prevents optimum SiC_4 linkage in the SiC structure. In Figures 2.4 (b) to (e) the hydrogen content increased progressively and thus the film's structure became less dense.

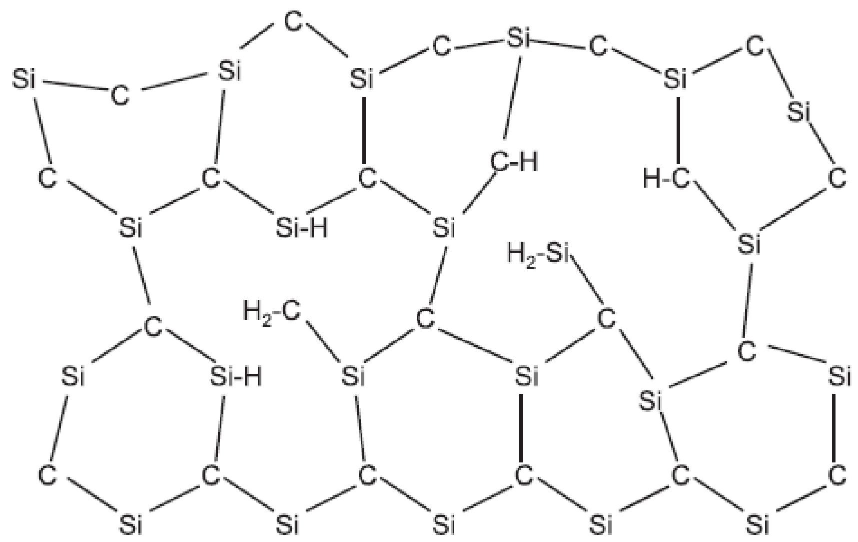

(a)

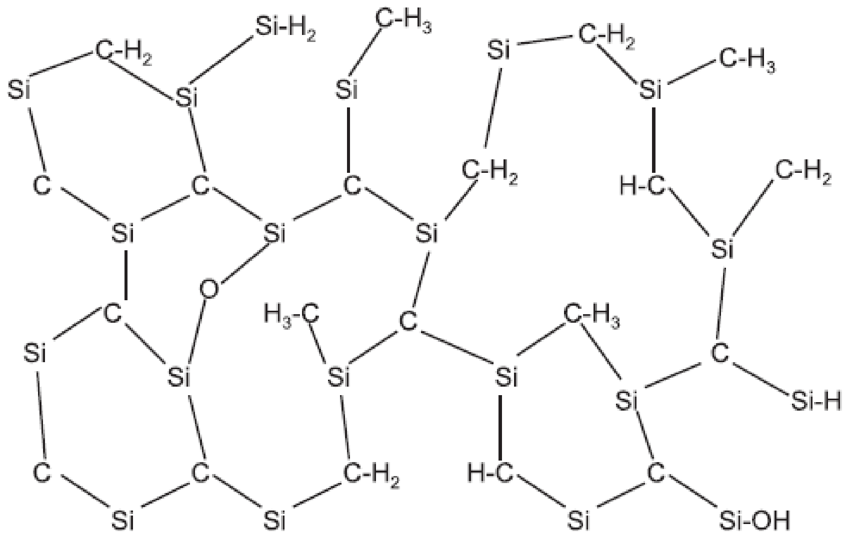

(b)

Figure 2.4: Atomic structure and bonding for a-SiC:H films with various hydrogen content (King, et al., 2011).

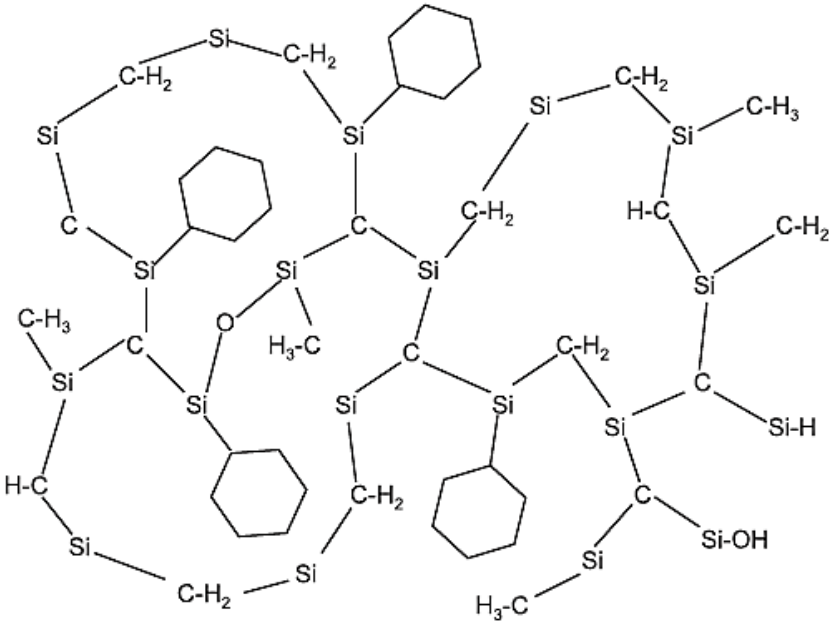

(c)

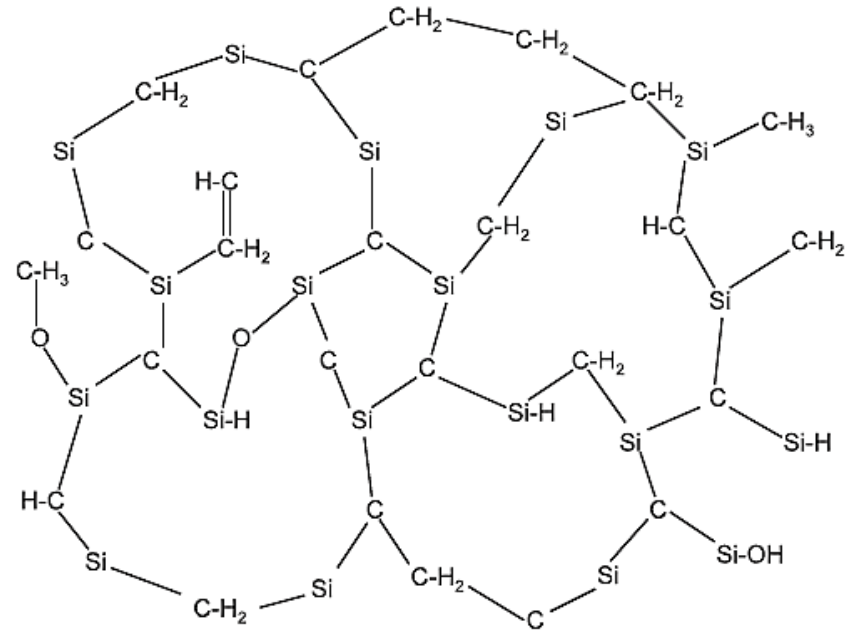

(d)

Figure 2.4, Continued.

2.3 Common Deposition Techniques Used for Preparation of SiC Films

The choice of the deposition technique usually depends on the desirable structure of SiC thin film. Moreover, the structural and optical properties of SiC thin

films strongly depend on deposition technique as well as deposition conditions. In this section, a preview of conventional deposition techniques for preparation of SiC films and highlighted properties of resulting films will be presented.

Based on the literature, two main groups of deposition techniques have been conventionally adopted for preparation of SiC thin films; chemical vapour deposition (CVD) and sputtering. It should be noted that each of them involves several sub-methods in terms of supplied activation source. However, beside these most widely used techniques, other deposition techniques have been also reported for preparation of SiC thin films such as Laser assisted deposition (LAD) (Sung et al., 1992), ion beam assisted deposition (Rivière, Zaytouni, & Delafond, 1996) and sublimation (Oulachgar, Aktik, Dostie, Gujrathi, & Scarlete, 2007). Nevertheless, this section will only concentrate on the mentioned main conventional techniques based on the literature.

2.3.1 Chemical Vapour Deposition (CVD) Methods

For deposition of SiC films in the forms of single and polycrystalline SiC and amorphous, chemical vapour deposition technique has been widely employed (Dhanaraj et al., 2007; Ellison et al., 2000; Ellison et al., 1999; Kordina et al., 1996; Morgan, 2006; Y. S. Park, 1998). In a typical chemical vapour deposition process the substrate is exposed to one or more unstable precursors, which react with the substrate surface to yield the desired deposit (Comninellis & Chen, 2009). In this process, the activation energy for chemical reactions can be supplied by various energy sources. If heating the substrate is used to activate the reaction of precursors, the process is called thermal CVD. For this purpose, usually high temperature above 1000°C is required. As a result, uniform and reproducible films are grown. However, the main limitation of this

technique is its required high temperature, which suffers from structural damage and formation of voids in the films (S. H. Feng & Chen, 2002).

Photo-assisted CVD is an alternative modification of CVD method, which has been used for amorphous and nano-crystalline SiC deposition (Chevaleevski, Myong, & Lim, 2003; Dasgupta, Ghosh, Kshirsagar, & Ray, 1997; Lim & Shevaleevskiy, 2008; Yeop Myong, Kew Lee, Yoon, & Su Lim, 2002). There are two main variants of this method as light source of excitation used in the decomposition process:

(i) Laser-induced Photo-CVD, which uses high-energy coherent radiations as light source to decompose reactive gases. In this manner, various gas lasers can be used. However, they are expensive while some effects such as damage due to high-energy photons are expected.

(ii) Lamp-induced Photo-CVD, which uses incoherent radiations to perform an indirect photolysis mechanism. Usually a low-pressure Hg lamp is used to dissociate the gas mixture due to high catalytic activity of mercury. It is a soft process because the damage of the film surface by the ions is negligible. Therefore, less bombardment-induced defects and sharper interfaces are expected especially in very thin films (Bullot & Schmidt, 1987).

Plasma-enhanced CVD (PECVD) is a modification of CVD method and undoubtedly has been the most conventional deposition technique for production of SiC films. In this method, plasma is used as a source of energy in order to dissociate the reactive gases at temperatures much lower than their pyrolysis temperature. Plasma can be defined as a gas vapour in which a part of the atoms (molecules) has been ionized. The main advantage of this method is its low operation temperature, which is usually below 400°C. Moreover, this method has ability to deposit films on various substrates

over a large area (Hori & Goto, 2002). However, decrease in optical gap for high carbon content SiC films have been observed due to graphite like sp^2 C-C bonding (Hu, 2004). In addition, presence of large density of ions in the plasma sometimes causes surface damages due to ion bombardment. It is worth noting that for deposition of nanocrystalline silicon carbide films, heavy hydrogen dilution is necessary that significantly decreases the deposition rate.

Next modification of CVD method is electron cyclotron resonance CVD (ECR-CVD) that have been used for deposition of amorphous and crystalline SiC films (Chew, 2002; Conde et al., 1999; Toal, Reehal, Barradas, & Jeynes, 1999; Xu, et al., 2000). The principle of this technique is that the frequency of the input source (usually in the microwave region) is matched with the cyclotron frequency set by magnetic field in a resonant chamber. When this matching occurs, electrons adsorb energy from the exiting electric field. Since in ECR-CVD the ion energy is low, the energy of impinging ions on the surface can be controlled independently of the microwave power by applying a bias voltage to the substrate electrode. In addition ECR plasma is usually operated at low pressures (< 10 mTorr) which avoids polymerization by reducing the number of gas-phase collisions and allow sharper interfaces (Conde, et al., 1999).

Catalytic CVD (also known as hot wire or hot filament CVD) is another simple modification of CVD technique, which is conventionally employed to produce Si-based and diamond films (Mahan, 2003; Mahan, Carapella, Nelson, Crandall, & Balberg, 1991; Martin, Teplin, Doyle, Branz, & Stradins, 2010; Matsumura, 1998; Soni, Phatak, & Dusane, 2010). This technique has become attractive in last two decades for deposition of device quality amorphous and nano-crystalline Si films at high deposition rate. Many research works have been published on both better understanding of this technique and toward optoelectronic applications especially in solar cells. However, much less references are available in the literature about the deposition of SiC thin films

by this technique. Since this technique is the subject of the present study, it will be described in more details in section 2.4.

2.3.2 Sputtering Methods

Cathodic sputtering is a multipurpose thin film deposition method used for a long time in different industrial developments. The principle of sputtering is that a solid is subjected to bombardment by high-energy particles such as ions. As a result, individual atoms or molecules achieve enough energy to escape from the surface. These ejected atoms or molecules can then form a new layer on the substrate surface. The sputter deposition is generally a more physical than chemical process. Physical sputtering of polycrystalline SiC target by argon ions always yields unhydrogenated and nearly stoichiometric materials. Co-sputtering from silicon and graphite targets allows variable Si/C ratio of the films. Sputtering in the presence of reactive gases such as H_2, CH_4 and SiH_4 leads to incorporation of desirable amount of hydrogen as well as Si/C ratio into the films (Bullot & Schmidt, 1987). Therefore, by this method it is possible to avoid use of toxic gases as well as accurately control the film thickness.

Deposition of various structures of SiC film by sputtering technique has been reported. Nano-crystalline SiC has been prepared by co-sputtering of silicon and carbon targets in H_2 environment (Kerdiles, 2000; Kerdiles, Madelon, & Rizk, 2001). Amorphous hydrogenated SiC films have been deposited by d.c. sputtering of polycrystalline Si target in the presence of CH_4 and H_2 gases as source of C and H in the film (Saleh, Munisa, & Beyer, 2003). Unhydrogenated amorphous SiC films have been obtained by sputtering of SiC target in the presence of Ar gas (Seo, Joung, Park, & Choi, 2011; Tang, Tan, Huang, Dong, & Jiang, 2005).

2.4 Hot-Wire Chemical Vapour Deposition (HWCVD) Technique

2.4.1 History of HWCVD Technique

Hot-wire chemical vapour deposition (HWCVD) technique was first introduced in 1979 by Weismann et al (Wiesmann, Ghosh, McMahon, & Strongin, 1979). They could deposit amorphous hydrogenated silicon (a-Si:H) thin films by high-temperature thermal decomposition of silane using a heated tungsten filament with relatively high deposition rate. However, their films were poor in quality due to low pressure they used in the deposition process. Therefore, researches on this method remained stagnated until 1988 that Matsumura et al (Matsumura & Ihara, 1988) obtained good quality a-Si:H films with high deposition rate by using much higher pressures. Since they discover the catalytic role of the heated filament in decomposition of SiH_4 molecules, they named it as "Catalytic-CVD (Cat-CVD)" method. Device quality a-Si:H films deposited by the same method with hydrogen content as low as 1%, which is desired for solar cell applications, was reported in 1991 by Mahan et al (Mahan, Carapella, et al., 1991; Mahan, Nelson, et al., 1991). This research group, however, called this deposition technique as "HWCVD". Since then, HWCVD has attracted much interest as a promising deposition technique for Si-based materials thin films.

2.4.2 Advantages of HWCVD

The highlighted advantages of HWCVD method and resulting Si-based thin films are listed below (Feenstra, Schropp, & Van der Weg, 1999; Gogoi, Jha, & Agarwal, 2010; Matsumura, 1998; Soni, et al., 2010):

i. High deposition rate: For deposition of Si-based thin films high deposition rates > 10 Å/s can be achieved without the deteriorating their device quality. This value is an order of magnitude higher than that expected using PECVD methods (Feenstra, et al., 1999; Takashi Itoh et al., 2001; Jadkar et al., 2007; Jadkar, Sali, Musale, Kshirsagar, & Takwale, 2002; Matsumura, Umemoto, & Masuda, 2004).

ii. Ion-free plasma: In HWCVD technique, only neutral atoms and molecules (radicals) are present in the gas phase. Therefore, the film surface does not suffer from plasma damage or charge-induced damage. This makes HWCVD a "gentle" process (Mahan, 2003; Matsumura, et al., 2004).

iii. Easily scalable deposition system: An extreme simplicity of geometry of the HWCVD system allows one to control the deposition process easily by adjusting only few parameters.

iv. Low cost of HWCVD system

v. Large area deposition: The deposition area can be easily widened by expansion of the spanned area of filaments.

vi. Low substrate temperature: The substrate temperature in HWCVD method is usually set to 300°C or less. Meanwhile, the radiations from the hot filament does not significantly effect on the substrate temperature when the distance between filament and the substrate is above 10 mm. Low-temperature deposition techniques are desired from the viewpoint of widening the application of SiC films in optoelectronic devices such as solar cells and thin film transistors. Moreover, for such applications, SiC film must be deposited on glass substrates that require low-temperature deposition method.

vii. Lower hydrogen incorporation into the film: To saturate dangling bonds in a-Si:H, theoretically about 0.1% hydrogen alloying is required. Materials

deposited by HWCVD show significant lower hydrogen content (about 1%) compared to those of deposited by PECVD (above 10%). Therefore, it is expected that low-hydrogen Si-alloys prepared using HWCVD are superior for optoelectronic applications (Mahan, 2003).

viii. High efficiency gas usage: It is generally accepted that for the filament temperatures above 1800 $^{\circ}$C, SiH_4 gas completely decompose into Si and H atoms. This high efficiency gas decomposition significantly reduces the deposition cost.

2.4.3 Some Physics and Chemistry of HWCVD

Since the invention of HWCVD technique, several research groups have studied the chemical reactions and kinetics in this method both experimentally and theoretically (Doyle, Robertson, Lin, He, & Gallagher, 1988; Duan, Zaharias, & Bent, 2002; Gallagher, 2001; Holt et al., 2001; Mahan, Carapella, et al., 1991; Matsumura & Ihara, 1988; Umemoto, 2002; van Veenendaal & Schropp, 2002; Zheng & Gallagher, 2006). These studies mostly have performed in Si deposition in the form of amorphous, poly-, micro, and nano- crystalline structures. Therefore, currently extensive works are available about the chemical reactions of different radicals produced in the HWCVD system. In this section, a brief explanation of what occur in Si deposition by HWCVD is presented.

The deposition process in the HWCVD system is generally composed of three stages:

i. Catalytically dissociation of source gases on a resistively heated filament surface,
ii. Gas phase reactions in the region between filament and the substrate, and

iii. Surface reactions on the substrate and growing surface that is heated by an external heater or by the radiations from the hot filament itself.

It has been established that a tungsten filament with a temperature of 1400°C and above is able to decompose silane (SiH_4) gas, which is usually utilized in Si deposition. However, filament temperature above 1800°C is advantageous since it avoids incorporation of Si atoms into and onto the filament surface i.e. silicide formation on the filament surface and hence shortening the filament lifetime due to breakage. Meanwhile, higher filament temperature (>1800 °C) leads to efficient decomposition of silane gas into atomic silicon and hydrogen as shown in following reaction (Gallagher, 2001; Jadkar, et al., 2002; van Veenendaal & Schropp, 2002):

$$SiH_4 \xrightarrow{\text{Hot filament (>1800 °C)}} Si + 4H \qquad (2.1)$$

Heintze et al. discovered that Si film could not be deposited when the W wire is covered with Al_2O_3, even if its temperature exceeds 1600°C. They concluded that the reaction at the hot filament is catalytic (Heintze, Zedlitz, Wanka, & Schubert, 1996). The catalytic role of the filament in this cracking reaction has been also proven by several investigations (Duan, et al., 2002; van Veenendaal & Schropp, 2002). They have shown that the decomposition probability is dependent on both filament material and temperature. Moreover, the small activation energy of silane decomposition strongly confirms that the cracking reaction of silane is catalytic rather than thermal (Duan & Bent, 2005; Mahan, 2003). The activation energy for pyrolytically cleave four Si-H bonds in SiH_4 is 12.9 eV, while decomposition of SiH_4 by a hot tungsten filament only needs 0.74 eV energy (Mahan, 2003).

Beside the generation of radicals, the transport of the radicals from the filament to the substrate surface has a critical influence on the film properties. The deposition pressure and the distance between the filament and the substrate influence the reactions on the path from the filament to the substrate. If the deposition pressure is too low in such a way that the mean free path of Si and H atoms emitted from the hot filament is equal or greater than the distance between filament and the substrate, they will reach and diffuse into the substrate without any further reactions. Otherwise, they will go through a chain of subsequent gas-phase reactions with the existing molecules and radicals in the chamber before reaching the growth surface. These reactions determine the growth species for the film deposition. It should be mentioned that the stability, sticking coefficient and surface mobility of the generated species are important for the film growth.

The gas phase reactions involve radical-molecule and radical-radical reactions.

i. Radical-molecule reactions

The insertion reaction of Si into silane and the abstraction reaction of hydrogen are the most important reactions in the gas phase. The insertion reaction of Si can be done in two possible forms as follows:

$$Si + SiH_4 \rightarrow SiH + SiH_3 \quad (2.2)$$

$$Si + SiH_4 \rightarrow HSiSiH_3 \quad (2.3)$$

However, the later reaction is energetically more favourable because it is an exothermic reaction. It should be noted that $HSiSiH_3$ compound is not stable and will be stabilized via reactions (Mahan, 2003; Muller, Holt, Goodwin, & Goddard, 2000; van Veenendaal & Schropp, 2002):

$$HSiSiH_3 \rightarrow H_2SiSiH_2 \quad (2.4)$$

or further reacts with SiH_4 :

$$HSiSiH_3 + SiH_4 \rightarrow SiH_2 + Si_2H_6 \quad (2.5)$$

The abstraction reaction of hydrogen has been proposed as follows:

$$H + SiH_4 \rightarrow SiH_3 + H_2. \quad (2.6)$$

It is generally accepted that SiH_3 is quite stable species and will not go through further gas phase reactions. Thus, it is a primary source of the film growth.

ii. Radical-radical reactions

The next gas phase reactions involve radical-radical collisions. Some of possible radical-radical reactions are:

$$H + SiH_3 \rightarrow SiH_2 + H_2 \quad (2.7)$$

$$H + Si_2H_2 \rightarrow Si_2H + H_2 \quad (2.8)$$

$$SiH_3 + SiH_3 \rightarrow SiH_4 + H_2 \quad (2.9)$$

These reactions become important at higher pressures due to increment of radical density in the chamber. Usually, generation of the above products as a result of radical-radical interactions has negative effects on the structural and optical properties of the film.

Reactive species, impinging onto a surface can react at the surface to form new species, which are adsorbed onto the substrate surface. The deposition rate of the film is

determined by the flux of radicals impinging on the substrate and the reaction probability with the film surface. Although the gas phase chemistry of HWCVD is believed to be very different compared to the conventional thermal CVD and PECVD, however, the it has been proposed that the deposition models used in PECVD and HWCVD should be similar (Gallagher, 2001; van Veenendaal & Schropp, 2002). Surface reactions generally involve (Pant, Russell, Huff, Aparicio, & Birkmire, 2001):

i. Adsorption of radicals and film precursors on the film surface,
ii. Surface rearrangement reactions.

Atomic Si, SiH, and SiH_2 have much higher surface reaction rate than SiH_3 because the former radicals can directly insert in SiH bond of the surface while SiH_3 requires a surface dangling bond. This is commonly described by a value called the sticking probability (s). Theoretical and empirical values of the sticking probability of SiH_x molecules have been reported for PECVD and HWCVD systems. The sticking probability of $SiH_{x\ (x=0-4)}$ has been shown to depend inversely on the number of H atoms bonded to Si in the growth radical (Pant, Huff, & Russell, 2001). However, I.T. Martin et al. have shown that the sticking coefficient of the growth radicals approach unity as the growing surface dehydrogenated at higher substrate temperature (Martin, et al., 2010). Hence, the reactions in the gas phase result in changes of surface reactivity of the precursors, the abstraction of hydrogen leads to generation of more reactive species, the insertion of Si in silane results in less reactive radicals.

W.M.M. Kessels et al. have proposed the surface reactions of SiH_3 as a primary growth species from their theoretical prediction (Kessels, et al., 2003). As shown in Figure 2.5, the first reaction is the absorption of SiH_3 on a surface dangling bond, which has no barrier. The second reaction is the abstraction of a surface H atom by SiH_3 that

creates a surface dangling bond. This reaction is important because it leads to formation of new sites for SiH_3 adsorption. The third reaction is the insertion of SiH_3 into a strained Si-Si bond at the surface.

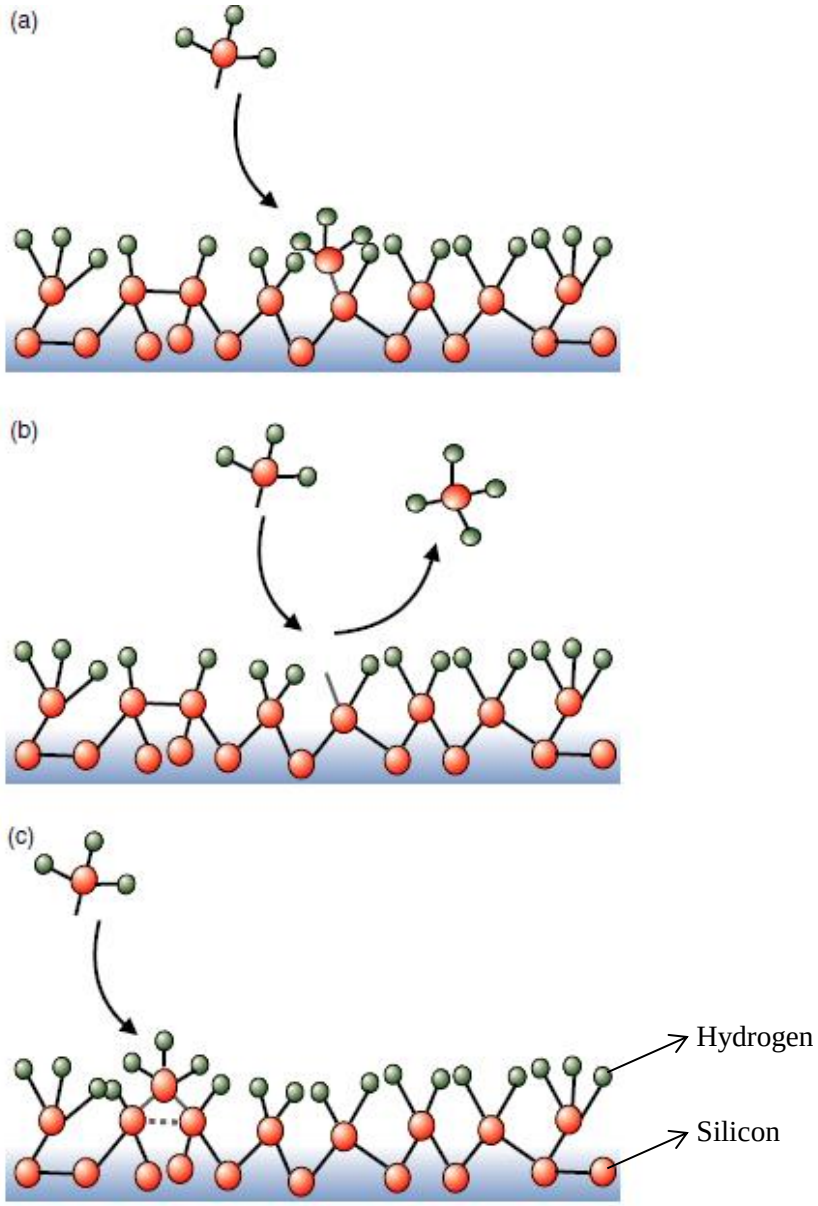

Figure 2.5: Proposed SiH_3 surface reactions during deposition of a-Si:H film as reported in the literature. (a) adsorption of SiH_3 from the gas phase onto a dangling bond; (b) abstraction of an H atom by SiH_3 creating a dangling bond and a gaseous SiH_4 molecule; (c) insertion of SiH_3 into a strained surface Si-Si bond. The five-folded coordinated Si atom can dissociate by the transfer of a H atom from the SiH_3 radical to a surface Si atom (Kessels, et al., 2003).

Researchers also have suggested other surface reactions as follows:

$$Si + SiH_{(s)} \rightarrow SiSiH_{(s)} = SiH_{(s)} + 2\ d.b. \quad (2.10)$$

$$H + SiH_{(s)} \rightarrow H_2 + d.b. \quad (2.11)$$

$$SiH_3 + d.b. \rightarrow SiH_{3(s)} \quad (2.12)$$

$$Si + d.b. \rightarrow Si_{(s)} + 3d.b. \quad (2.13)$$

$$H + d.b. \rightarrow SiH_{(s)}. \quad (2.14)$$

where subscript (s) refers to a radical bonded to Si in the film and d.b. stands for dangling bond. The first two reactions are the reactions of Si and H with hydrogen-passivated surface, while the rest are reactions of SiH_3, Si, and H with a dangling bond. The second reaction also known as the etching reaction that is believed to be very important in growth of high quality ordered amorphous and crystalline films.

2.4.4 Development of HWCVD Technique for SiC Deposition

Silicon carbide thin films have been deposited commonly by using plasma-enhanced chemical vapour deposition (PECVD) technique. However, since the HWCVD method was proposed as a promising technique to grow Si based materials, much effort have been paid to deposit better quality silicon carbon thin films without any help from plasma at higher deposition rate and by this new technique. First work on preparation of silicon carbon alloys was reported in 1995 by Kumbhar et al (A. S. Kumbhar, et al., 1995). They used a gas mixture of $SiH_4/CH_4/H_2$ and varied the silane fraction in the mixture. Their silicon carbon films were amorphous in structure as indicated by XRD broad peak. They proposed the growth mechanism in such a way that

SiH_4 species are adsorbed on the hot filament and subsequently energetic Si atoms are evaporated from the filament. They suggested the following reactions to be occurred:

$$SiH_{4(gas)} \rightarrow Si_{(liquid)} + 2H_{2(gas)} \quad (2.15)$$

$$CH_{4(gas)} \rightarrow C_{(solid)} + 2H_{2(gas)} \quad (2.16)$$

$$Si_{(liquid)} + C_{(solid)} \rightarrow SiC_{(gas)} \quad (2.17)$$

$$Si_{(hot\ gas)} + CH_{4(gas)} \rightarrow Si\text{-}C\text{-}H_{2(gas)} + H_{2(gas)} \quad (2.18)$$

However, at low silane fraction (<10%) reactions (2.16) and (2.17) have been proposed to be dominant during deposition process. They indicated that low silane fraction (silane starvation) in HWCVD method yields growth of a-SiC:H films. Later in 1998, another research group reported formation of micro-crystalline silicon phase in amorphous silicon carbon alloy using HWCVD method (A. A. Kumbhar, et al., 1998). They synthesized silicon-carbon alloy films from pure SiH_4 and CH_4 gases without hydrogen dilution. Formation of micro-crystalline silicon phase has been verified by the observed sharp peak near 520 cm^{-1} in the Raman spectra of the films. However, the crystalline-SiC phase did not exist in their films. Deposition of nano-crystalline cubic SiC (nc-3C-SiC) using HWCVD method was first reported in 2000 by Yu et al (M. B. Yu, Rusli, Yoon, Chen, et al., 2000). They utilized SiH_4/CH_4 gas mixture diluted with pure hydrogen gas and successfully deposited nc-3C-SiC film on Si substrate. However, the relatively high substrate temperature of 600°C used in their film deposition, limited the optoelectronic application. Moreover, this research group did not propose any growth mechanism of SiC nano-crystallites in the HWCVD system.

Next two years, in 2002, George et al. successfully deposited β-SiC on Si substrate using bias enhanced HWCVD technique from methane and hydrogen gas mixture (George et al., 2002). They used Si substrate as a source of Si in their

deposition. They found that the formation of highly oriented β-SiC films was due to applying of bias and use of low pressure during the deposition. The bias resulted in the bombardment of the substrate and the growing film by high-energy positive ions. Low pressure leads to the mean free path of the precursor species comparable to the distance between filament and the substrate. However, this method has limitation of deposition of SiC films at high temperatures (> 700°C) and only on Si substrate.

The interest in SiC deposition by HWCVD technique has been significantly increased and many other researchers have attempted to prepare SiC films by this technique in order to understand the properties of the resulting films as well as growth mechanism of SiC films in HWCVD. However, different structures of SiC such as amorphous, microcrystalline and nano-crystalline structures have been obtained from different deposition conditions. For example, Tabata group have obtained amorphous and nano-crystalline SiC films using $SiH_4/CH_4/H_2$ gas mixture under different conditions (A. Tabata, Hoshide, & Kondo, 2010; A. Tabata & Komura, 2007; A. Tabata, Komura, Narita, & Kondo, 2009; A. Tabata, Kuroda, M., Mori, M., Mizutani, T., Suzuoki, Y., 2004; A. Tabata & Mori, 2008). Chen *et al.* have deposited microcrystalline SiC (μc-SiC) films from decomposition of monomethylsilane (MMS) diluted in H_2 gas (Chen et al., 2012; Chen, Huang, Yang, Carius, & Finger, 2010; Chen, Huang, Yang, Carius, & Finger, 2011; Chen, Yang, Carius, & Finger, 2010). It should be noted that formation of this kind of SiC structure has only reported from HWCVD using MMS as a source gas. It seems that the presence of Si-C bond in this molecule has important role for growing stoichiometric and highly crystalline films. While deposition of a-SiC embedded with nano- or micro-crystalline silicon by HWCVD has also been reported by other groups (I. Ferreira, Fernandes, & Martins, 1999; Takashi Itoh, et al., 2001; Mao, et al., 2012; Shen, et al., 2012). It has been shown that high hydrogen dilution of the gas mixture enhances the formation of SiC crystallites into the films

(Mao, et al., 2012; A. Tabata & Mori, 2008; Q. Zhao et al., 2004). In addition it has been concluded that higher deposition pressures and filament temperature are suitable condition for growth of nc-3C-SiC (Shen, et al., 2012; A. Tabata et al., 2006; A. Tabata, et al., 2009; Wu, 2011; Q. Zhao, et al., 2004). Now, after about two decades from the first SiC deposition by HWCVD technique, many aspects remained unknown. In addition, because of lack of theoretical calculations and/or experimental measurement of chemical reactions and radicals in the HWCVD of SiC, the growth mechanism of SiC material from the SiH_4 and CH_4 gas mixture has not been explored clearly yet. However, it is generally believed that presence of large flux of H radicals is required for improvement of the crystallinity in SiC films. This is due to the effect of H radicals in etching of the weak and strained bonds and nucleation for crystalline growth.

Beside studies on growth of SiC films by HWCVD, some attempts have been taken toward doping of amorphous and crystalline SiC to improve the electrical properties for potential applications in optoelectronic devices such as solar cells. T. Itoh *et al.* have shown for the first time the possibility of doping of a-SiC films including μc-Si grains by HWCVD technique using B_2H_6 and PH_3 gases for n-type and p-type doping, respectively (T. Itoh, Fukunaga, Katoh, Fujiwara, & Nonomura, 2002; Takashi Itoh, et al., 2001). They demonstrated that the dark and photoconductivity of the B- and P-doped films was larger than undoped samples. A year later, Miyajima's group successfully fabricated a-Si solar cells with p-layer (B-doped a-SiC films containing μc-Si grains) and obtained a conversion efficiency of 10.2% (Shinsuke Miyajima, Yamada, & Konagai, 2003). They also deposited n- and p-type nano-crystalline cubic SiC films by HWCVD. It has been shown that p-type doping significantly affected absorption coefficients above the band gap of nc-3C-SiC:H compared with n-type doping (Shinsuke Miyajima, Yamada, & Konagai, 2007). Recently, several works have been reported the development in application of microcrystalline SiC films deposited by

HWCVD as transparent window layer in silicon solar cells (Chen, et al., 2012; Chen, Huang, et al., 2010; Chen, et al., 2011; Mao, et al., 2012).

It is concluded that the HWCVD method is a promising deposition technique for preparing device quality SiC films. Therefore, more information about the details of SiC growth mechanism and influence of various deposition parameters on the properties of SiC films deposited using this technique would be useful for further development in this field.

CHAPTER 3

Experimental

and

Analytical Procedure

3.1 Introduction

The SiC thin films were deposited using a home-built hot-wire chemical vapour deposition, HWCVD system and characterized by using a series of characterization methods. This chapter contains two main parts, the experimental and analytical methods involved in this work. The first part of this chapter describes the HWCVD deposition system, pre-deposition, and film deposition procedures, while the second part of this chapter presents the instruments, characterization procedure and calculation methods utilized in characterizing the films and analysis of results. These characterization methods include mechanical profilometry, Fourier transform infrared spectroscopy (FTIR), Micro-Raman scattering spectroscopy, X-ray diffraction (XRD), Auger electron spectroscope (AES), field emission scanning electron microscope (FESEM), UV-Vis-NIR spectroscopy, and photoluminescence (PL) spectroscopy.

3.2 Hot-Wire Chemical Vapour Deposition (HWCVD) System

In this work, a home-built HWCVD system in the low dimensional material research centre (LDMRC), University of Malaya, was utilized for deposition of SiC thin films. This system comprises a reaction chamber, a vacuum pumping system, the gases supply and distribution system, the electrical power supply system, and detoxification system. A schematic diagram of the HWCVD system used in this study is shown in Figure 3.1.

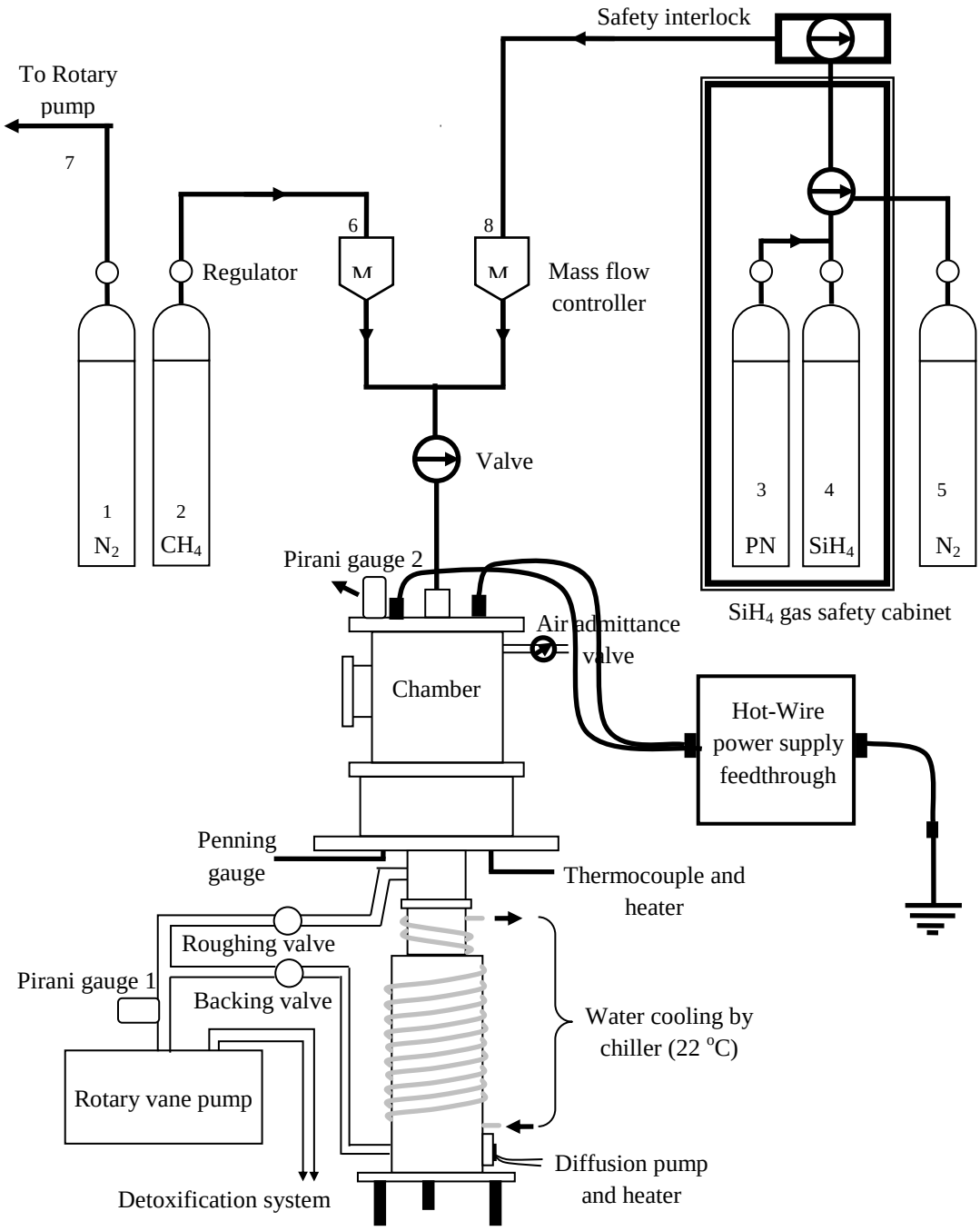

Figure 3.1: Schematic diagram of HWCVD system.

The vacuum pumping system provides a clean environment in the reaction chamber for the film deposition. In the HWCVD system, a rotary vane pump (model Edward E2M28) is utilized to evacuate the deposition chamber and to maintain the required pressure during the deposition process. This rotary vane pump is able to evacuate the deposition chamber to a pressure of 6.0×10^{-3} mbar. For high vacuum

condition, the chamber is pumped down until base pressure is as low as 2.0×10^{-5} mbar for 1 hour pumping by diffusion pump (model Edward F603 with heating power of 1300 W). The cooling system for the diffusion pump is circulated by chiller to enhance pumping efficiency of the diffusion pump. The cooling temperature of the chiller is fixed at 22°C. The pressure in the chamber for low and high level vacuum is measured using pirani (Leybold vacuum gauge with model TTR91) and penning (Leybold vacuum gauge with model PTR 225) gauge respectively.

The rotary vane pump is connected to a 10 kVA Uninterruptible Power Supply (UPS) in order to make sure that there is no abrupt interruption in the power supply during the deposition. This UPS can sustain the power supply for about 2 hours when there is any break in power supply. This is to confirm that silane gas is always in pumping and vacuum condition.

The nitrogen gas is used to purge the gas line and reaction chamber before and after deposition to remove any contaminants in the gas lines and deposition system. In addition, the nitrogen gas is directed into the rotary vane pump to prevent the silane gas from condensing in the pump during deposition and to dilute the gas before leaving through the exhaust lines. The excess silane gas exits via the exhaust line into the detoxification system, which is located outside the laboratory.

A cross-sectional overview of HWCVD reaction chamber is shown in Figure 3.2. The chamber is made of stainless steel, which is a passive material in the presence of the reactant gases. The dimensions of the reaction chamber are 200 mm in height, 180 mm in diameter and 6 mm in wall thickness. The mixed source gases enter the chamber from the top plate through a shower head and exit from the bottom of the chamber to the rotary pump. Two stainless steel rods are the filament holders, which are connected to the top plate of the chamber. These holders are connected to the DC power

supply to heat up the filament during the deposition. The filament is a 99.9% pure tungsten wire with a diameter of 0.5 mm coiled into 2 cm length helix. It is fixed between two holders by screws at the desired distance to the substrate holder. The filament temperature is controlled by adjusting the applied voltage on it. The substrate holder is placed 10 cm below the gas shower. It consists of two stainless steel plates and is attached to the heater and thermocouple that are sandwiched between the plates. Four glass stands are used to isolate the substrate holder from the electrical connections.

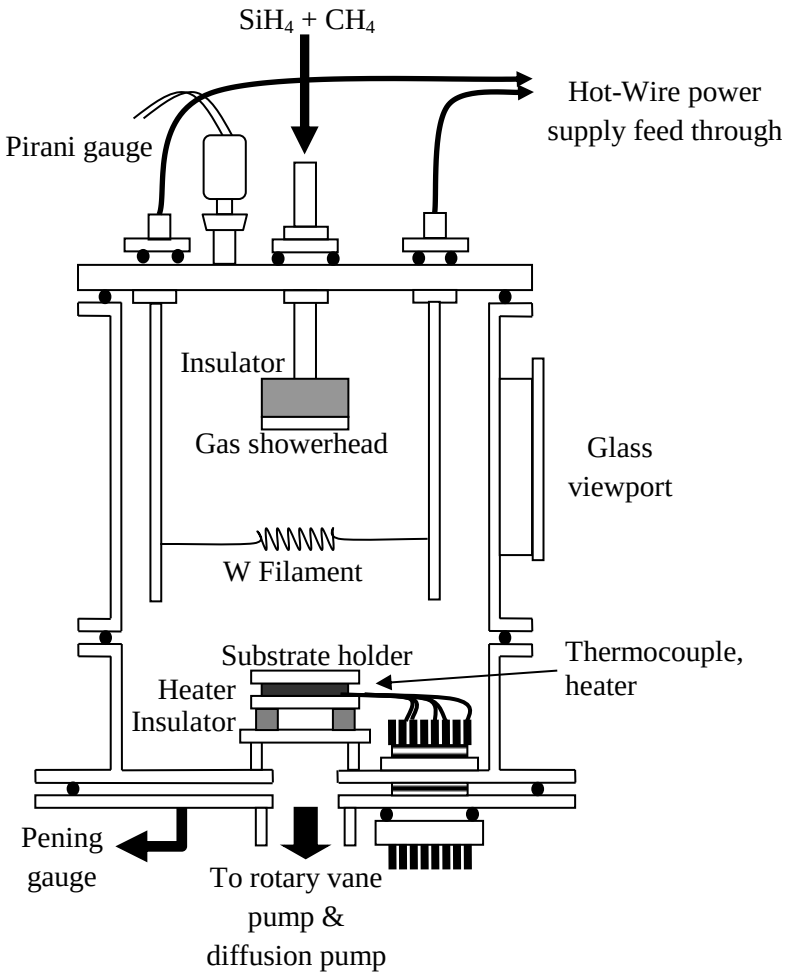

Figure 3.2: Schematic diagram of the HWCVD reaction chamber.

The gases used in this work are silane, SiH_4 (99.9995 %), purified methane, CH_4 (99.999 %), purified nitrogen, PN (99.999 %) and industrial nitrogen, N_2 (99.9 %). The

SiH_4 and CH_4 are used as the source gas for Si and C in SiC thin films deposition, while PN and N_2 are used for purging the HWCVD system, which includes the gas line, reaction chamber and roughing after every deposition. All these gases are distributed from the gas cylinders inside the gas room to the reaction chamber. The gases are carried through ¼" stainless steel tubing using Swagelock connectors and valves to a gas distribution panel.

The SiH_4 is a highly inflammable gas and thus, its cylinder is kept in the safety cabinet attached to an exhaust system which is able to remove any SiH_4 gas in case of leakage. A photograph of this safety cabinet is shown in Figure 3.3. The SiH_4 gas cylinder has a special gas regulator, model AP1510S, which is connected to a special purging system. This purging system is connected to an N_2 gas cylinder. This special gas regulator has a pneumatic valve, which allows gas through it only when the pressure of N_2 is about 50 psi. This N_2 gas is connected to the regulator through a safety system. This safety system, which is particularly used for SiH_4 gas can stop the SiH_4 gas from flowing into the chamber instantly in the case of emergency.

From the gas distribution panel, the gases separately pass through metering valves (Swagelock, SS-4MG) and then the mass flow controller (MFC) with model (Aalborg, GFC17), to display the gas flow-rate. Metering valves control the gas pressure to avoid high pressure gases entering the MFC. On exiting the MFC, the gases pass through check valves (Swagelock, SS-CHS4-1/3) which are used to prevent back flow of the gases. The gases are mixed before inflowing to the reaction chamber.

For the SiH_4 gas, the bypass line is provided for safety purposes, which allow the SiH_4 gas to be pumped out via the rotary pump directly if any blockage occurs at the entrance of the MFC. Also, it is used to remove excess SiH_4 and other gases at a faster purging rate after the deposition process.

Figure 3.3: Photograph of the safety cabinet for SiH_4 gas tank.

The last part of the HWCVD system is the detoxification system. The excess of SiH_4 gas in the reaction chamber is diluted with nitrogen gas in the rotary pump and delivered from rotary pump to detoxification tank through the exhaust line to avoid explosion in the air. The detoxification tank, which is made of hard polymer, contains a solution of potassium permanganate ($KMnO_4$, M=158.04 g/mol). This solution reacts with SiH_4 and converts it to non-toxic products according to the following chemical reaction:

$$8KMnO_4 + 3SiH_4 \rightarrow 8MnO_4 + 3SiO_2 + 8KOH + 2H_2O \qquad (3.1)$$

This process starts from the opening of the SiH_4 gas line until a few hours after deposition.

The electrical power supply system includes two parts, the DC power supply for the filament heating, and the power supply for the substrate heating. An automatic voltage regulator (VMARK AVR-1000VA) is connected to the substrate heater to stabilize the voltage. The applied voltage to the filament and the substrate is adjusted by the voltage regulator (IBC Regavolt, 0-240 V A.C., 1 KVA). A temperature controller (Taishio TS501) is used to monitor the substrate temperature during the deposition process. The substrate temperature is measured by a chromel-alumel k-type thermocouple, which operates from room temperature up to 500°C.

3.3 Sample Preparation

3.3.1 Pre-deposition Procedure

Before film deposition, it is essential to clean the substrates and filament according to the standard procedures in order to avoid absorption of dusts and contaminations in the film during the deposition.

3.3.1.1 Substrate Cleaning

In this work, SiC films are deposited on glass and p-type c-Si (111) simultaneously. They are first cut into 2 cm × 2 cm squares. Before deposition, it is essential to clean the substrates properly to remove any types of contamination from the substrate surface in order to deposit films having better properties. The method of substrate cleaning varies for different substrates.

For cleaning the glass substrates, they are placed in a clean beaker and rinsed with deionized water several times. Then they are immersed in a beaker containing soap solution (Decon 90 diluted with distilled water). Next, this beaker is placed in the ultrasonic bath for 15 minutes followed by rinsing with deionized water. Finally, they are immersed in acetone and ethanol, and dried thoroughly by industrial nitrogen gas.

The cleaning process for the c-Si substrates starts with rinsing the substrates with deionized water similar to glass substrates. Then, they are immersed in a beaker containing H_2O:HCL:H_2O_2 = 86:11:3 solution for 6 minutes to remove inorganic contaminations from the Si-substrate surface. Then, the substrates are rinsed again with deionized water. The Si substrates are then put in a beaker containing a solution of H_2O:H_2O_2:NH_4OH = 4:1:1 for 6 minutes followed by rinsing with deionized water to remove any organic contaminations. Finally, the Si-substrates are immersed in a solution of H_2O: HF = 10:1 for 6 minutes and then rinsed with deionized water to remove native oxides from the Si surface. The last step is to dry the substrates using nitrogen gas.

After the cleaning process, the cleaned substrates are immediately put into the reaction chamber, which is directly pumped down.

3.3.1.2 Filament Pre-heating

The W filament was pre-heated before every deposition to remove existing oxides from the filament surface. For this purpose, the W-filament was heated at 1900°C under flow of hydrogen gas (40 sccm) for 10 minutes. The procedure of filament pre-heating is carried out after evacuation of the system by rotary pump to the pressure of 8×10^{-3} mbar.

3.3.2 Film Deposition Procedure

In order to deposit SiC thin films, it is important to ensure that all the components of the reaction chamber are clean. The cleaning of the chamber's wall and components is performed first by rubbing with sand paper and then cleaning thoroughly with acetone.

After cleaning the chamber and the substrates, the latter are fixed on the substrate holder by using a stainless steel mask. It is of importance to double check all the electrical connections of the substrate heater, thermocouple, and the filament before closing the chamber. Next, the chamber is completely sealed to prevent any leakage, and evacuated by using rotary and diffusion pump. Before turning on the rotary pump, it is required to check and ensure that all the valves in the system are closed. After starting the rotary pump and the pressure display, the roughing valve should be slowly opened until fully opened to prevent damaging the pump. The rotary pump is able to evacuate the system to 6×10^{-3} mbar in 1-2 hours. During this stage, it is important to empty all the gas lines from the gas tank to the chamber. For this purpose, all the valves of SiH_4 and CH_4 lines including metering valves, MFCs, and valves in the distribution panel are opened respectively from the chamber to the tank. After the pressure 6×10^{-3} mbar is obtained, the metering valves are closed and the MFCs are switched off. The diffusion pump would help to reach the base pressure of 2×10^{-5} mbar after around 1 hour. To start pumping with diffusion pump it is essential to turn on the water chiller 30 minutes before heating the diffusion pump. This, makes the body of diffusion pump cold ($22^{\circ}C$) and enhances the pumping efficiency. The last step before switching on the diffusion pump is opening the backing valve and waiting until the pressure becomes stable. The diffusion pump is then switched on and left to warm up for about 30 to 40 minutes before opening the high vacuum valve. A fan is usually used to prevent excess heating

at the bottom part of the diffusion pump. Before opening main vacuum valve, the roughing valve must be completely closed. Afterwards, the high vacuum valve is gradually opened. Now, the pressure is decreasing with higher rate and to lower values. After the pressure of 2×10^{-5} mbar is obtained, the high vacuum valve is slowly closed and the roughing valve is opened again. The diffusion pump is then switched off while the cooling system is kept operating to cool the body of the diffusion pump. Then, the backing valve is closed tightly. The next step before starting the film deposition is heating the substrates to reach the desired temperature. In this work, the substrate temperature is always kept constant at 300°C and set to this value by the temperature controller. Subsequently, the heating is started by applying the AC voltage of 80 V by Regavolt. Once the temperature of substrates reaches 300°C and the pressure is stable, the gases are flowing into the chamber. Before SiH_4 is allowed to flow into the deposition chamber, the N_2 gas cylinder (see Figure 3.2, labelled as 5) is opened. This will automatically turn on the pneumatic valve and allow the SiH_4 gas to flow through it. The excess flow switch (EFS) in the gas line will be activated if the SiH_4 pressure in the line is abruptly increased above 70 psi and the alarm in the safety cabinet will ring. Concurrently, nitrogen gas labelled as 1 in Figure 3.2, is allowed to flow into the rotary pump in order to dilute the excess SiH_4 gas during deposition for safety purposes. To flow the SiH_4 into the reaction chamber, first the SiH_4 gas tank is opened slightly until the gas pressure reaches 100 psi and then the valve is closed. Then the MFC of SiH_4 is switched on and the metering valve slowly opened. The CH_4 gas flows into the reaction chamber simply by opening the gas tank followed by switching on the CH_4 MFC and opening the corresponding metering valve. The flow rates of SiH_4 and CH_4 are monitored by their individual MFCs as fixed at the desired values for every film deposition. The deposition pressure is controlled by adjusting the roughing valve connected to the reaction chamber.

The deposition process begins when the filament is heated up until 1900°C by applying AC voltage to it. The voltage must be gradually increased from zero until the filament temperature reaches 1900°C. First stages of increasing the applied voltage should be done very carefully and slowly to prevent sudden expansion of filament and likely deformation or disconnection of the filament. The temperature of the filament is monitored by an optical pyrometer (model Raytek), which operates at spectral range of 1.0 μm. The emissivity value is set at 0.35 as mentioned in the pyrometer's manual. The deposition time is started once the filament temperature reaches 1900°C, and is ended when the applied voltage is decreased to zero. The deposition time is fixed at 30 minutes for every deposition. During the deposition, all the deposition parameters including substrate temperature, deposition pressure, filament temperature, and gases flow rates are monitored and maintained. However, the radiations from the hot filament sometimes influence the substrate temperatures. This depends mostly on the distance between filament and substrates. The variation of substrate temperature because of filament radiation during the deposition process for two sets of samples prepared at different deposition pressure and filament-to-substrate distance is shown in Figure 3.4. From this figure, it is seen that the substrate temperature is almost independent of deposition pressure. Similar results were observed for the films deposited at various gas flow rates and gas pressures. Nevertheless, it was found that the decrease in the distance between substrate and filament significantly increased the substrate temperature.

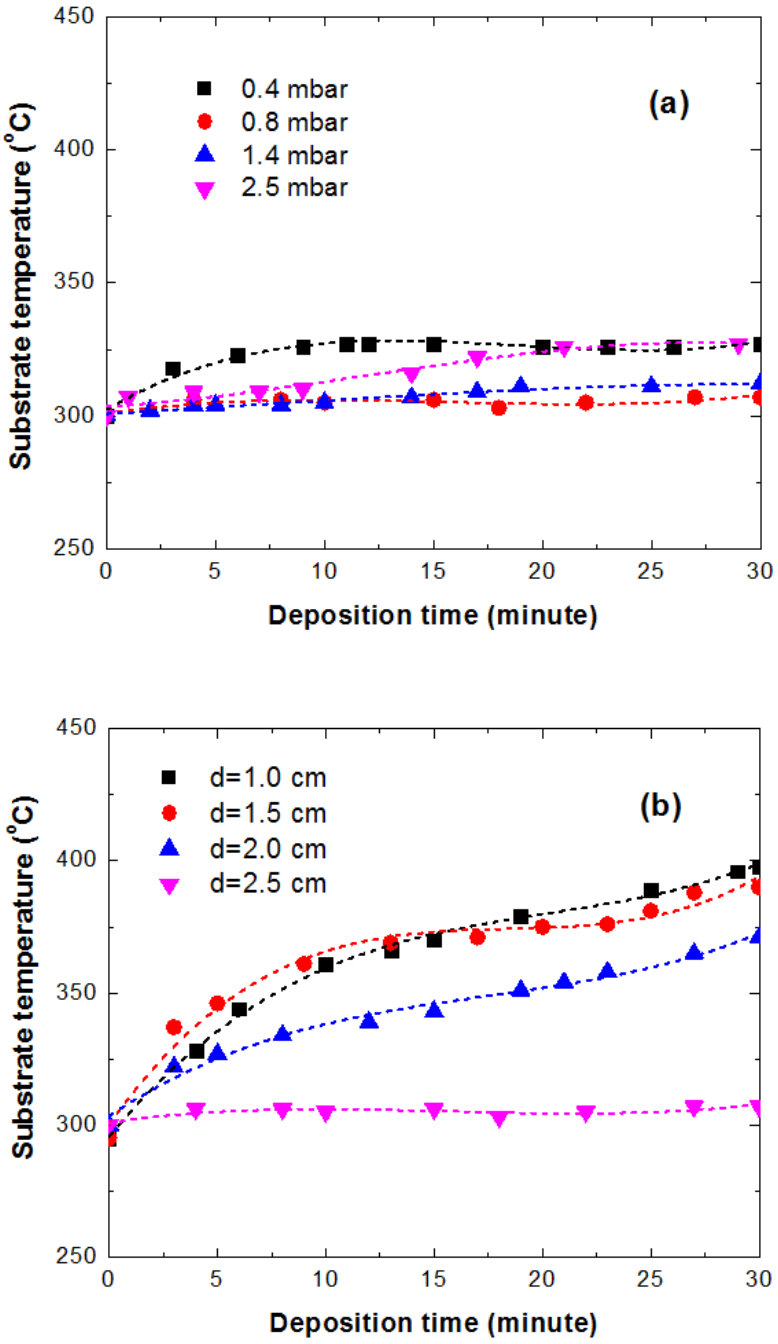

Figure 3.4: Variation in substrate temperature as a function of deposition time at different (a) deposition pressures and (b) filament-to-substrate distances. The data are obtained from this work.

Once the deposition process is completed, the applied voltage is decreased to zero, the substrate heating is stopped by decreasing the AC voltage to zero. Subsequently, the CH_4 gas tank is closed and the roughing valve is fully opened. The

gas lines are pumped until the pressure reaches the pre-deposition pressure. This means that all gases are finished, which is also indicated by the MFCs that show zero flow rate for both SiH_4 and CH_4 gases. This verifies that no excess gas remains in the gas lines. Subsequently, the SiH_4 line must be purged by purified nitrogen gas several times to flush out any excess silane in the gas line. For this purpose, firstly, the valve in the SiH_4 line to the system is closed. Then, the PN gas tank (labelled as 3 in Figure 3.1) is opened to fill the SiH_4 line with the nitrogen gas and then it is closed. Subsequently, the valve on the SiH_4 line is opened to allow nitrogen to flow in the line with high pressure through the metering valve and MFC toward the chamber. The pumping is continued until the nitrogen gas pressure reaches zero. This action is repeated several times to ensure that all the excess SiH_4 gases are purged from the line.

When all gases in the lines are pumped out and the system evacuated until the pressure of 6×10^{-3} mbar, we just have to wait until the samples are cooled down to near room temperature. The system can be switched off by closing all the gas valves and roughing valve and switching off the rotary pump. Now, the chamber can be opened in order to take out the deposited films for characterization. The films are transferred into a clean sample container and kept in the dry cabinet for future characterizations.

In this work, the filament and substrate temperatures were fixed at 1900°C and 300°C; respectively for deposition of total six sets of silicon carbide thin films. Two sets of samples were deposited by varying the CH_4 gas flow rate from 10 to 100 sccm while SiH_4 flow rate was fixed at 0.5 and 1 sccm. To investigate the effect of gas pressure, two sets of films were prepared at fixed SiH_4 to CH_4 flow rate ratio of 0.05 while the total gas partial pressure was varied from 12 to 33 Pa. For one set, the deposition pressure was kept constant at 80 Pa by adjusting the roughing valve, and in another set, the deposition pressure was equal to the total gas partial pressure by leaving the

roughing valve fully opened. Lastly, the effect of deposition pressure and the filament-to-substrate distance (d) on the properties of SiC films were studied by preparing films at SiH_4 and CH_4 flow rates of 1 and 20 sccm, respectively, and changing the deposition pressure and d.

3.4 Characterization and Analytical Procedures

This section describes the characterization and analytical procedures performed to characterize the SiC films and analyse the data obtained. These characterization techniques include surface profilometery to determine the film thickness and deposition rate, Fourier transform infrared (FTIR) spectroscopy and Raman scattering spectroscopy to investigate the bonding configurations, Auger electron spectroscopy (AES) for elemental composition, field emission scanning electron microscope (FESEM) to study the morphology, and UV-Vis-NIR spectroscopy for optical characterization of the films.

3.4.1 Thickness Measurement by Surface Profilometry

The thickness of SiC films deposited on glass and c-Si was determined using a KLA-Tencor P-6 surface profiler system, shown in Figure 3.5, which works in contact mode.

Before SiC film deposition, a mask was placed on the substrates in order to create a well-defined edge between substrate and SiC film. The profiler measures the step height between the edge of the film and the substrate. A horizontal scan across the step from the substrate to the middle of the film provides the thickness of the film deposited on the substrate. The average of four measurements from different edges was taken as the average film thickness.

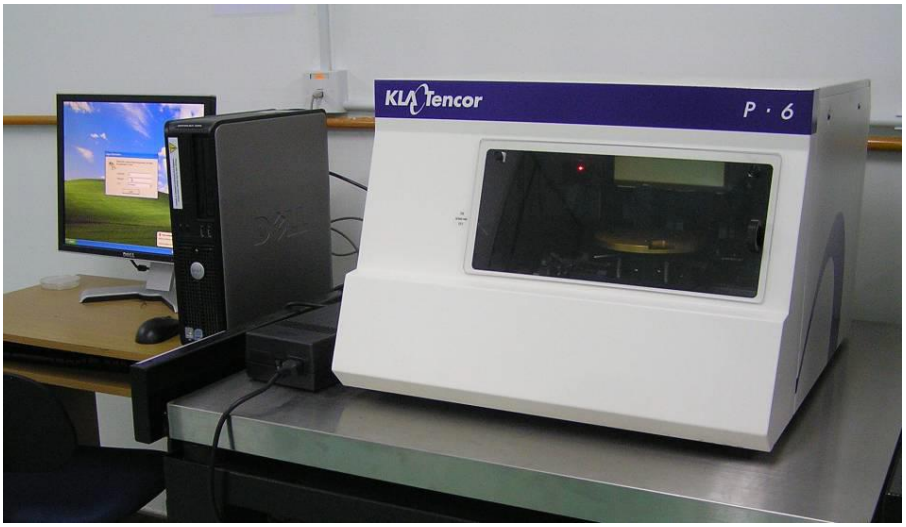

Figure 3.5: KLA-Tencor P-6 surface profiler system used for thickness measurement.

3.4.2 Fourier Transform Infrared (FTIR) Spectroscopy

Chemical bonding of silicon carbide films was studied using Fourier transform infrared (FTIR) spectroscopy. It is a non-destructive chemical analysis method, which is particularly sensitive to the asymmetrical bonding in semiconductor materials such as silicon carbide. In this work, FTIR spectra of HWCVD deposited amorphous and nano-crystalline SiC thin films on c-Si substrates were recorded using a Perkin Elmer System 2000 FTIR as shown in Figure 3.6. The measurement was done in the range of 400-4000 cm^{-1} at the resolution of 4 cm^{-1}. A bare Si substrate was used as a reference.

A chemical covalent bond can be considered as an elastic spring connected with two balls (atoms). The stronger the spring (i.e. the bond), the faster the vibration. Thus, the frequency of vibration is an indication of bond strength or can be related to the type of bond.

A molecular vibration occurs when atoms in a molecule are in periodic motion while the whole molecule undergoes translational and rotational motions. All molecules

have their inherent frequencies of vibration. A simple diatomic molecule such as H_2 has only one bond, which may stretch. Molecules that are more complex have many bonds, and vibrations can be conjugated.

Figure 3.6: Perkin Elmer System 2000 FTIR used for chemical bonding investigation.

When molecules are irradiated with an IR of a continuous wavelength, the IR with the same wavelength (or wavenumber) as the frequency of an inherent vibration (or other modes) of the molecular bonds will be absorbed, and an absorption peak will appear at the wavelength (or wavenumber). In other words, the molecular vibration with the same frequency will be activated or accumulated (also called "resonated") (Zhang, Li, & Kumar, 2009). Infrared radiation interacting with a vibrating molecule will only occur if there is oscillation of the electric vector of the radiation field with similar frequency, as the molecular dipole moment. If the normal vibration modulates the molecular dipole moment, a vibration is considered infrared active.

$$\left(\frac{\partial \mu}{\partial q}\right) \neq 0, \tag{3.2}$$

where μ is the molecular dipole moment and q stands for the normal coordinate describing the motion of the atoms during a normal vibration (Schrader, 1995). Molecular vibrations that can cause a change in the dipole moment include stretching, wagging, rocking, bending and twisting of an asymmetrical nature. Symmetrical bonds cannot be detected by this method because they do not pose any dipole moment. The vibrational modes of each molecule produce an absorption peak in the FTIR spectrum. The position of the peaks depends on the dipole moment or relative electronegativity of the two bonded atoms. The integrated intensity of the absorption peak is proportional to the concentration of the respective bonds in the material. How wide the absorption peaks are is due to the way the structure of the film is ordered (Prado et al., 2001). Thus, important information regarding the chemical structure and the bonding characteristics of the film are provided by its FTIR spectrum.

Based on the theory, for SiC films, homonuclear bonds such as Si-Si and C-C do not have dipole moment and thus cannot be detected in FTIR spectra. However, other bonds such as Si-C, Si-H and C-H are IR active. A typical FTIR spectrum of a SiC film is shown in Figure 3.7, which shows broad, shallow interference fringes in the transmittance IR spectra. This is due to the refractive index of the film, which is between that of Si substrate and air. The result is index contrast between the film and the substrate (Rajagopalan, 2003). Three main absorption bands are observed centred at around 800, 2080, and 2900 cm^{-1} corresponding to stretching vibrations of Si-C, Si-H, and C-H bonds, respectively. The CH_3 symmetric deformation mode in ($Si-CH_3$) group results in the absorption band at 1250 cm^{-1}. Another absorption peak at ~1000 cm^{-1} is usually observed in FTIR spectrum of SiC films deposited by HWCVD technique, which is attributed to wagging/rocking modes of C-H bonds in the $Si:C-H_n$ configuration. However, it should be noted that this absorption band is not correlated to C-H stretching vibration at 2800-3000 cm^{-1}. Vasin et al. have suggested that the main

contribution of the absorption band at 2800-3000 cm^{-1} comes from hydrogenated carbon clusters, i.e. from vibration of carbon-hydrogen bonds in the C:C-H configuration, while the contribution of Si:C-H_n bonds is minor (Vasin, 2008).

In order to analyse FTIR results quantitatively, it is important that the absorption coefficient (α(ω)) for the films should be measured, which can be done employing Lambert-Beer's law:

$$\alpha(\omega) = \frac{1}{d}\ln[T_0(\omega)/T(\omega)] \tag{3.3}$$

where d is the film thickness and $T_0(\omega)$ is the fitted baseline corresponding to zero absorption as indicated by a dashed line in Figure 3.7.

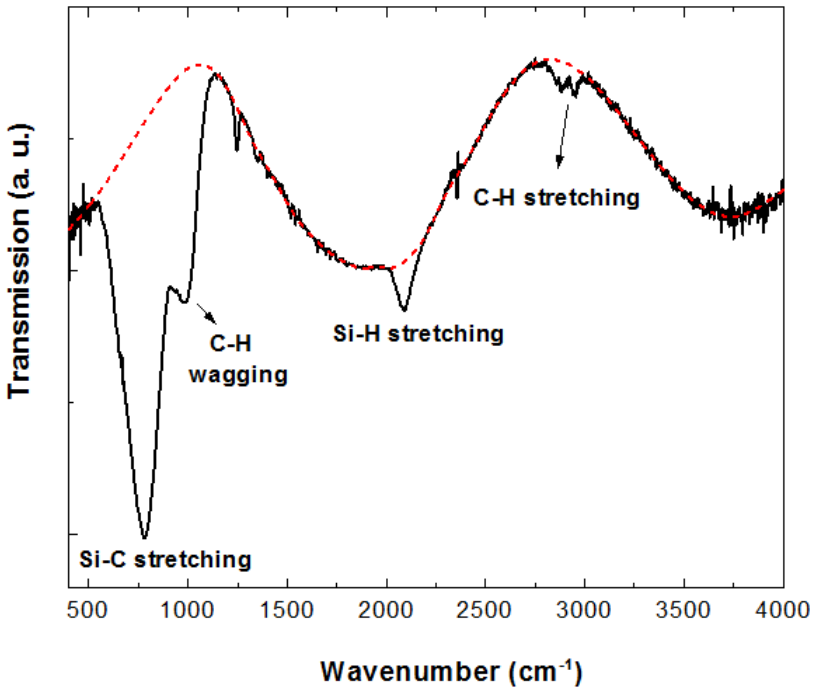

Figure 3.7: A typical FTIR spectrum for silicon carbide films. The dashed line is the baseline used to subtract the interference fringes in the spectrum.

The bond density is directly proportional to the integrated intensity of its IR absorption band as follows:

$$N = A \int \frac{\alpha(\omega)}{\omega} d\omega, \tag{3.4}$$

where A is inverse absorption cross section constant of the considered absorption mode. Table 3.1 lists this constant corresponding to various absorption bands of the SiC films.

It should be noted that the absorption band around 600-1100 cm^{-1} is usually a superposition of various absorption peaks at ~650 cm^{-1}, 800 cm^{-1}, and 1000 cm^{-1} corresponding to Si-H wagging mode, Si-C stretching mode, and C-H wagging in Si-CH_3 respectively. Therefore, to calculate the Si-C bond density, the deconvolution of this band into constituents is required. In this work, the deconvolution was done by using Origin 8.0 software. An example of such deconvolution is presented in Figure 3.8.

Table 3.1: Inverse absorption cross sections (A) of various absorption bands in FTIR spectrum.

Absorption band	A (cm^{-2})
Si-H wagging mode (650 cm^{-1})	3.6×10^{19}
Si-H stretching (2080 cm^{-1})	1.4×10^{20}
Si-C stretching mode (800 cm^{-1})	2.13×10^{19}
C-H (2800-3000 cm^{-1})	1.35×10^{21}

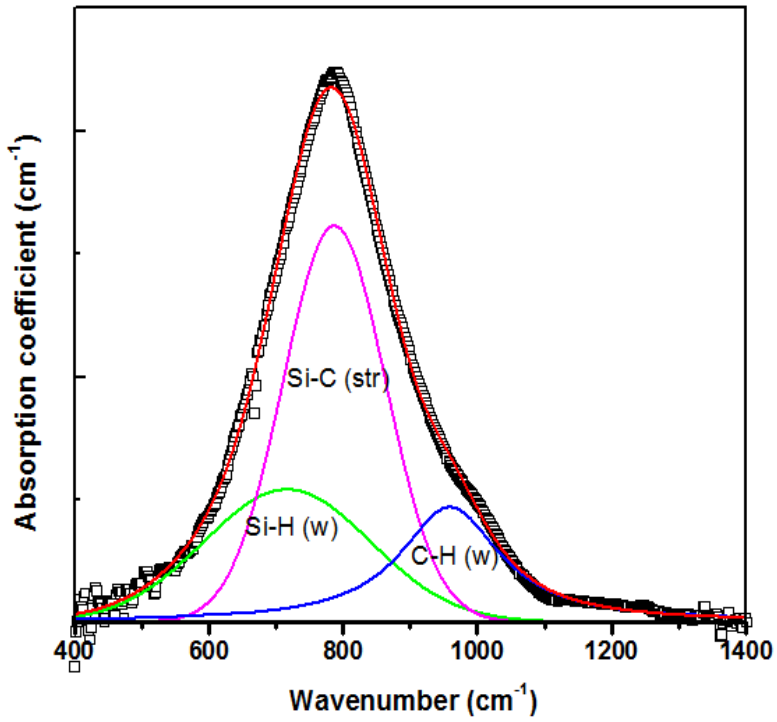

Figure 3.8: A typical deconvolution of IR absorption band of SiC film in the region of 400-1400 cm^{-1}.

3.4.3 Micro-Raman Scattering Spectroscopy

Raman scattering spectroscopy provides information about molecular vibrations that can be used for sample identification and qualification. Raman spectroscopy is based on the Raman Effect, which consist of the inelastic scattering of photons by the sample. Vibrational transitions are observable in either IR or Raman spectra, but there is a significant difference between the origin of Raman spectra and IR spectra. In the case of Raman scattering spectroscopy, irradiation of the sample is done by intense laser beam in the UV-visible region (ν_0), and the scattered light is normally seen a perpendicular direction to the incident beam (Figure 3.9).

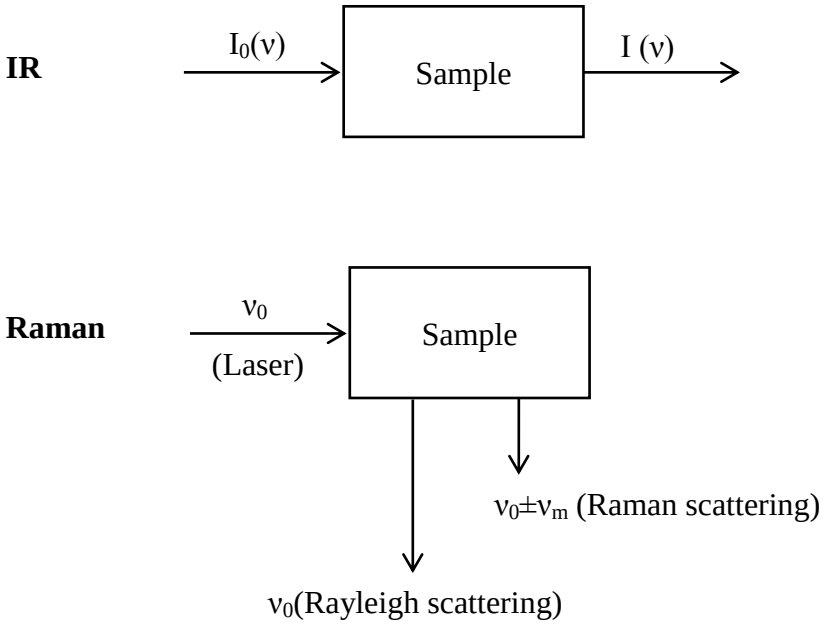

Figure 3.9: Differences in mechanism of Raman vs IR (Ferraro, et al., 2003).

There are two types of scattered lights: one, known as *Reyleigh scattering*, is strong and with frequency similar to that of the incident beam (ν_0); and the other, referred to as *Raman scattering*, is significantly weak (~ 10^{-5} of the incident beam) and with frequencies $\nu_0 \pm \nu_m$, where ν_m is a vibrational frequency of a molecule. The $\nu_0 - \nu_m$ and $\nu_0 + \nu_m$ lines are known as *Stokes* and *anti-Stokes* lines, respectively. Therefore, in Raman spectroscopy the vibrational frequency (ν_m) is measured as a shift from the incident beam frequency (ν_0) (Ferraro, et al., 2003).

A similar condition that was mentioned for IR must be met to observe the Raman spectrum vibration. When there is exposure of a molecule to an electric field, electrons and nuclei are forced to move in opposite directions, creating a dipole moment, which is proportional to the strength of the electric field and to the molecular polarizability α. A molecular vibration is observable in the Raman spectrum when the molecular polarizability is modulated by the vibration (Schrader, 1995),

$$\left(\frac{\partial \alpha}{\partial q}\right) \neq 0 \qquad (3.5)$$

The intensities of bands in the Raman spectrum of a compound are governed by the change in the polarizability that occurs during the vibrations. The intensity of any band in the Raman spectrum is given by the following expression:

$$I_{Raman} = KI_L(\nu_0 - \nu_m)^4 \left(\frac{d\alpha}{dq}\right)^2 \quad (3.6)$$

Where I_L is the power of the laser at the sample (ν_0-ν_m), the wavenumber at which the band is measured, and *dα/dq,* the change in the polarizability of the vibration. This parameter is the Raman equivalent of absorptivity and is sometimes called the Raman cross section (Griffiths & De Haseth, 2007).

In silicon carbide films, Si-Si and C-C bonds satisfy the above condition and thus can produce a Raman peak. However, Si-C bonds have low Raman cross section particularly in amorphous structure. It has been reported that the Raman cross section of Si-C bond is around 40 times smaller than that of C-C bonds (W. Yu, Lu, W., Han, L., Fu, G., 2004). Therefore, usually only a broad, weak Raman band can be observed due to Si-C from SiC films.

The Raman scattering spectra of the films were recorded using a Renishaw inVia Raman Microscope as shown in Figure 3.10. The measurements were carried out with two different excitation sources i.e. 514 nm Ar^+ laser and 325 nm He-Cd laser with the laser power of 10 mw. A schematic diagram of the Raman spectrometer is shown in Figure 3.11. From the figure, the laser beam is passed through a sample. Light scattered sideways from the sample is collected by a lens and passed into a grating monochromator. The signal is measured by a sensitive photomultiplier and after amplification a computer that plots the Raman spectrum processes it. In this work, the Raman shift was measured in the range of 100-2000 cm^{-1}.

Figure 3.10: Renishaw inVia Raman Microscope used to study the bonding configuration in the SiC films.

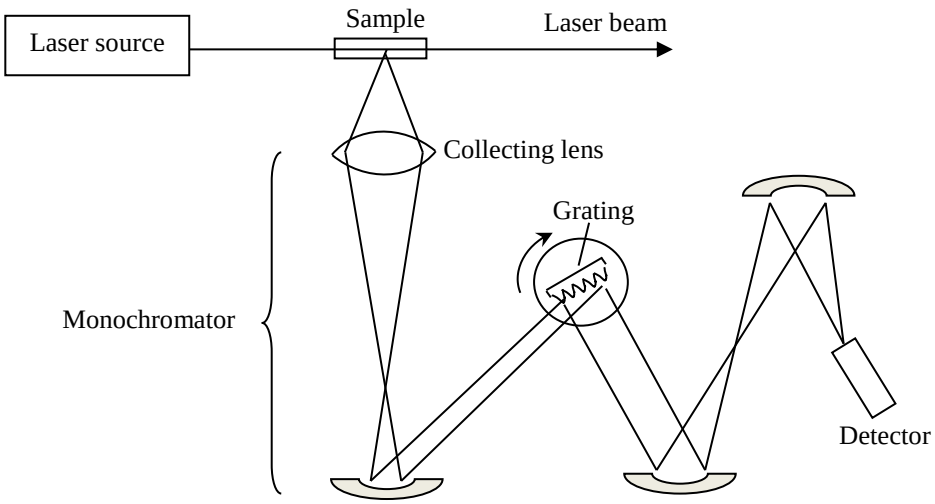

Figure 3.11: Schematic diagram of a Raman Spectrometer.

An example of a Raman scattering spectrum of SiC films is shown in Figure 3.12. In this figure, three main Raman bands in the spectrum are indicated

corresponding to Si-Si, Si-C and C-C vibrations in the SiC film. This shows that the film consists of separated phases. However, the intensity of each band depends on the Raman cross section of respective bonding vibrations.

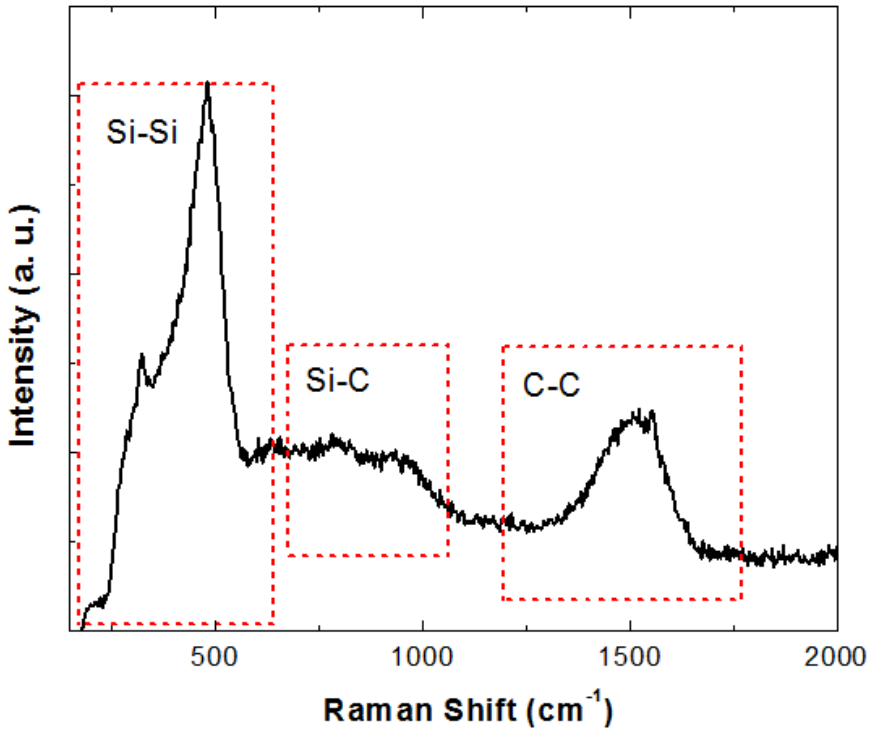

Figure 3.12: A typical Raman scattering spectrum (excitation laser: 325 nm) of HWCVD deposited SiC films.

3.4.4 X-Ray Diffraction (XRD)

X-Ray Diffraction (XRD) is a powerful and established technique that provides information about material identification and crystal size. It is based on the diffraction of X-ray radiation within the film structure. In this work, the XRD pattern of SiC films was recorded using SIEMENS D5000 X-ray diffractometer, with Cu Kα (λ=1.5418 Å) in the range of 2θ=5-80º. A photograph of the XRD instrument is shown in Figure 3.13.

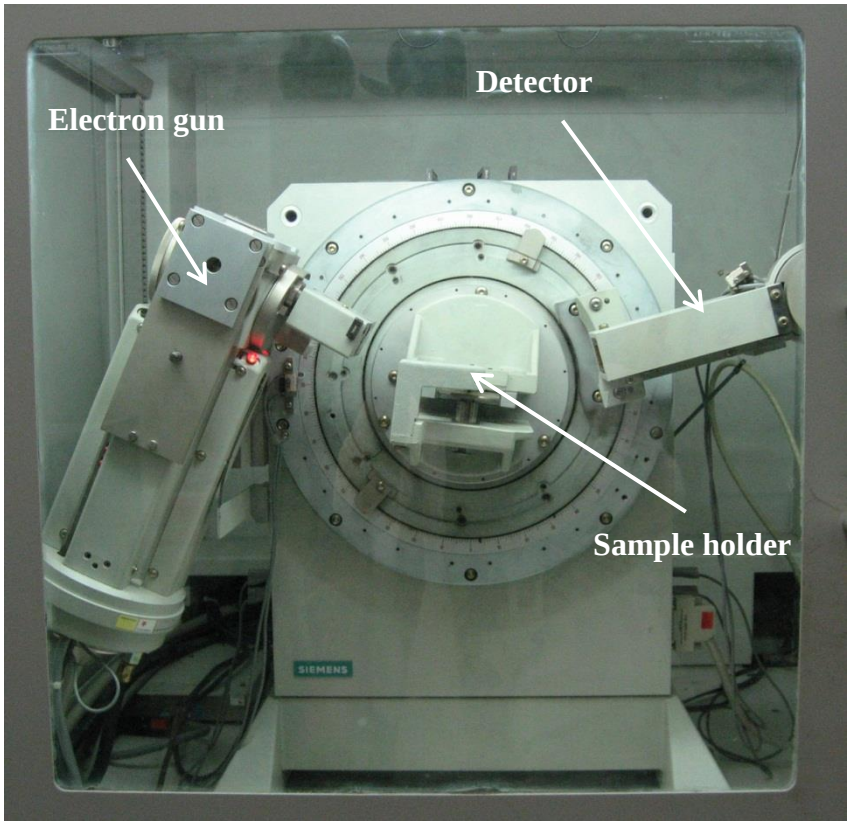

Figure 3.13: SIEMENS D5000 X-ray diffractometer used to investigate the crystalline structure of the films.

There are diffraction effects when there is impingement of electromagnetic radiation on periodic structures with geometrical variations on the length scale of the wavelength of the radiation. The crystals and molecules interatomic distances of 0.15-0.4 nm match to the electromagnetic spectrum with the wavelength of X-ray, with photon energies between 3 and 8 keV. Therefore, phenomena such as constructive and destructive interference should be observable when there is exposure of crystalline and molecular structures to X-ray.

The condition of constructive interference of two parallel X-ray beams which are reflected by two parallel atomic planes with a distance *d*, is given by Bragg's law:

$$2d\sin(\theta) = n\lambda \tag{3.7}$$

where θ is angle of incident X-ray beam with respect to the atomic plane, λ is the wavelength and n is an integer number, corresponding to the reflection order (see Figure 3.14 (a)).

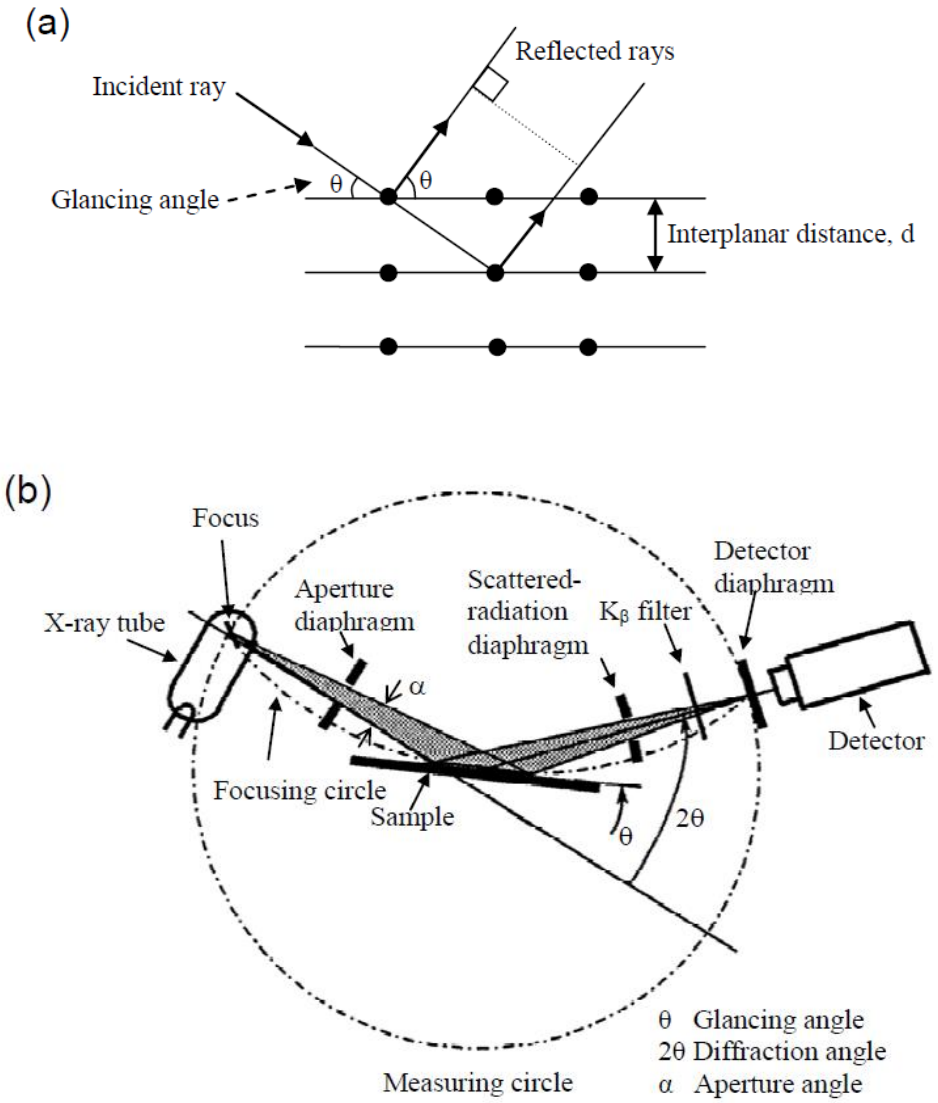

Figure 3.14: (a) The principle of X-ray diffraction and (b) schematic diagram of X-ray diffractometer.

A schematic description of an X-ray diffractometer is shown in Figure 3.14 (b). The X-rays coming from the X-ray tube are incident on the sample which is set at any

desired angle to the incident beam. The collection of the diffraction pattern is by varying the incidence angle of the incoming X-ray beam by θ and the scattering angle by 2θ while measuring the scattered intensity $I(2\theta)$. A real picture of X-ray diffractometer is shown in Figure 3.13.

If the atoms in a crystal are regularly arranged in a long range, the diffraction pattern contains sharp interference peaks. The size of crystallites (t) can be determined from Scherrer formula:

$$t = \frac{0.9\lambda}{B \cos \theta_B} \tag{3.8}$$

where B is the width at an intensity level equal to half the maximum (FWHM) of the diffraction peak and θ_B is the Bragg angle, which is the angle of incident X-ray beam. From this formula, it is obvious that bigger crystals result in sharper diffraction peaks at the position of $2\theta_B$.

The Bragg condition is not fulfilled in liquids and amorphous solids due to lack of long range order. The amorphous phase can only produce a broad peak in the diffraction pattern.

3.4.5 Auger Electron Spectroscopy (AES)

In 1925, Auger observed that an ionized atom could eject another electron (second ionization) if the first ionization occurs in the inner shell. Because the kinetic energy of the second ejected electron is dependent on the electronic structure of the element, it can be used to identify the element from which the electron is ejected. This is called Auger effect. The ejected electron is known as Auger electron. Based on the

auger effect, Auger electron spectroscopy (AES) was developed to identify the elements in a given material (Zhang, et al., 2009).

In depth analysis of samples, AES instrument uses ion beam etching to eliminate the material from the sample surface. One cycle of a typical depth profile involves etching a small increment into the sample, stopping, measuring relevant portions of Auger spectrum, and employing the equation for elemental quantification in the film structure.

Elemental composition of SiC films was investigated by using Auger electron spectroscopy (AES) technique. This measurement was performed using a JEOL JAMP-9500F field emission Auger microscope, as indicated in Figure 3.15. The concentration of constituent atoms was made available by Auger Electron Spectroscopy with depth profiling with Ar^+ ions (4 kV accelerating voltage) etching rate of 14.8 nm/min. An example of Auger depth profile of HWCVD deposited SiC film is shown in Figure 3.16. Here, the SiC film, SiC/Si interface and Si substrate regions are indicated. Relative atomic concentration of constituent elements is calculated using their relative sensitivity factors (RSF). The RSFs are 0.121, 0.122, 0.365, and 0.238 for carbon, nitrogen, oxygen, and silicon, respectively.

Figure 3.15: JEOL JAMP-9500F field emission Auger microscope used for elemental composition measurements.

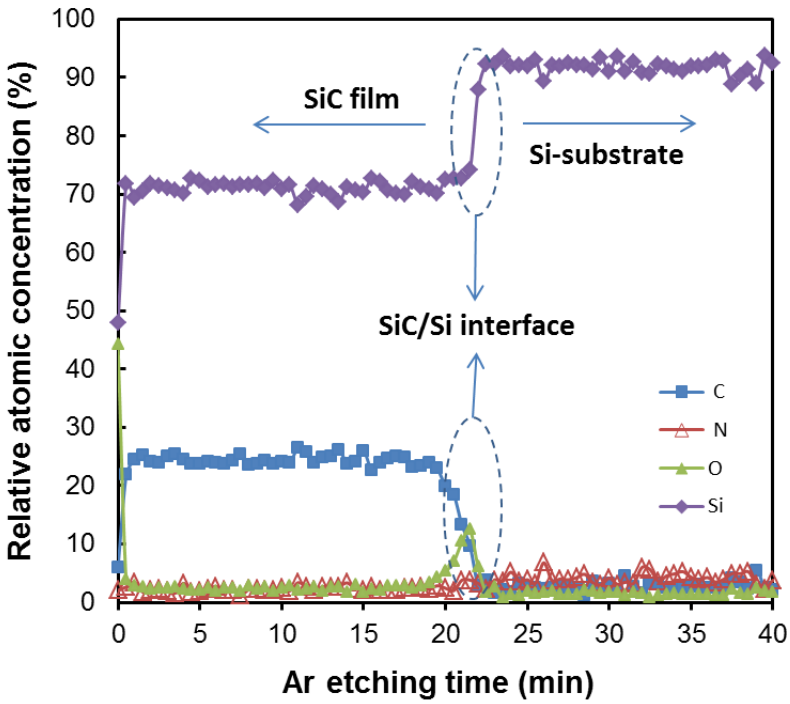

Figure 3.16: Typical Auger depth profile of SiC film deposited by HWCVD technique.

3.4.6 Field Emission Scanning Electron Microscope (FESEM)

The surface and morphological properties of SiC films were examined using Field Emission Electron Microscope (FESEM). High-resolution images were taken using an FEI Quanta FESEM as shown in Figure 3.17. The images were taken in high vacuum at acceleration voltage 0f 20 kV.

Figure 3.17: FEI Quanta Field Emission Electron Microscope (FESEM) used for high-resolution imaging of SiC films.

The principle of scanning electron microscopy (SEM) is the detection and visualization of secondary and backscattered electrons because of the interaction between an electron beam and the sample surface. An SEM mainly consists of an

electron gun, a lens system, detector and display as shown in Figure 3.18. A high-energy electrons beam is emitted and moves downward through a series of magnetic lenses designed to direct the electrons to a very fine spot. When a focused electron beam strikes the sample surface, different types of signals are generated from the sample and detected by various sensors. Secondary electrons with lower energy give information about the surface of the specimen while backscattered electrons come from a deeper interaction zone of interest.

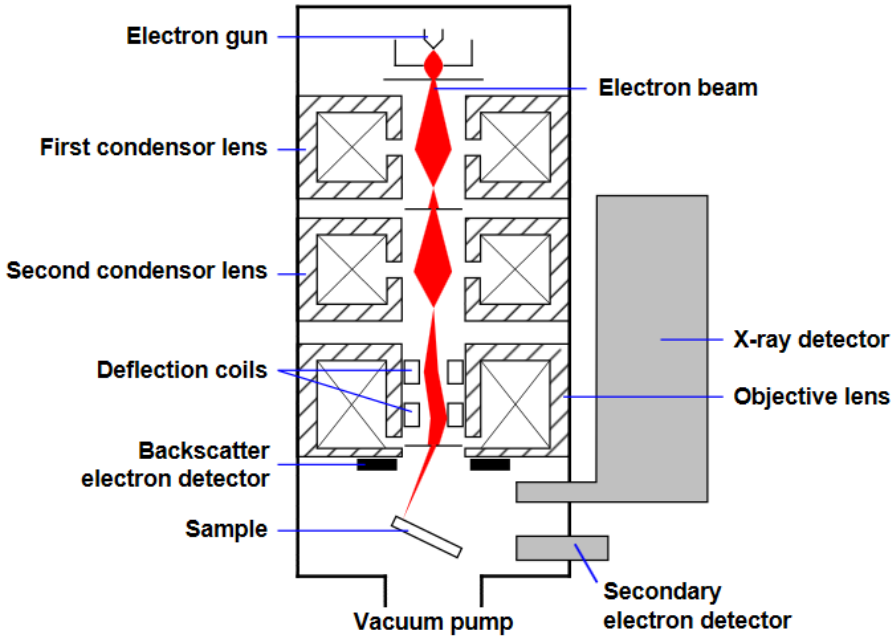

Figure 3.18: A schematic diagram of FESEM system.

3.4.7 UV-Vis-NIR Spectroscopy

When photons impinge on a semiconductor, the photons of energy $h\nu \geq E_g$ are absorbed, while those of energy less than the band gap are transmitted. The ratio of the transmitted and the incident light is a function of the photon wavelength and the thickness travelled. The absorbance is given according to Beer-Lambert's law,

$$Absorbance = 1 - log\left(\frac{I}{I_0}\right) = \varepsilon cl \tag{3.9}$$

where ε, c, and l are molar absorptivity, molar concentration, and path length of sample respectively. I_0 is the intensity of incident beam and I is the intensity of transmitted beam.

Optical characterization of SiC films deposited on glass substrates were carried out using a Jasco V-750 UV-Vis-NIR spectrophotometer, as shown in Figure 3.19.

Figure 3.19: Jasco V-750 UV-Vis-NIR spectrophotometer used for optical characterization.

The measurements were performed in both transmission and reflection modes. For transmission, a bare glass substrate was employed as a reference while in reflection mode an aluminium-coated glass was used as a reference with total reflection. Incident beam was normal to the film surface for transmission measurement. However, in the reflection mode the incident angle was fixed at 5º in respect of the normal direction to the film surface. The measurement was performed in the spectral range of 190-2500 nm with interval of 2 nm. The absorption region in the transmittance spectrum was where

the transmission intensity showed significant decrease. A typical optical transmission and reflection spectra of SiC thin films is shown in Figure 3.20.

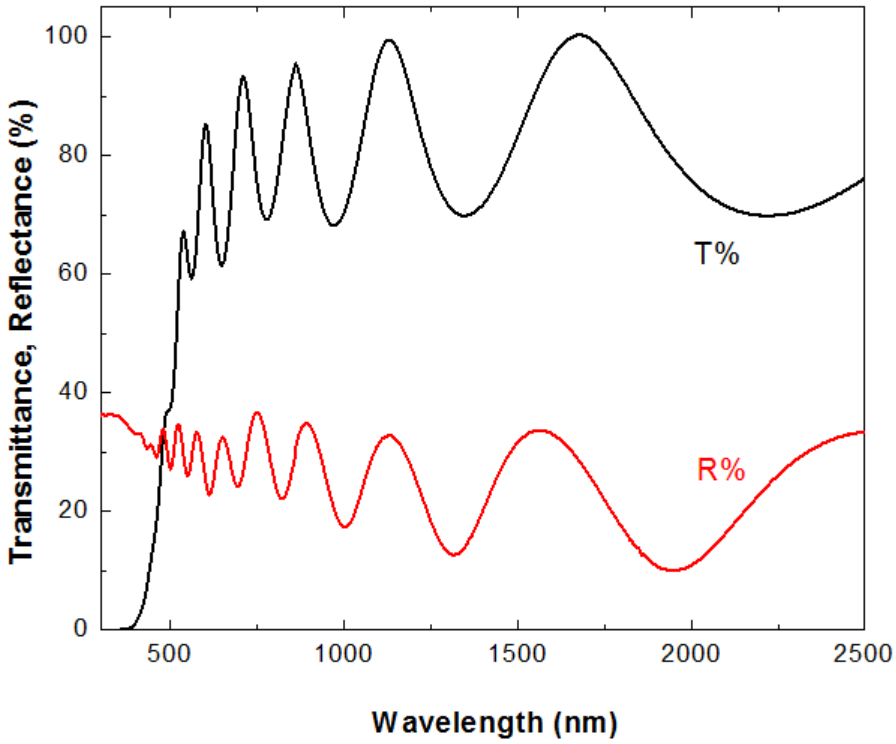

Figure 3.20: A typical transmission and reflection spectra of SiC film deposited by HWCVD. (The data are extracted from this work.)

From transmission and reflection spectra, optical constants of the film including refractive index, thickness, and energy band gap can be calculated.

3.4.7.1 Determination of Film Thickness and Refractive Index

In this section, a method introduced by Manifacier et al. (Manifacier, Gasiot, & Fillard, 1976) is presented that will be utilized for optical characterization of SiC films. According to this method, the refractive index (n) of the films can be written as follows:

$$n(\lambda_i) = \left(N + (N^2 - n_o^2 n_1^2)^{\frac{1}{2}}\right)^{\frac{1}{2}} \tag{3.10}$$

where

$$N = \frac{n_o^2 + n_1^2}{2} + 2n_o n_1 \frac{T_{Max} - T_{min}}{T_{Max} T_{min}} \tag{3.11}$$

n_o is the refractive index of air;1.00 and n_1 is the refractive index of glass substrate; 1.52. T_{Max} and T_{min} are the values of transmission obtained from the interference fringes of the spectrum using an envelope method as shown in Figure 3.21.

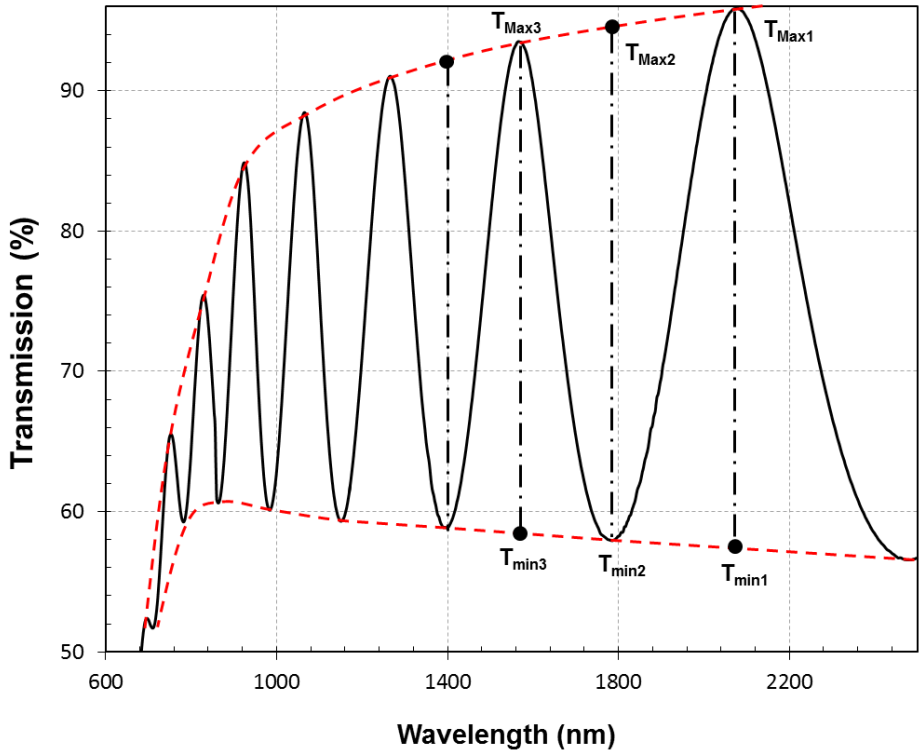

Figure 3.21: The transmission spectrum of SiC film with envelope functions of T_{Max} and T_{min} used for refractive index calculation (The data corresponds to the film deposited under deposition pressure of 40 Pa).

The optical thickness can be determined using a method proposed by Davis et al. (Davis, Piggins, & Bayliss, 1987):

$$m\lambda = 2nd, \tag{3.12}$$

where *m* is interference order, λ, n and *d*, are the wavelength, refractive index and optical thickness of the corresponding interference order, respectively.

The interference order is taken from the smallest value for the first extreme point and increases by half for next maximum or minimum point. It should be noted that the value of *m* is the integer for maximum points and half integer for minimum points. By varying the *m* value for a series of interference fringes, a set of *mλ/2* values are produced which is equal to *nd*. To determine the *m* values, a simple graphical method introduced by Swanepoel et al. (Swanepoel, 1983) is used. If the order number (integer or half integer) of the first extreme is m_1, the equation for the extreme points can be written as follows:

$$2nd = \left(m_1 + \frac{k}{2}\right)\lambda, \qquad k = 0, 1, 2, 3 \ldots \tag{3.13}$$

or

$$k/2 = 2nd/\lambda - m_1 \tag{3.14}$$

If *k/2* is plotted versus *n/λ*, the amount of m_1 can be obtained from the intercept of the straight line. By selecting the correct first interference order, the optical thickness (*d*) can be simply determined by dividing *nd* by *n* at the longest wavelength obtained from the Manifacier method. The values of the refractive index as a function of wavelength are then calculated using this thickness. These values must satisfy the Cauchy function:

$$n = \frac{a}{\lambda^2} + n_0' \tag{3.15}$$

where a and n_0' are linear slope and static refractive index of the film, respectively.

3.4.7.2 Optical Absorption and Band Gap

From the transmission and reflection spectra, the absorption coefficient of the films can be obtained using the following equation:

$$\alpha = \frac{1}{d} ln\left(\frac{1-R}{T}\right), \tag{3.16}$$

where d is the optical thickness of the film as determined following the method explained in above section. T and R are the transmission and reflection data as obtained from UV-Vis-NIR measurement.

The energy band gap of SiC films, E_g can be determined from the Tauc relation (Tauc & Abeles, 1972):

$$\alpha E = B\left(E - E_g\right)^2, \tag{3.17}$$

where B is a constant and E is the photon energy. In order to determine the value of E_g, graph of $(\alpha E)^{1/2}$ versus photon energy, E, is plotted as an example as shown in Figure 3.22. Extrapolation of the linear part of this plot for $(\alpha E)^{1/2} = 0$ gives the value of E_g.

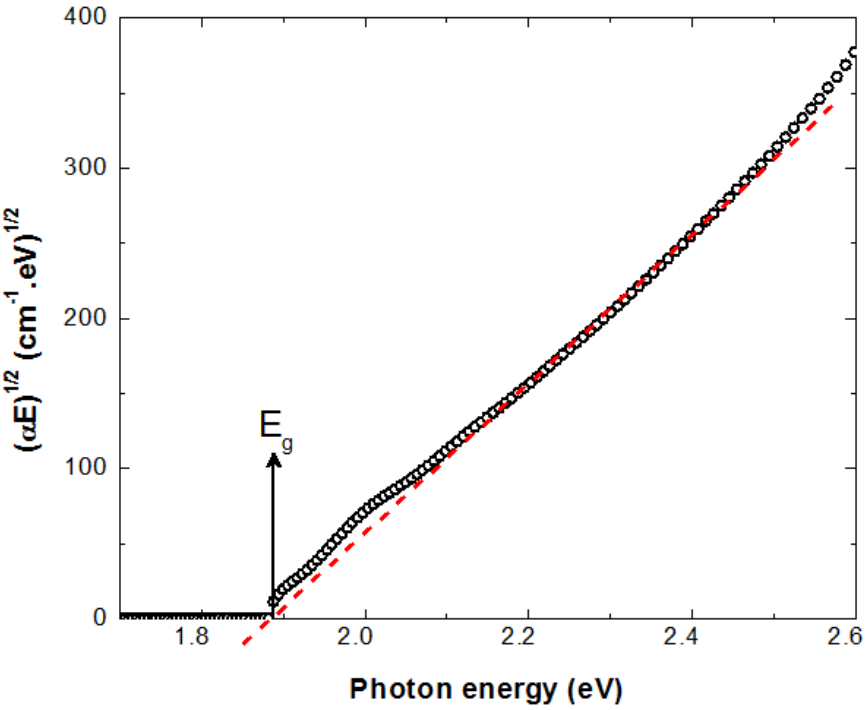

Figure 3.22: An example of Tauc plot of SiC film for determination of energy gap.

3.4.8 Photoluminescence Spectroscopy

Photoluminescence (PL) spectroscopy is a powerful tool for semiconductor material characterization. This characterization technique is fast, simple, and non-destructive. This technique is based on the emission of light by a semiconductor material when it is photo-excited by a monochromatic light of certain energy. Therefore, PL can provide information on radiative recombination centres like defects and impurities in the material.

PL characteristics of the films in this work were recorded using a Renishaw 2000 at room temperature. This system is an integrated PL/Raman measuring system which was also used for Raman measurement. A helium cadmium laser was used as an excitation source with the wavelength of 325 nm.

CHAPTER 4

Silicon Carbide Thin Films Prepared by HWCVD Technique from Pure Silane and Methane: Part 1

4.1 Introduction

In this chapter, the deposition of SiC thin films using hot-wire chemical vapour deposition (HWCVD) from pure silane and methane gas mixture is presented. The influence of precursor gas concentration on chemical bonding, crystallinity and elemental composition properties of the films are studied from analysis done on the Fourier transform infra-red (FTIR), Raman scattering, X-ray diffraction, and Auger depth profiling measurement of the films deposited on c-Si substrate. Two series of SiC films were studied in this part. The FTIR transmission spectra were carried out to study the heteronuclear bonds such as Si-C, Si-H and C-H bonds present in the films. While Raman scattering spectroscopy was performed to detect the homonuclear bonds i.e. Si-Si and C-C bonds and carbon bonding configuration. The first series of films consisted of two sets of films deposited at two different silane flow-rates of 0.5 and 1 sccm while the flow-rates of methane gas were varied from 10 to 100 sccm in each set. The choice of SiH_4 flow rate was based on earlier reports in the literature that verified 'silane starving' condition is necessary to obtain better quality SiC films (A. A. Kumbhar, et al., 1998; A. S. Kumbhar, et al., 1995). The second series of films also consisted of films deposited at different silane (SiH_4) and methane (CH_4) flow-rates with the gas flow ratio fixed. Two sets of films were deposited for this series. The films in the first set were deposited at the deposition pressure of the total gas partial pressure by setting the rotary pump valve fully opened while the deposition pressure of the second set of films was fixed by controlling the rotary pump valve. It should be noted that the other deposition parameters not mentioned above were fixed and will be detailed in the following section.

Three main objectives of the work done in this chapter are:

1. To deposit SiC films by HWCVD technique from pure silane and methane gas mixture.
2. To determine the effect of methane flow rate on the quality of the films i.e. Si-C bond density, crystallinity and deposition rate by varying the methane flow rate at two different fixed silane flow rate. The films in series 1 are used to study the structural properties of the films with increase in the concentration of methane molecules.
3. To determine the influence of total gas partial pressure on the structural properties of the SiC films. The films deposited in series 2 are studied to establish that the flow-rate ratio of silane to methane is not a determining factor to the structural properties of the films and increase in the concentration of precursor gases silane and methane at fixed silane to methane flow-rate ratio has significant influence on the structural properties.

4.2 Deposition Parameters of SiC Thin Films Highlighted

The deposition parameters of the SiC films prepared by HWCVD technique studied in this chapter are listed in Table 4.1.

It should be noted that for the samples prepared in series 1, the methane flow rate, [CH_4], was varied from 10 to 100 sccm, while keeping silane flow rate, [SiH_4], constant at either 0.5 or 1 sccm. In addition, two sets of samples were deposited in series 2. Silane to methane flow-rate ratio, [SiH_4]/[CH_4], was fixed at 0.05, while the flow rate of each gas was varied. This process was performed in two different conditions. Firstly, the deposition pressure was set to be equal to the total gas partial pressure. For this purpose, the roughing valve was kept fully opened during deposition.

Therefore, the deposition pressure was a variable parameter. This set of samples is called "VP" which stands for "Variable Pressure". For the second set, however, the deposition pressure was always kept constant at 80 Pa regardless of the

partial pressure. Adjusting the deposition pressure in this set was done by regulating the roughing valve until the pressure reading is equal to 80 Pa. This set is named "FP" which stands for "Fixed Pressure".

Table 4.1: Deposition parameters for SiC films used in this chapter.

Deposition Parameter	Value
Filament temperature	1900°C
Substrate temperature	300°C
Methane flow rate	10-100 sccm (series 1)
	10-40 sccm (series 2)
Silane flow rate	1 sccm (series 1, first set)
	0.5 sccm (series 1, second set)
	0.5-2 sccm (series 2)
Deposition pressure	80 Pa
	12-33 Pa (series 2, VP set)
Filament-to-substrate distance	25 mm
Deposition time	30 min

4.3 Deposition of SiC Films Under Fixed Silane Flow-Rate with the Methane Flow-Rates Varied

4.3.1 *Chemical Bonding Investigation by FTIR Spectroscopy*

The bonding configurations of the films were studied by FTIR spectroscopy. Figure 4.1 (a) and (b) show the thickness-normalized FTIR absorption spectra of SiC films deposited at SiH_4 flow rate of 0.5 and 1 sccm, respectively, and indicated CH_4 flow rates.

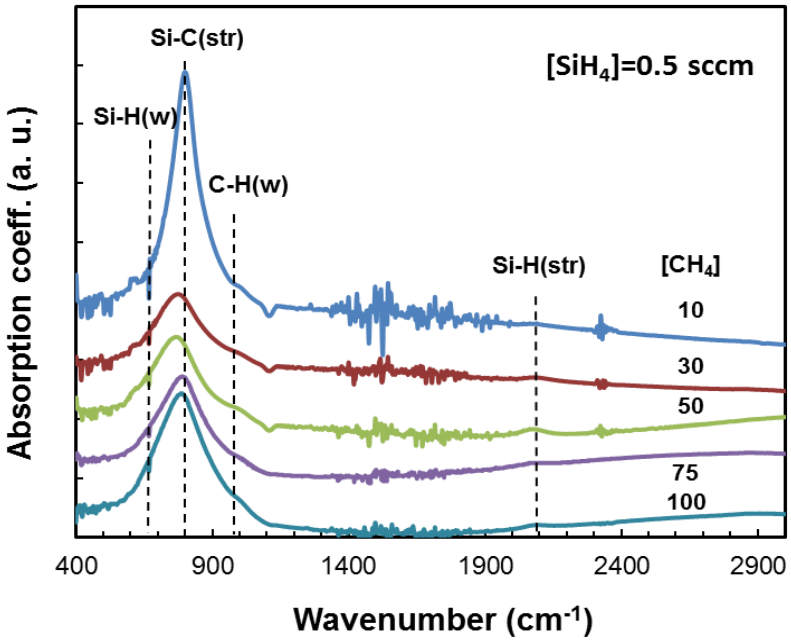

(a)

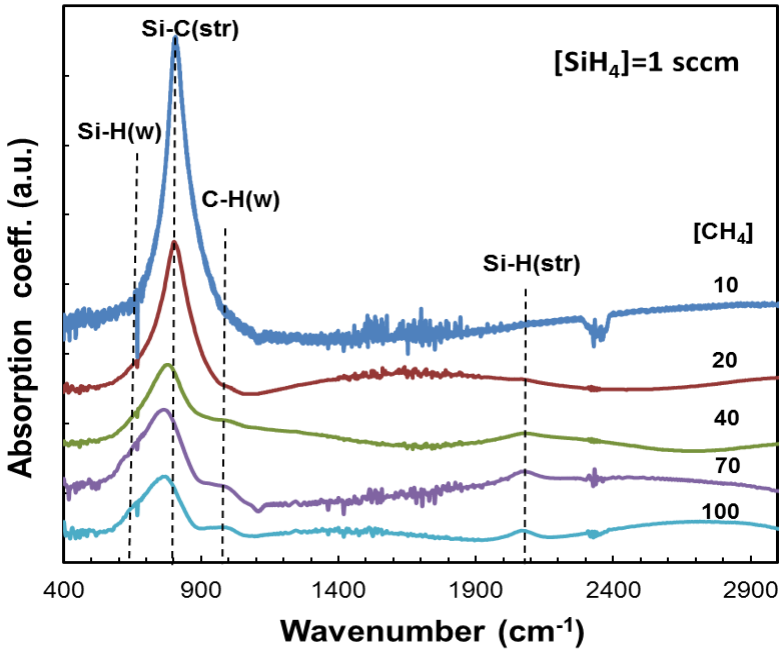

(b)

Figure 4.1: FTIR absorption spectra of SiC film deposited under different CH_4 flow rate and SiH_4 flow rate of (a) 0.5 sccm and (b) 1 sccm.

The main feature of these spectra was a sharp and intense absorption band in the range of 600 cm^{-1} to 1100 cm^{-1}. This band is contributed by the superposition of absorption peaks located at about 650 cm^{-1}, 800 cm^{-1} and 980 cm^{-1} corresponding to the Si-H wagging (w), Si-C stretching (str) and C-H_n wagging (w) vibration modes, respectively (Hartel, 2010). Additionally, a weak absorption band in the range of 1900 to 2200 cm^{-1} was detected which is attributed to Si-H (str) vibration mode (Chew, 2002). C-H_n stretching vibration at the range of 2800-3000 cm^{-1} (Ritikos, Siong, Ab. Gani, Muhamad, & Rahman, 2009), usually observed in hydrogenated a-SiC films was absent in our spectra. It was observed that the former absorption band increased in intensity with the decrease in CH_4 flow rate, while the Si-H (str) band followed the opposite trend. The decrease in the Si-H (str) intensity indicates a decrease in the hydrogen concentration in the films prepared at lower CH_4 flow rate. Moreover, the evolution in the shape and width of the Si-C (str) band suggested a phase transformation from amorphous to crystalline (Kerdiles, 2000; Rajagopalan, 2003) with decrease in CH_4 flow rate. In order to verify this transformation, the standard deconvolutions have been done for this absorption band. The Si-C (str) band was fitted to both Gaussian and Lorentzian distribution curves to determine the amorphous and crystalline components of the SiC phase in the film structure respectively. Many researchers working on SiC films have widely adopted this technique (Finger et al., 2009; Rajagopalan, 2003; W. Yu, Wang, X., Lu, W., Wang, S., Bian, Y., Fu, G., 2010). The Lorentzian component of Si-C (str) mode was dominant in the films deposited at lower CH_4 flow rate with insignificant presence of Si-H (w) and C-H (w) modes. The presence of Gaussian Si-C (str), Si-H (w) and C-H (w) modes became more significant compared to the Lorentzian Si-C (str) mode at higher CH_4 flow rate. The SiC crystalline volume fraction of the films prepared at different CH_4 flow rate was estimated following the formula $A_L/(A_G+A_L)$ where A_L and A_G were the areas under Si-C Lorentzian and Gaussian

components, respectively. Figure 4.2 shows the variation of SiC crystalline volume fraction as a function of CH_4 flow rate for the films deposited under SiH_4 flow rate of 1 and 0.5 sccm. It was noticed that the volume fraction of SiC crystallites considerably decreased with increase in CH_4 flow rate and similar trends were observed for both sets of films. This variation indicates a phase transition from crystalline to amorphous in the film structure.

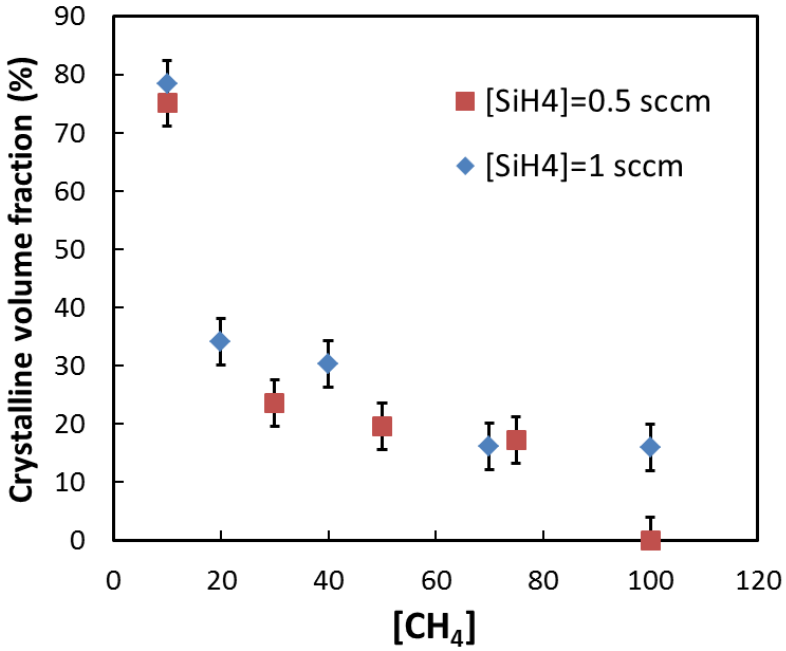

Figure 4.2: Variations of SiC crystalline volume fraction of the films deposited at SiH_4 flow rate of 0.5 and 1 sccm as a function of CH_4 flow rate.

The bond density (N) of Si-C and Si-H can be calculated by using the following formula:

$$N = \frac{A}{\nu_0} \int \alpha(\nu) d\nu \tag{4.1}$$

where A, ν_0, and $\alpha(\nu)$ are reverse cross section, position of the absorption peak and absorption coefficient, respectively. The standard values of A for Si-C and Si-H

stretching vibration modes adopted from literature are 2.13×10^{19} and 1.40×10^{20} cm^{-2}, respectively (Kaneko, 2005). Figure 4.3 shows a decrease in bond density of Si-H and increase in Si-C bond with the decrease in CH_4 flow rate. The absence of C-H (str) indicates there were no a-C:H clusters in the films while the presence of C-H (w) vibration mode, was associated to the C-H bonds attached to Si atom (Si-C-H) (Vasin, 2008). It can be concluded that the films deposited at high CH_4 flow rate are generally amorphous with a mixture of a-Si:H phase embedded within a more dominant a-SiC:H phase, while the films deposited at lower CH_4 flow rate showed lower hydrogen concentration with more ordered Si–C matrix. The Si-C and Si-H bond densities in the films were calculated and listed in Table 4.2.

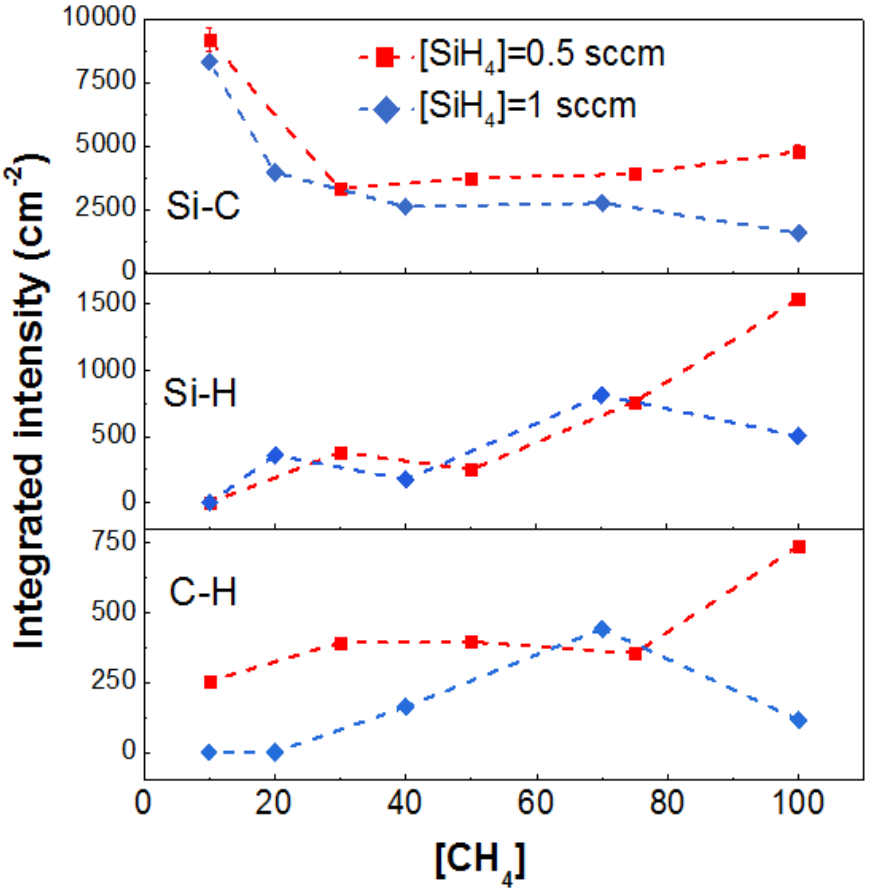

Figure 4.3: Variations of integrated intensities of Si-C, Si-H, and C-H bands in the films prepared under various methane and silane flow rates.

Table 4.2: Si-C and Si-H bond densities of SiC films deposited under different methane and silane flow rate.

CH_4 (sccm) ± 0.1 sccm	SiH_4 (sccm) ± 0.01 sccm	N_{Si-C} (cm^{-3}) ± 0.1×10^{23}	N_{Si-H} (cm^{-3}) ±0.5×10^{21}
10.0	0.50	2.0×10^{23}	3.5×10^{21}
30.0	0.50	7.1×10^{22}	4.0×10^{21}
50.0	0.50	7.9×10^{22}	6.0×10^{21}
75.0	0.50	8.3×10^{22}	6.5×10^{21}
100.0	0.50	1.0×10^{23}	6.0×10^{21}
10.0	1.00	1.8×10^{23}	8.0×10^{20}
20.0	1.00	8.4×10^{22}	1.5×10^{21}
40.0	1.00	5.6×10^{22}	5.5×10^{21}
70.0	1.00	5.9×10^{22}	8.0×10^{21}
100.0	1.00	3.4×10^{22}	8.0×10^{21}

4.3.2 Raman Scattering Spectroscopy

Figures 4.4 (a) and (b) show the Raman scattering spectra (excitation wavelength of 325 nm) of the SiC films deposited at different CH_4 flow rate with SiH_4 flow rate fixed at 1 and 0.5 sccm, respectively. The broad band centred at 480 cm^{-1} attributed to Si-Si TO mode indicates the presence of a-Si phase in all the films. For the films prepared at SiH_4 flow rate of 1 sccm, the intensity of this band monotonically increased with the increase in CH_4 flow rate, indicating the increase in presence of a-Si phase in the film structure. In the case of the films prepared at SiH_4 flow rate of 0.5 sccm, an initial increase in the intensity of this band was observed with increase in CH_4 flow rate from 10 to 30 sccm followed by a continuous decrease in its intensity with further increase in CH_4 flow rate. The band located in the region between 700 and

1000 cm^{-1} which is associated with Si-C bonds was weak due to the low Raman efficiency of SiC (Q. Cheng & et al., 2008; Bibhu P. Swain & Dusane, 2006).

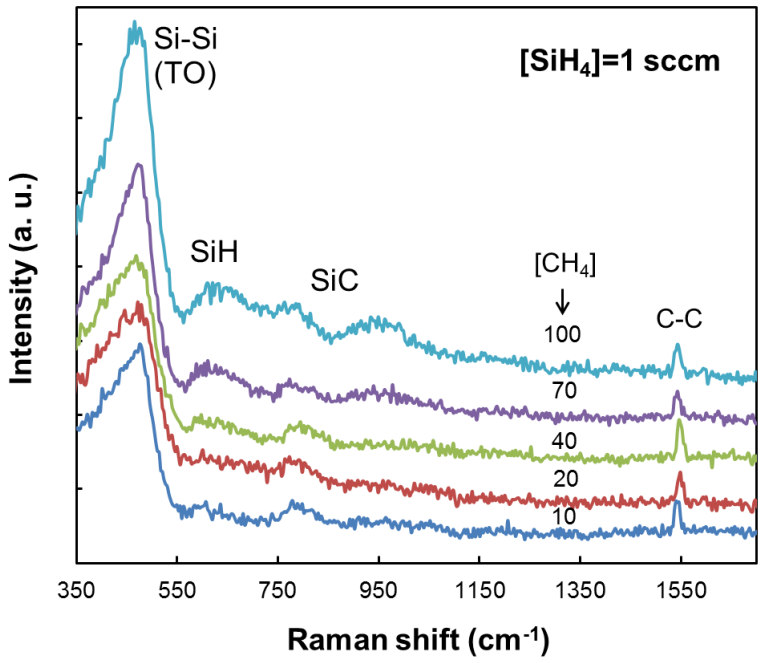

(a)

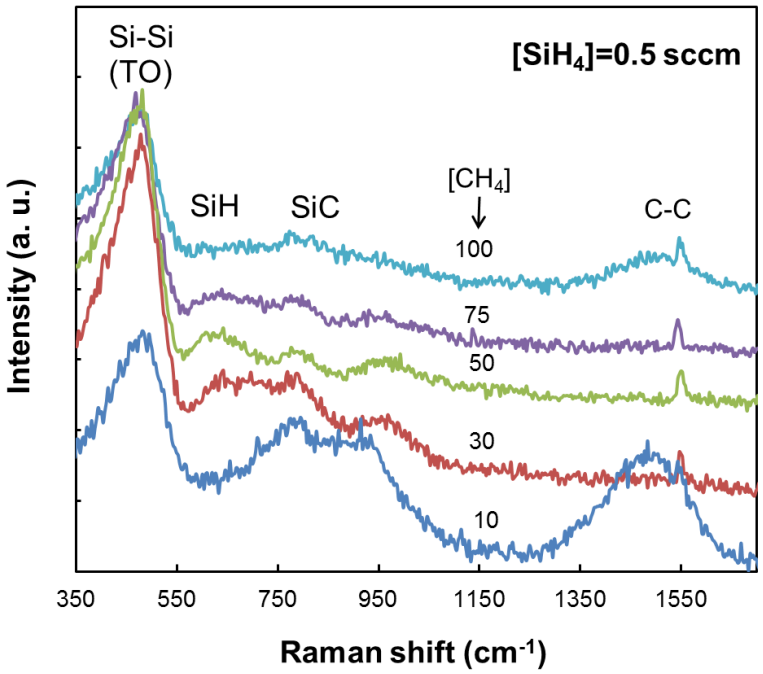

(b)

Figure 4.4: Raman scattering spectra of SiC films deposited at indicated CH_4 flow rates and SiH_4 flow rate of (a) 0.5 sccm and (b) 1 sccm.

A sharp observable peak at 1550 cm^{-1} is attributed to atmospheric oxygen (Huang, 2002; J. R. Shi, et al, 2000). However, for the films prepared at SiH_4 flow rate of 0.5 sccm and CH_4 flow rate of 10 and 100 sccm, this peak was accompanied by a broad band centred at ~1500 cm^{-1}. This band is usually associated with the C-C sp^2 bonds in a-C:H films; however this band was red-shifted compared to the positions of the G bands of a-C:H films at 1590 cm^{-1} (A. C. Ferrari & Robertson, 2000; Andrea Carlo Ferrari & Robertson, 2004) which is due to the addition of Si to the carbon matrix (Guruvenket, 2010). Therefore, the formation of multi-phased films consisting of a-Si, a-C and SiC phases was obviously confirmed by the Raman results.

4.3.3 XRD Analysis

Figures 4.5 (a) and (b) show the XRD patterns of the SiC films deposited at various SiH_4 and CH_4 flow rate. As shown in both figures, all samples revealed an XRD peak at 2θ of 56.7° corresponding to the crystalline Si (311) orientation plane. This preferred orientation of Si crystallites is due to Si substrates, since the XRD pattern of Si substrate showed an XRD peak at the same position. Three XRD peaks were observed at 2θ of 35.7°, 60.0° and 71.8° corresponding to the (111), (220) and (311) reflection planes of 3C-SiC, respectively from the films deposited at CH_4 flow rate below 30 sccm (A. Tabata, et al., 2010). This shows that SiC crystallites are formed in the films deposited at lower CH_4 flow rate (< 30 sccm) and this is consistent with FTIR results, which showed a high SiC crystalline volume fraction for these films. This is particularly obvious for the set of films prepared at SiH_4 flow rate of 1 sccm.

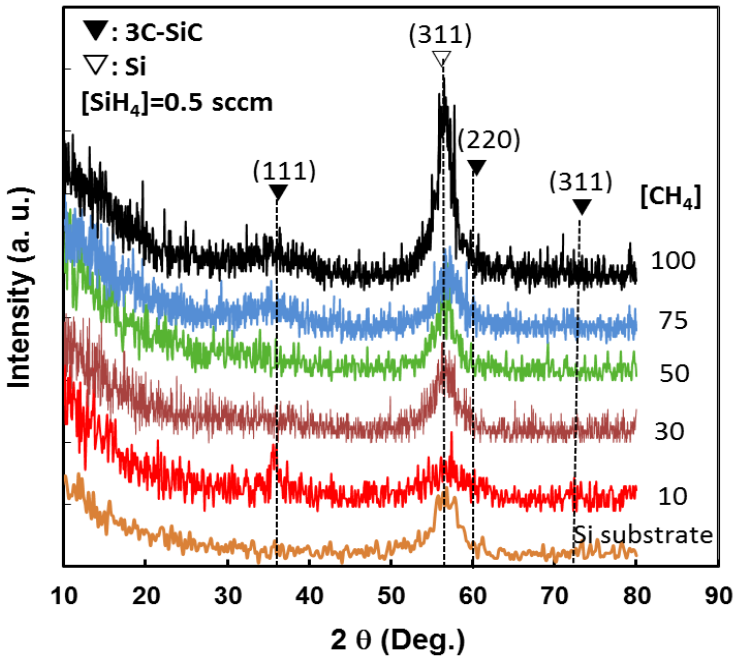

(a)

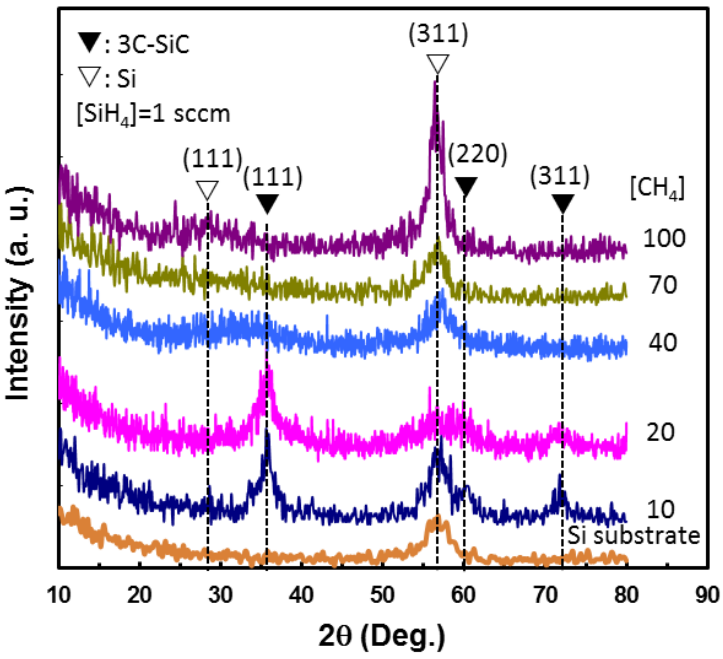

(b)

Figure 4.5: XRD patterns of SiC films deposited at indicated CH_4 flow rates and SiH_4 flow rate of (a) 0.5 sccm and (b) 1 sccm. The XRD pattern of c-Si bare substrate was also shown in both graphs. The XRD peaks corresponding to Si and 3C-SiC were labelled in the figure.

The SiC mean crystallite size of the films estimated from the XRD peak of 3C-SiC (111) using Scherrer's formula (Klug & Alexander, 1974), was in the range of 2-6 nm. The samples prepared at CH_4 flow rate above 30 sccm are amorphous. It should be noted that the films prepared at SiH_4 flow rate of 1 and 0.5 sccm, showed the formation of 3C-SiC nano-crystallites and exhibited high density of Si-C bonds when the CH_4 flow rate is 20 sccm and 10 sccm, respectively. The SiH_4 to CH_4 flow rate ratio for both of them was the same and equal to 0.05 showing that the formation of SiC crystallites can be manipulated by controlling the SiH_4 to CH_4 flow rate ratio.

4.3.4 AES Analysis

The relative atomic concentrations of silicon, Si, and carbon, C, in the films were obtained from the Auger electron spectroscopy. Figure 4.6 shows the variation of C/Si ratio with $[CH_4]/[SiH_4]$ ratio. The inset shows this plot as a function of $[CH_4]$. Since the C/Si appears to show stronger dependence on $[CH_4]/[SiH_4]$ gas ratio than the $[CH_4]$, the discussion on the results will be focused on the former. The C/Si ratio was less than 1 in all films indicating that the relative concentration of Si was higher than that of C in all of the SiC thin films studied in this work. High $[SiH_4]$ of 1 sccm resulted in higher C/Si ratio at each $[CH_4]/[SiH_4]$ ratio. The increase in $[CH_4]/[SiH_4]$ ratio up to 100 decreased the C/Si ratio in both set of films. However, further increase in $[CH_4]/[SiH_4]$ ratio to 200 which was observed only in the films deposited at $[SiH_4]$ of 0.5 sccm for the range of $[CH_4]$ studied in this work, intensely increased the C/Si ratio. These results show that C incorporation into the film structure was strongly influenced by the partial pressure of CH_4 with respect to the SiH_4 gas. At $[SiH_4]$ of 1 sccm, higher density of H radicals, generated from decomposition of SiH_4 gas by the heated W-filament, go through the secondary gas-phase reactions with the CH_4 molecules and

enhances the density of C-related radicals reaching the growth sites. This explains the higher incorporation of C atoms in the films deposited at the [SiH_4] of 1 sccm at each [CH_4]/[SiH_4] ratio. The increase in [CH_4]/[SiH_4] ratio decreased the partial pressure of SiH_4 gas and consequently limited the number of Si and H radicals generated during SiH_4 decomposition by the hot filament and thus reduced the density of C-related radicals reaching the growth sites. Further increase in [CH_4]/[SiH_4] ratio from 100 to 200 resulted in a significant decrease in Si-related radicals reaching the growth sites. However, the H radicals produced still contributed to the secondary gas-phase reactions with CH_4 molecules and resulting in the production of C-related radicals. Thus an increase in C/Si ratio was seen in this region of [CH_4]/[SiH_4] ratio. The decrease in a-Si phase in the film as shown by the Raman results with increase in [CH_4] for the films prepared at [SiH_4] of 0.5 sccm also confirmed these results.

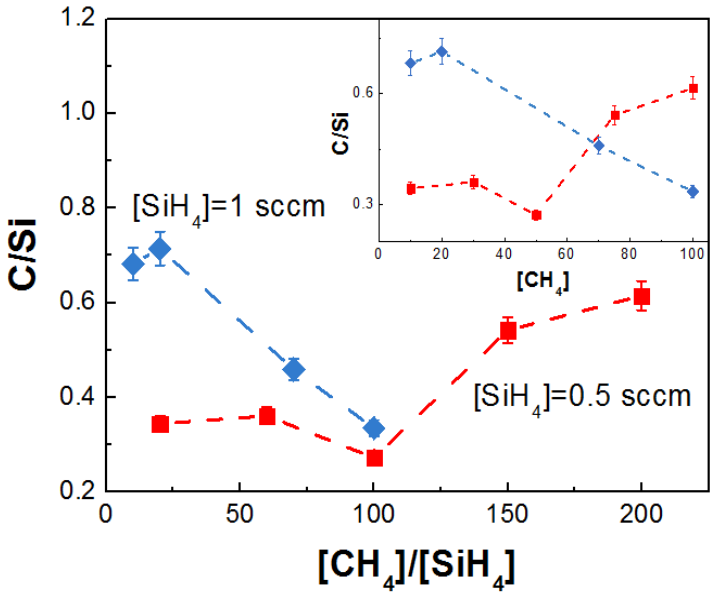

Figure 4.6: Dependence of carbon to silicon content ratio (C/Si) of SiC films on CH_4 to SiH_4 flow rate ratio. The inset displays C/Si ratio as a function of CH_4 flow rate.

The films deposited at the lowest and highest [CH_4]/[SiH_4] ratio with [SiH_4] of 1 and 0.5 sccm respectively showed the most near stoichiometric composition. However, the latter films were inhomogeneous and consisted of a-Si:H, a-C:H and a-SiC:H phases as confirmed by Raman and FTIR results. The film deposited at the lowest [CH_4]/[SiH_4] ratio with [SiH_4] of 0.5 sccm had low C/Si ratio but showed high SiC crystalline volume fraction indicating that the SiC nano-crystallites were embedded within the a-SiC:H, a-Si:H and a-C:H phases. These results were partly different from those reported by Y. Hoshide et al (Y. Hoshide, Komura, Y., Tabata, A., Kitagawa, A., Kondo, A., 2009) in their work on HWCVD SiC films. They showed that increasing [CH_4]/[SiH_4] ratio to 2 resulted in an amorphous film structure, but the configuration of the deposition system used in this work and the different parameters such as pressure and filament temperature used in this work enabled nano-crystalline SiC film structure to be grown at much higher [CH_4]/[SiH_4] ratio.

4.3.5 Deposition Rate

The average deposition rate of the films was calculated by dividing the film thickness by the deposition time. Figure 4.7 shows the dependence of the deposition rate of SiC thin films on the SiH_4 and CH_4 flow rates. The deposition rate of the films deposited at SiH_4 flow rate of 1 sccm is generally higher than those of 0.5 sccm. It is worth noting that the deposition rates of the films deposited in this work, are higher than those reported by other researchers using plasma-enhanced CVD (PECVD) technique (G. Ambrosone, Coscia, U., Ferrero, S., Giorgis, F., Mandracci, P., Pirri, C.F. , 2002; Q. Cheng, Xu, S. , 2007; A. Tabata, Kuno, Y., Suzuoki, Y., Mizutani, T., 1997). Interestingly, these deposition rates are also higher compared to those reported by other research groups under similar conditions using HWCVD (Y. Hoshide, Tabata, A.,

Kitagawa, A., Kondo, A., 2009; Bibhu P. Swain & Dusane, 2006; A. Tabata, et al., 2009).

It is well known that in HWCVD systems, SiH_4 molecules are efficiently decomposed at the heated W-filament above 1800°C resulting in the generation of high densities of Si and H radicals (Zheng & Gallagher, 2006). In contrast, although the decomposition of CH_4 molecules may occur in the same way as SiH_4, they decompose mainly via gas phase reactions (A. Tabata & Komura, 2007). An increase in SiH_4 flow rate leads to the production of more Si and H radicals, which in turn, increases the number of reactions with CH_4 molecules and the generation of more C-related radicals. This enhances the density of the reactive precursors and thus leads to higher film deposition rate for the films deposited at SiH_4 flow rate of 1 sccm.

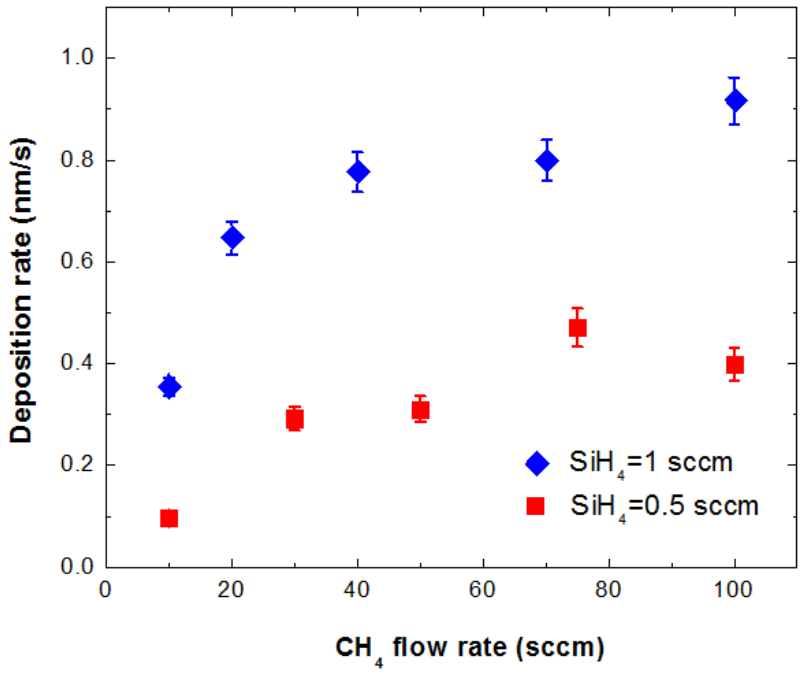

Figure 4.7: Deposition rate of SiC films deposited at different CH_4 flow rate and SiH_4 flow rate of 0.5 and 1 sccm.

The increase in [CH_4] produced similar trends in deposition rates of the films prepared at [SiH_4] of 1 and 0.5 sccm. It increased significantly with initial increase in [CH_4] from 10 to 40 sccm and tended to saturate with further increase in [CH_4]. The films deposited at the lowest [CH_4] showed the highest SiC crystalline volume fraction indicating high coverage of the growth surface with H atoms. The low [CH_4] allowed generation of higher density of Si and H radicals from SiH_4 decomposition at the heated W-filament and enhanced the density of H atoms reaching the growth sites. This also resulted in more effective etching of the amorphous phase by the H atoms leading to lowest deposition rate of the films deposited at the lowest [CH_4]. Increase in [CH_4] from 10 to 40 sccm increased the deposition rate of the films significantly, but further increase in [CH_4] did not produce much change in the deposition rate. It is believed that the increase in deposition rate with the increase in [CH_4] was contributed by a significant reduction in the density of H radicals reaching the growth sites thus reducing H etching effects. Although the density of Si and C related radicals reaching the growth sites was also decreasing, the decrease in H etching effect was more significant as the density of H radicals was dramatically reduced through gas phase reactions with the increase in [CH_4]. This resulted in the increase in the deposition rate. Similar variation in the deposition rate had been reported in the region where the structure of SiC phase transformed from nano-crystalline to amorphous (Komura, 2008), comparable to what had occurred here. However, when [CH_4] increased further beyond 40 sccm, the significant decrease in the density of H, Si and C-related radicals reaching the growth surface resulted in an equilibrium state between the growth and etching rate of the films during the growth process. This contributed to the almost constant deposition rate with the increase in [CH_4] above 40 sccm. These findings show that the [SiH_4] is an important parameter affecting the deposition rate with [CH_4] being influential at lower flow rates.

4.4 Deposition of SiC Films Under Different Gas Pressures with the Silane to Methane Flow-Rate Ratio Fixed

4.4.1 Introduction

It is generally known that the deposition pressure and gas flow rate are the two key parameters controlling the SiC film properties. With regards to gas flow-rate, researchers generally consider the ratio of gases introduced into the reaction chamber as an important deposition parameter and put no emphasis on the effects of the actual gas flow-rates used on the film properties. When considering the effects of deposition pressure on the film properties, most studies focus on the effects on the film properties when the gas ratios are fixed with the gas flow-rates fixed and the deposition pressure changed by controlling the pumping rate evacuating the deposition chamber. In this part of this work, the effects of varying the reactant gas flow-rates which directly influences total gas partial pressure at a fixed SiH_4 to CH_4 flow-rate ratio on the properties of the films produced are investigated. Thorough literature search done to gather information on similar work done by other researchers reveals that there is no reported work available so far covering this aspect. Two sets of samples were deposited for this study. For the first set of samples (labelled as VP samples), the deposition pressure was fixed at the lowest stable pressure recorded in the deposition chamber when the reactant gases were fully admitted. The pumping rate evacuating the reaction chamber was maintained at the highest rate by fully opening the roughing valve. In other words, the films in this set were deposited at the same pressure as the total gas partial pressure. For the second set of films (labelled as FP samples), the deposition pressure was kept constant by regulating the pumping rate using the roughing valve. As a result, for each total gas partial pressure, two films deposited at two different deposition pressures were studied.

The influence of these deposition pressures on the properties of the films at similar total gas partial pressure was also investigated.

The SiH_4 to CH_4 flow rate ratio for all samples was fixed at 1:20 while the total gas partial pressure used during the deposition ranged from 12 to 38 Pa. For the FP samples, the process pressure was maintained at 80 Pa by controlling the pumping rate with the roughing valve of the rotary pump. For the VP samples, the roughing valve was kept fully opened, thus resulting in the reaction chamber pressure increasing with the increase in the gas flow rates. For clarity, the gas flow rates and deposition pressures for the deposition of these samples are listed in Table 4.3.

Table 4.3: Methane and silane gas flow rates, total gas partial pressure and deposition pressures in deposition of SiC films in the FP and VP series.

Sample ID	CH_4 flow rate (sccm) ± 0.1	SiH_4 flow rate (sccm) ± 0.01	$[SiH_4]/[CH_4]$	Total gas partial pressure (Pa) ± 1	Deposition Pressure (Pa) ± 1
FP-1	10.0	0.50	0.05	12.	80
FP-2	20.0	1.00	0.05	20	80
FP-3	30.0	1.50	0.05	27	80
FP-4	40.0	2.00	0.05	33	80
FP-5	50.0	2.50	0.05	38	80
VP-1	10.0	0.50	0.05	12	12
VP-2	20.0	1.00	0.05	20	20
VP-3	30.0	1.50	0.05	27	27
VP-4	40.0	2.00	0.05	33	33
VP-5	50.0	2.50	0.05	38	38

4.4.2 Chemical Bonding Investigation by FTIR Spectroscopy

Figures 4.8 (a) and (b) show the FTIR spectra for both the FP and VP samples, respectively. In the case of the VP samples, VP-1 showed a dominant absorption peak centered at about 800 cm^{-1}. The other VP samples showed small absorption peaks centred at approximately 660, 770, 1000 and 2000 cm^{-1} correspodning to Si-H_n wagging modes, Si-C stretching mode, C-H_n wagging mode or Si-O stretching mode and Si-H_n stretching mode, respectively. The dominant absorption peak produced by VP-1 sample was actually due to the overlapping of these peaks but the significant presence of SiC phase in this film resulted in the Si-C stretching band becoming very significant. The Si-C stretching band appeared to be suppressed when the total gas partial pressure was increased. The increase in total gas partial pressure with this set of samples also resulted in an increased presence of Si-O bonds. Increase in the total gas partial pressure above 12 Pa for this set of samples suppressed the formation of Si-C phases and favoured the formation of a-Si:H and SiO phases in the films.

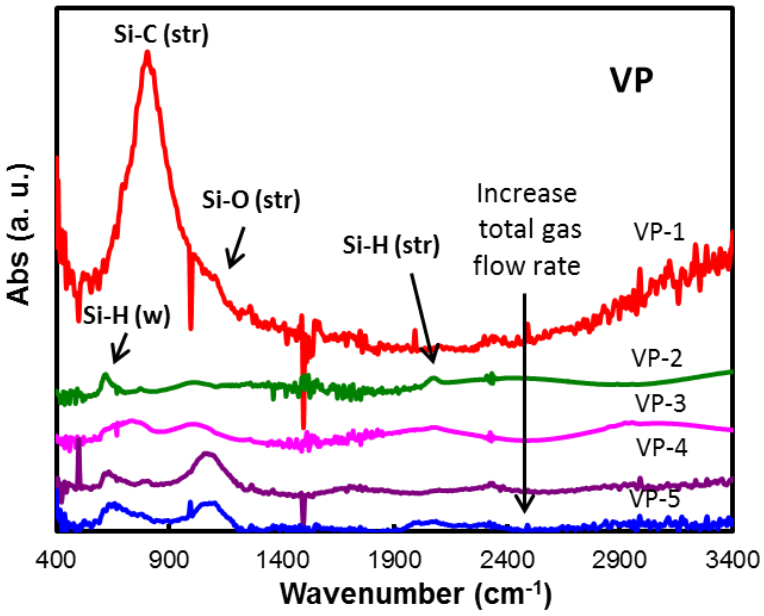

(a)

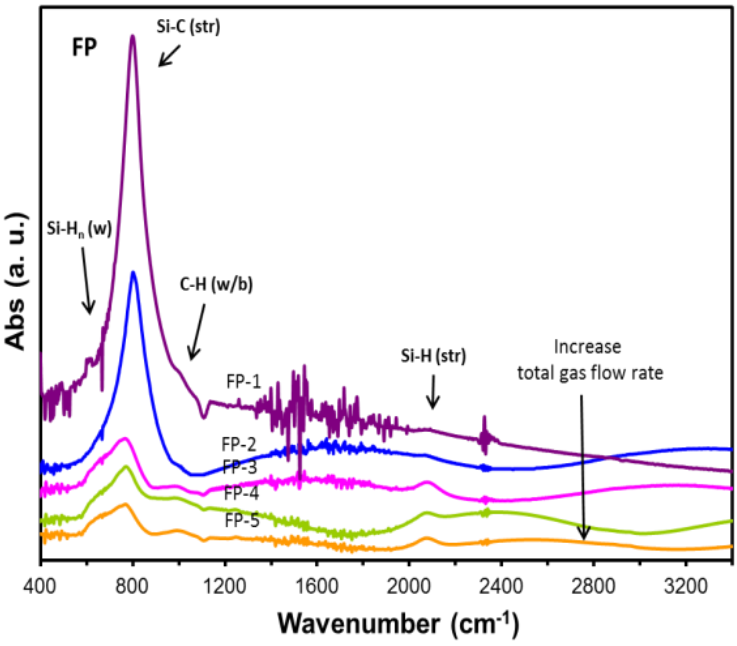

(b)

Figure 4.8: FTIR spectra of films deposited at different gas partial pressures with the SiH_4 to CH_4 flow-rate ratio fixed at 1:20: (a) The deposition pressure was fixed at the total gas partial pressure (VP samples) and (b) The deposition pressure was fixed at 80 Pa (FP samples).

In the case of FP samples, significant presence of SiC phase was observed in all the films as indicated by the presence of a dominant peak centred at 800 cm^{-1} in the FTIR spectra of these films. This absorption peak centred at 800 cm^{-1} was sharp and very intense for the VP-1 and VP-2 films. However, the intensity of this absorption band significantly decreased and appeared to be red-shifted for the other three films in this set. This absorption band also broadened for these films transforming from the Lorentzian to the Gaussian line shape. Additionally, two more absorption bands associated to Si-H and C-H wagging modes at 660 and 1000 cm^{-1}, respectively, appeared in the FTIR spectra of these films. The decrease in the Si-C peak intensity, red-shift in the peak position, transformation in the line shape from Lorentzian to Gaussian of the Si-C peak along with the increase in Si-H and C-H bond densities with increases in the total gas partial pressure for this set of films showed the transformation of the SiC phase in the films from nano-crystalline to amorphous phase and a relative increase in the presence of a-C:H and a-Si:H phases with increase in total gas partial pressure when the pressure in the reaction chamber is fixed at 80 Pa.

Consequently, maintaining the reaction chamber pressure at a higher pressure than the total gas partial pressure allowed the radicals to have longer residence time in chamber resulting in higher probability of secondary gas phase reactions. This favoured the formation of SiC phases in the film structure. However, formation of nano-crystalline SiC phase in the films was shown to be more favourable at low total gas partial pressure especially when the pressure in the reaction chamber during the deposition process was higher than the total gas partial pressure. Increase in the total gas partial pressure by increasing the SiH_4 and CH_4 flow-rates keeping the flow-rate ratio constant only resulted in the suppression in the formation of SiC phases in the film structure. The increased presence of SiH_4 molecules produced more secondary gas phase reactions of the Si based radicals with these molecules favouring the formation of

more Si-Si and Si-H bonds compared to Si-C bonds in the films during surface interactions. This explained the decrease in SiC phases in the films and the relative increase in a-Si:H phases in the films when the total gas partial pressure was increased.

4.4.3 Raman Scattering Spectroscopy

The presence of pure silicon in the crystalline or amorphous phase can be determined from Raman scattering spectra. Figures 4.9 (a) and (b) show the Raman scattering spectra (excitation wavelength: 325 nm) of VP and FP films, respectively. Bulk crystalline silicon produces a very sharp and narrow peak at 520 cm^{-1} that is the characteristic of Si-Si transverse optical (TO) vibrational mode. The amorphous silicon, on the other hand, gives a broad peak centred at around 480 cm^{-1}. A sharp Raman peak around 515 cm^{-1} together with broad band near 480 cm^{-1} was observed for the VP-2, VP-3, and VP-4 films. This indicates the presence of nano-crystalline silicon phases in the film where the silicon nano-crystallites were embedded in the amorphous Si matrix. The downshift of the peak position to lower wavenumber on the other hand gave a clear indication of the reduction in the size of the crystallites. A typical deconvolution of this band into component bands was shown in Figure 4.10. It was found that another component at about 500 cm^{-1} was necessary to fit this Raman band. This band represents the amorphous grain boundary (GB) surrounding the Si nano-crystalline grains. However, the Raman scattering spectrum of the VP-1 sample exhibits a broad peak centred at 480 cm^{-1} which indicates that only amorphous silicon phases were present. The FTIR spectra of all the FP films show broad absorption peak centred at 480 cm^{-1} in the region of 100-600 cm^{-1} indicating an increase in gas phase reaction due to the lower pumping rate resulting in the formation of a-Si:H phases in the film structure instead of nano-crystalline Si phases as in the VP samples.

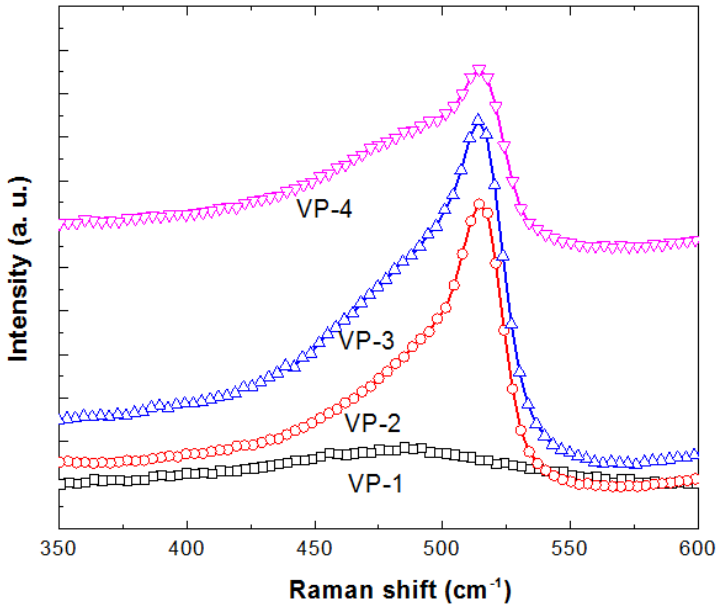

(a)

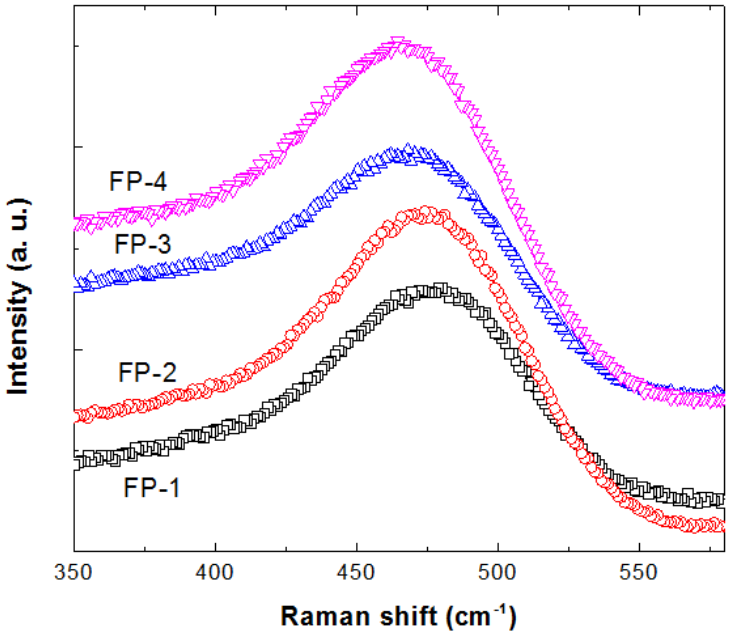

(b)

Figure 4.9: Raman scattering spectra of (a) VP and (b) FP films.

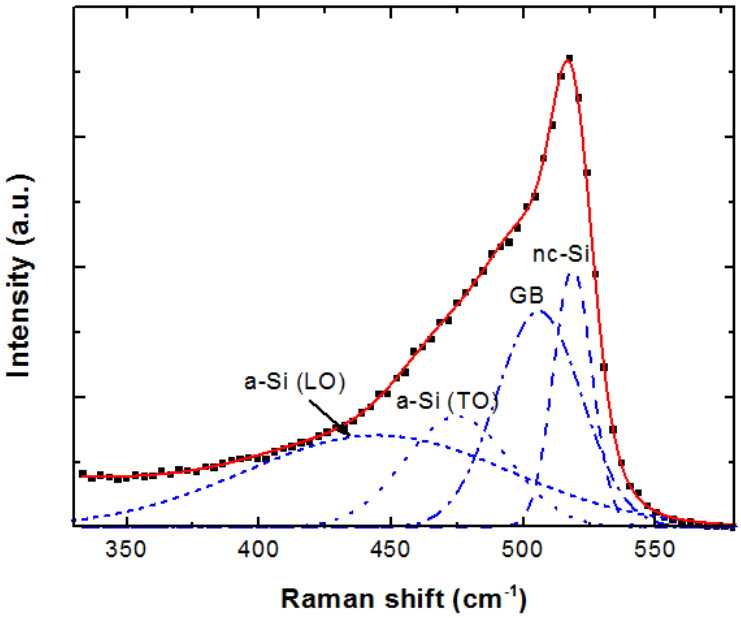

Figure 4.10: Typical deconvolution of Raman spectrum in the ranged of Si-Si vibrations.

In this section, the results show that formation of Si nano-crystals were more favourable when the films were deposited at the pressure maintained at the total gas partial pressure (VP samples) and the crystalline Si peak appears to be most dominant compared to the a-Si peak for the VP-3 sample. The nano-crystalline phase was totally suppressed in the VP-1 sample suggesting that a reduction in gas phase reactions reduces the number of energetic H radicals reaching the growth sites resulting in low H etching effects thus reducing the formation of nano-crystalline Si phases. The decrease in the nano-crystalline phase present in the VP-4 sample indicates that an increase in occurrence of collisions during gas phase reactions resulting in less energetic H radicals reaching the growth sites thus suppressing the formation of nano-crystalline phases. Therefore, an optimum total gas partial pressure was required in the formation of nano-crystalline phases in the films.

4.4.4 XRD Analysis

Figures 4.11 (a) and (b) show the XRD spectra of the SiC films grown at various total gas partial pressures for VP and FP samples respectively. For the VP samples, three XRD peaks located at 2θ of 28.5°,47.2° and 56.7° assigned to the diffraction peaks of crystalline Si with orientations of (111), (220), and (311) planes, respectively were observed. These results confirmed the Raman results that nano-crystalline Si phases were present in these films although the peak at 56.7° is mainly contributed by the c-Si substrate as confirmed from the XRD spectrum of the bare Si substrate. The mean crystallite size estimated from the XRD peak of Si(111) was increased from 3.2 to 5 nm which indicates an increase in crystallinity of the silicon phases in the film with increasing total gas partial pressure. Additionally, the film deposited at lowest total gas partial pressure, VP-1, shows XRD peak at 2θ of 35.6° assigned to the diffraction peak of crystalline cubic silicon carbide with orientation (111) indicating the presence of 3C-SiC phase in the film structure with orientation of (111). All the FP samples showed a dominant single Si peak at 56.7° which was believed to be from the c-Si substrate as the Raman results showed that nano-crystalline phase were not present in these films. The presence of 3C-SiC phases in the FP-1 and FP-2 samples were also shown from the XRD spectra of these samples. The presence of 3C-SiC phases in the films deposited at the lowest total gas partial pressures further confirmed the FTIR results showing that low total gas partial pressure was more favourable in the formation of crystalline SiC phases in the film structure and longer residence time of the radicals through increasing the deposition pressures further enhanced the presence of crystalline SiC phases.

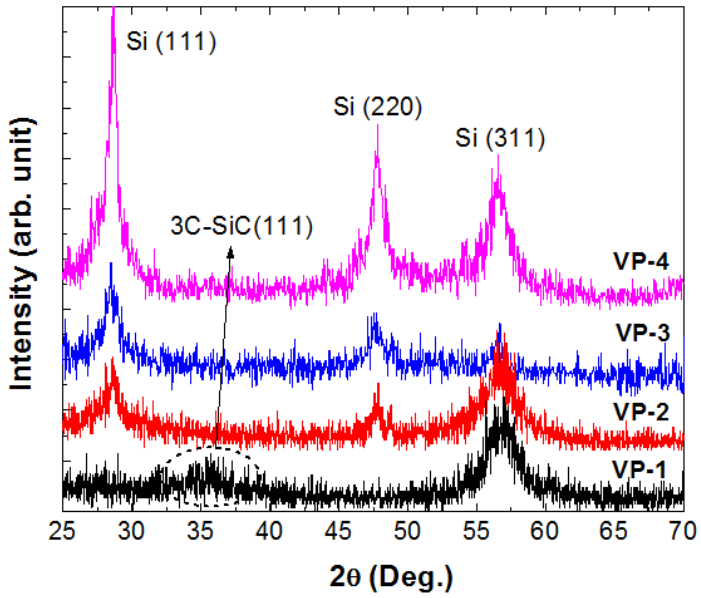

(a)

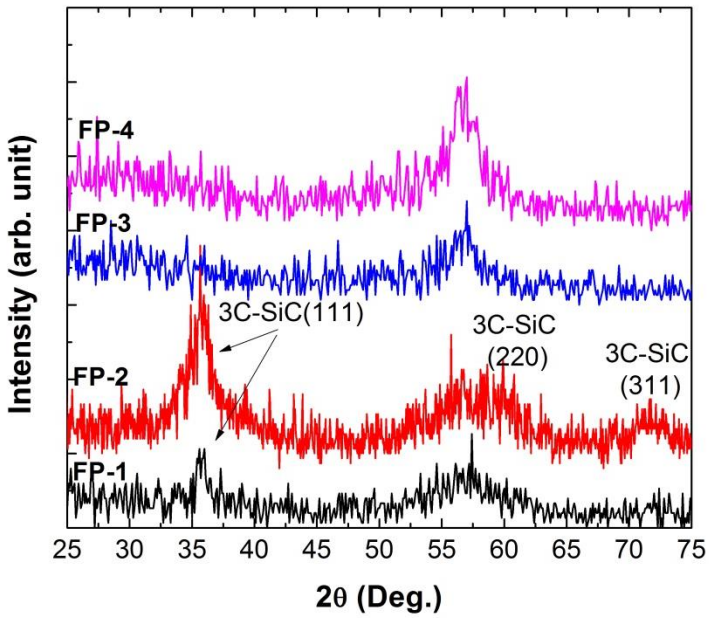

(b)

Figure 4.11: XRD pattern of SiC films prepared under different total gas partial pressures (a) VP (b) FP.

4.4.5 AES Analysis

Figure 4.12 shows the Auger depth profile of the VP and FP samples. The atomic composition of each element and the integrated intensities of Si-H wagging mode and Si-C stretching mode are presented in Table 4.4. Since the composition of Si and C atoms were not constant for the FP samples, two values obtained from the maximum and minimum values of relative atomic concentration were provided. By having a closer look at the Auger depth profiles of the films, the following analyses were made:

1. For both series, the relative atomic concentration of Si was increased while the relative atomic concentration of C was decreased with increasing total gas partial pressure. This was due to the increase in the number of SiH_4 molecules decomposed at the heated filament. Although the number of CH_4 molecules was also increased, these molecules needed a filament temperature of 2400°C to decompose, thus these molecules were mostly not decomposed at the filament temperature of 1900°C used in this work. C-related radicals were mainly produced during gas phase reactions between CH_4 molecules and H radicals in the plasma. The abundant presence of Si-related radicals generated at the filament produced even more Si-related radicals during the secondary gas phase reactions. These explain the higher incorporation of Si atoms in all the samples with increase in total gas partial pressure. The Si-radicals were also more energetic on reaching the growth sites for the VP samples due to the less frequent collisions during gas phase reactions thus inducing the formation of highly nano-crystalline Si phase in the VP samples as indicated by the XRD results.

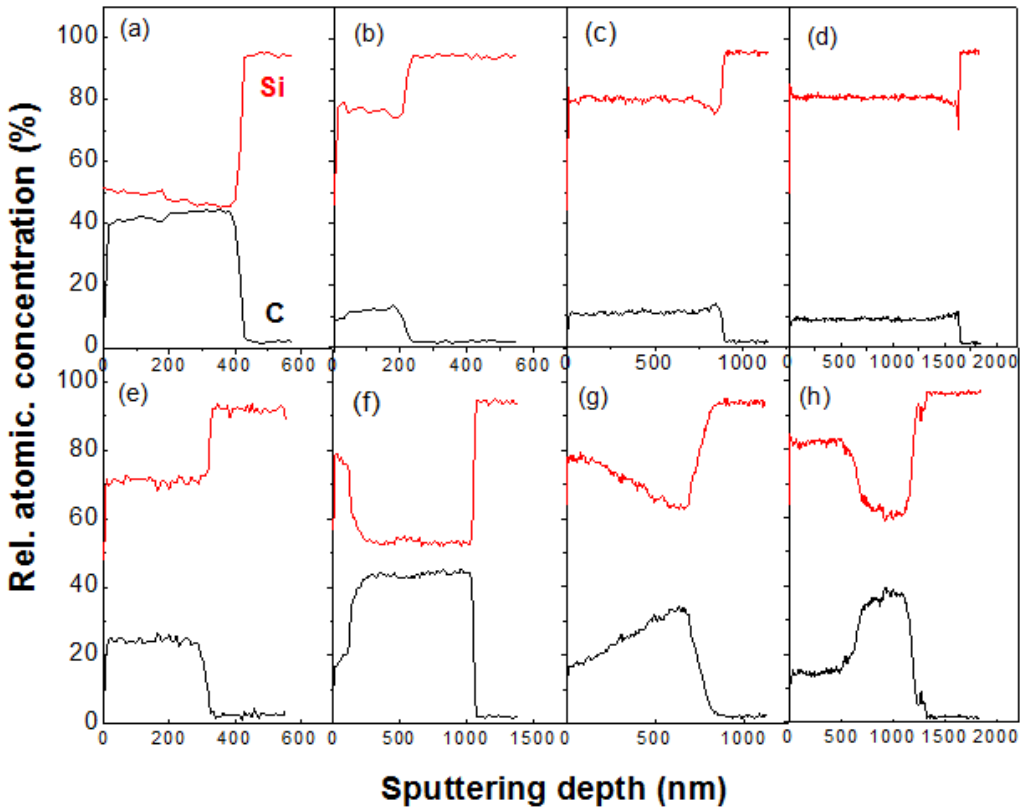

Figure 4.12: Auger depth profile of SiC films. (a): VP-1, (b): VP-2, (c): VP-3, (d) VP-4, (e): FP-1, (f): FP-2, (g): FP-3, (h): FP-4.

2. The carbon incorporation in FP samples was generally higher than that of VP samples. As mentioned before, FP samples were prepared at higher pressure by increasing the dwell time of the molecules in the reactor. This has increased the probability of collisions between molecules and radicals. Therefore, gas phase reactions became more important in contributing to the growth of these films. As a result, more C-related radicals were generated during the growth process of the FP films. This is necessary for formation of 3C-SiC crystallites, which occurs only when the carbon incorporation is high enough (near stoichiometric).

Table 4.4: Relative atomic concentration of constituent elements in SiC films (set VP and FP) as obtained from Auger depth profile, and Si-H and Si-C bond densities in the films calculated from FTIR spectra.

Sample ID	Si% ± 0.02		C% ± 0.02		O% ± 0.01	I_{Si-H} (10^5 cm^{-2})	I_{Si-C} (10^5 cm^{-2})
VP-1	50.16		40.50		7.20	ND	15.66
VP-2	76.44		11.46		9.63	0.677	0.120
VP-3	79.74		11.16		6.97	0.258	0.171
VP-4	80.78		9.20		7.84	0.483	0.133
	Max	min	Max	Min			
FP-1	71.02	-	24.44	-	2.20	ND	68.6
FP-2	80.00	56.42	40.32	15.00	1.25	3.41	36.0
FP-3	78.28	64.22	34.90	16.00	1.21	3.19	6.97
FP-4	82.50	60.50	37.50	13.50	1.21	2.18	5.96

In should be noted that the carbon content of sample FP-1 detected by AES is low. However, the FTIR shows a very high intensity Si-C peak. These results appeared to be contradictory, however it was obvious here that the higher presence of energetic H atoms reaching the growth sites was necessary in the formation of Si-C bonds particularly for the nc-SiC phases. Although a higher presence of C atoms was necessary to form nc-SiC, but higher concentration of H radicals reaching the growth sites was also necessary to form Si-C bonds in the film through H etching effects. The higher concentration of C atoms present in the films deposited at high total gas partial pressure may result in the formation of a-C:H phases instead of SiC phases.

3. Oxygen contamination detected in the VP samples is about 7-10% that is much higher than that of FP samples. It has been reported that the surface Si dangling bonds are easily passivated by oxygen (Goh, 2012; Hartel, 2010). This suggests that during the deposition of VP samples, many Si dangling bonds were present which passivated by oxygen atoms in the chamber. Presence of oxygen in these samples is also detected in the FTIR spectra that show an absorption peak located at 1000-1080 cm^{-1} that attributed to stretching mode of Si-O bonds. In contrast, FP samples show negligible oxygen content which might be due to formation of more hydrogen terminated Si in these samples that is also supported by FTIR results and by comparing the integrated intensity of Si-H bonds between FP and VP samples (see Table 4.4).

4. The atomic concentration of Si and C in each of VP samples is almost constant along its depth but not in FP samples. This is related to different dominant reactions that took place during deposition. In the process of VP samples deposition, the gas phase reaction is not very significant because of low pressure and short dwell time of molecules. Therefore, the most controlling reaction is surface reaction. The radicals produced by dissociation of SiH_4 are very energetic when they reach the substrate surface. This allows them to continuously find the favourable growth site for growth of crystalline Si. On the other hand, in the case of FP samples, by increasing the total gas partial pressure the more Si and H radicals are generated near the heated filament. Then, they undergo gas phase reactions to decompose the CH_4 molecules and produce C-related radicals. Depth profiles of these samples show that carbon incorporation increases toward the interface of film and substrate. This means at initial growth of the film, the C-related radicals react with the surface of substrate and bond to Si atoms. However, the C-related radicals are not so energetic and they form relatively weak Si-C bonds. It is known that the sticking coefficient of C-based radicals is lower than that of Si-based radicals (Q. Cheng & et al., 2008; Q. Cheng, Eugene Tam, Shuyan Xub and

Kostya (Ken) Ostrikov, 2010). By continuing the deposition process, the weak C bonds can be easily broken and replaced by more energetic Si and H radicals, which reduces the carbon content. This effect becomes more visible at higher total gas partial pressures i.e. FP-3 and FP-4.

4.4.6 Deposition Rate

Figure 4.13 shows the variations of the deposition rate of FP and VP films as a function of the total gas partial pressure. The values of deposition rates were estimated from dividing the average film thicknesses measured via surface profiler by the deposition time. Generally, the deposition rate of VP films are higher than that of FP films and the deposition rate increases from 0.1 to 1.2 nm/s with increase in total gas partial pressure for both sets of the films.

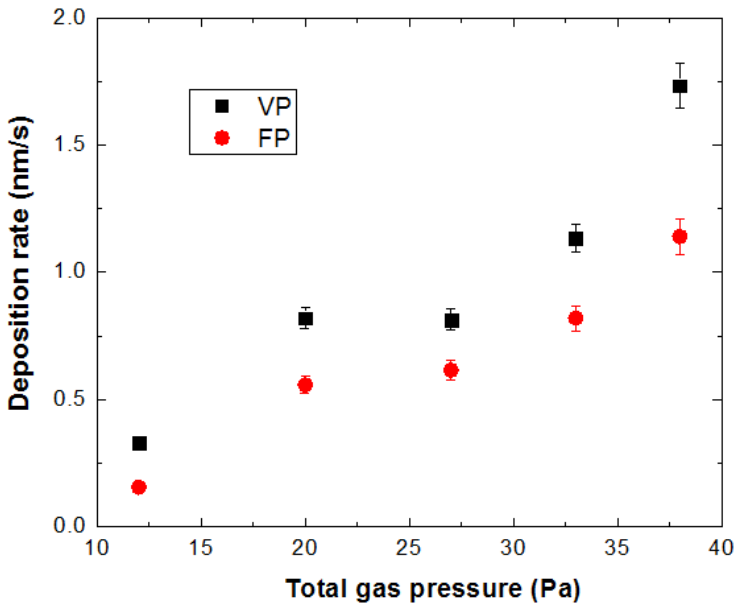

Figure 4.13: Deposition rate of VP and FP films as a function of total gas partial pressure.

The SiC film deposition in HWCVD systems occurs by the decomposition of silane and methane gas molecules with the hot filament and gas phase reactions. SiH_4 molecules are known to be preferentially decomposed on the heated-filament surface with the temperatures above 1800°C via reaction (2.1) (Gallagher, 2001). CH_4 molecules are mainly decomposed through reaction with the H radicals that generated near the filament resulting from silane dissociation (A. Tabata & Komura, 2007). The produced Si and C related radicals contributed to the film growth at the surface of substrate. Therefore, introducing more silane and methane gases, results in more growth radical production, which enhanced the deposition rate.

In contrast, it was found that applying higher deposition pressure at similar gas pressures, in contrast, leads to a slight decrease in deposition rate. This was the result of increment of dwell time of the radicals and molecules due to higher probability of their collisions with other species on the way to reach the growth surface. The other research groups have reported similar variations of deposition rate with gas pressure (Komura, 2008; A. Tabata, Kuroda, M., Mori, M., Mizutani, T., Suzuoki, Y., 2004).

4.5 Summary

In this chapter, it has been established that multi-phased SiC thin films can be deposited using a HWCVD system built in-house for this work from pure silane and methane gas mixture without hydrogen dilution. The formed films were multi-phased in structure consisting of a-Si:H, a-C:H, nc-Si:H, a-SiC and nc-SiC phases. The influence of methane flow rate at fixed silane flow-rates of 0.5 and 1 sccm on the structural, chemical bonding and elemental composition properties of the films has been investigated in the first part of the work. In the second part of the work, the influence of

total gas partial pressure with the silane to methane flow-rate ratio fixed on these properties was studied at deposition pressure equal to the total gas partial pressure and a fixed deposition pressure.

An increase in CH_4 flow rate with the SiH_4 flow-rate fixed at low flow-rate of 0.5 and 1 sccm resulted in a transition from crystalline to amorphous phase of the SiC phases present in the film structure. The films deposited at high CH_4 flow rates are generally amorphous with a mixture of a-Si:H phase embedded within a more dominant a-SiC:H phase, while the films deposited at low CH_4 flow rates have a more ordered Si-C matrix with lower hydrogen concentration. SiC crystallites are formed in the films deposited at low CH_4 flow rate. The formation of SiC crystallites can be manipulated by controlling the CH_4 to SiH_4 flow rate ratio but this is only possible at low SiH_4 flow-rates not larger than 1 sccm.

Maintaining the reaction chamber pressure at a higher pressure than the total gas partial pressure has been shown to favour the formation of SiC phases in the film structure. However, formation of nano-crystalline SiC phase in the films is shown to be more favourable at low total gas partial pressure especially when the pressure in the reaction chamber during the deposition process was higher than the total gas partial pressure. An optimum total gas partial pressure is required for the formation of nano-crystalline phases in the films. Low total gas partial pressure and longer residence time of the radicals through increasing the deposition pressures are shown to be more favourable in the formation of crystalline SiC phases in the film structure.

This work establishes that nano-crystalline SiC film structure can be grown at much higher CH_4 to SiH_4 flow-rate ratio and the deposition rates are higher than those reported by other research groups under similar conditions using HWCVD. The

deposition mechanism of the films studied in this work has been established through studying the properties of the films deposited under the different deposition conditions.

CHAPTER 5

Silicon Carbide Thin Films Prepared by HWCVD Technique from Pure Silane and Methane: Part 2

5.1 Introduction

In Chapter 4, the home- built HWCVD system used for this work was shown to be capable of depositing multi-phased SiC thin films from pure silane and methane gas mixture without hydrogen dilution. The influence of methane flow rate at fixed silane flow-rates and total gas partial pressure at fixed silane to methane flow-rate ratio on the structural, chemical bonding and elemental composition properties of the films was studied. It was established that nano-crystalline SiC film structure can be grown using this system at high growth rate. However, the capability of this system to grow films with higher crystallinity needs to be explored. In this chapter, the influence of deposition pressure and filament to substrate distance on the structural properties of the films is studied for this purpose.

Information on the refractive index and optical band gap of SiC films is very important for applications of the thin films in the optoelectronic devices. The high refractive index of SiC is very useful in reducing solar cell reflectivity. The wide band gap of SiC makes it a good candidate for solar cell window layer material. This property of SiC is also useful for applications in short-wavelength blue and ultraviolet optoelectronics devices. Therefore, it is very useful to explore the possibility of controlling the refractive index and band gap of SiC films through identifying the deposition parameters which can strongly influence these parameters. The correlation between the structural properties and optical properties of SiC films is important information that can be utilized to control the refractive index and energy gap of the films. However, not much work on this aspect of SiC films deposited by HWCVD has been reported in the literature. Another flaw is that the measurement of refractive index and band gap energy is usually done on films deposited on transparent substrates like glass and quartz and characterizations done using FTIR spectroscopy can only be done

on films grown on c-Si substrates. Therefore, valuable information giving accurate correlation between these properties derived from optical transmission spectroscopy measurements cannot be obtained. The objectives of this work presented in this chapter as outlined below are to address these issues. The objectives are

1. To investigate the influence of deposition pressure and substrate to filament distance on the growth rate, structural and optical properties of SiC films prepared by HWCVD.
2. To identify the structural properties, which control the refractive index and band gap energy of the SiC films.
3. To correlate the optical properties to the structural properties of the SiC films.
4. To show that the structural properties of SiC films deposited by the home-built HWCVD from silane and methane discharge are not substrate dependent.

5.1 Deposition Parameters of SiC Thin Films

Two series of SiC films were deposited under five deposition pressures and four filament-to-substrate distances. Details on the deposition parameters used during the deposition of these series of films are tabulated in Tables 5.1 and 5.2. The deposition pressures are adjusted by controlling the opening of the roughing valve between the rotary pump and the deposition chamber. The SiH_4 and CH_4 flow-rates are fixed at 1 and 20 sccm respectively since these were the best flow-rates for these gases for obtaining SiC nano-crystalline phases in the films as shown by the results in Chapter 4. The substrate temperature is fixed at 300°C as done in Chapter 4 since this temperature is the highest temperature that contamination effects from the heating of the Viton O-rings in the system are minimized. The filament temperature of 1900°C is used because

this is the highest filament temperature achieved in this system at the present filament configuration and power supply used. The effects of deposition pressure and filament-to-substrate distance on the growth rate, parameters obtained from the optical transmission spectra of the films, photoluminescence properties and structural properties will be studied in this chapter. The optical energy gap and refractive index of the films will be derived from the parameters obtained from the optical transmission spectra of the films deposited on glass substrates. The structural properties like the chemical bonding properties studied from the FTIR spectra, the morphology and elemental composition of the films will be analysed from the films deposited on c-Si substrates only. On the other hand, XRD and micro Raman scattering analysis will be done on films deposited on both c-Si and glass substrates to show that the structural properties are not substrate dependent. When this can be confirmed, the properties of the films obtained from films deposited on glass substrates only can be studied in respect of all the structural properties of the SiC films irrespective of the substrates used so that a complete correlation between these properties to each other can be analysed.

Table 5.1: The deposition parameters for the preparation of SiC thin films at various deposition pressures.

Deposition Parameter	Value
SiH_4 flow rate	1.0 sccm
CH_4 flow rate	20 sccm
Deposition pressure	20, 40, 80, 140, 250 Pa
Substrate temperature	300 $^{\circ}$C
Filament temperature	1900 $^{\circ}$C
Filament-to-substrate distance	25 mm

Table 5.2: The deposition parameters for the preparation of SiC thin films at different filament-to-substrate distances.

Deposition Parameter	Value
SiH_4 flow rate	1.0 sccm
CH_4 flow rate	20 sccm
Deposition pressure	80 Pa
Substrate temperature	300 $^{\circ}$C
Filament temperature	1900 $^{\circ}$C
Filament-to-substrate distance	10, 15, 20, 25 mm

5.2 Influence of the Deposition Pressure on the Properties of SiC Films

5.2.1 FTIR Spectroscopy Analysis of SiC Films Deposited on c-Si Substrate

The bonding configurations present in the films were studied by FTIR spectroscopy. Figure 5.1 shows the thickness-normalized FTIR absorption spectra of SiC films grown at different deposition pressures.

The main features observed in the spectra of the SiC films studied in Chapter 4 are also observed. The absorption peaks detected from the films include the Si-H wagging mode (w) at 650 cm^{-1}, Si-C stretching mode (str) at 800 cm^{-1}, C-H (W) at 980 cm^{-1}, Si-CH_3 (w) at 1250 cm^{-1}, Si-H (str) at 2080 cm^{-1}, and C-H_n (str) at 2800 - 3000 cm^{-1}.

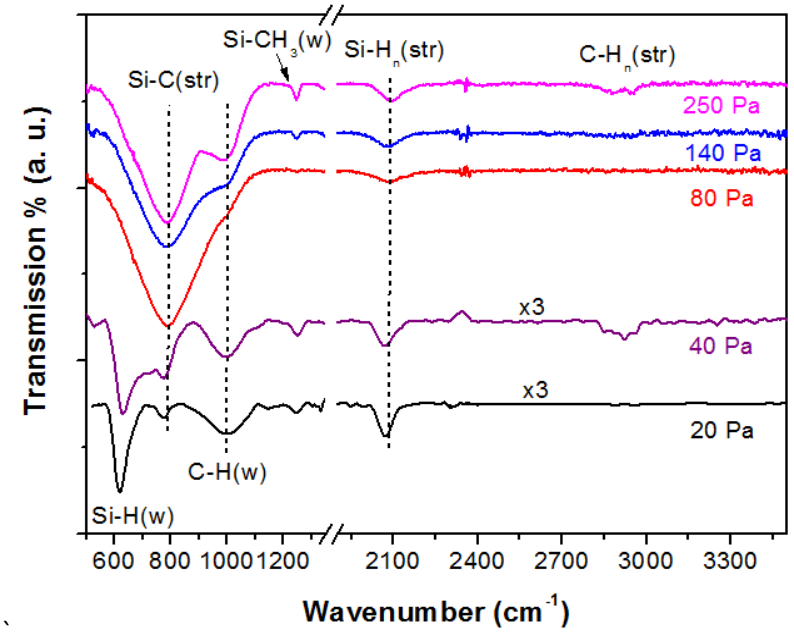

Figure 5.1: FTIR spectra of SiC films deposited at different deposition pressures.

Since Si-C bond is highly IR active, the presence of Si-C bonds in the films is confirmed by the presence of an absorption band at around 800 cm^{-1}. The spectra of the films deposited at pressures below 80 Pa exhibited very weak Si-C peaks but strong presence of Si-H wagging and stretching bands indicating that these films were Si-rich SiC films. However, higher deposition pressures showed an increase in dominance of the Si-C band and the position of the peak was shifted to higher wavenumbers compared to the Si-rich SiC films deposited at lower pressure. Since the absorption band located between 600 and 1100 cm^{-1} is produced by the superposition of Si-H (w), Si-C (str) and C-H (w) vibration modes, it is necessary to deconvolute this band into these component peaks in order to determine the integrated intensity of Si-C bonds. The integrated intensities of deconvoluted Si-C (str), C-H_n (w), and Si-H (str) peaks for the SiC films deposited at various deposition pressures are plotted in Figure 5.2. It was observed that the density of Si-H and Si-C bonds followed similar trends with the increase in deposition pressure, both showing a maximum at 80 Pa. The density of C-H bonds in the films showed a gradual increase with increase in pressure from 20 to 80 Pa followed

by a significant increase to saturation for the films deposited at pressure of 140 Pa. It was also observed that the intensity of C-H and Si-CH_3 peaks progressively increased with the increase in deposition pressure from 80 to 250 Pa. This implies that at high deposition pressure, through secondary gas phase reactions high density of CH_3 radicals were formed and these radicals were more readily incorporated into the film structure through surface interaction process. From these results, it was found that the most stoichiometric SiC film with highest Si-C bond density were deposited under intermediate deposition pressure of 80 Pa. Below this pressure, the a-SiC:H films formed were Si-rich while the films grown at pressures above 80 Pa were shown to be rich in hydrocarbon (C-H_n bonds) content.

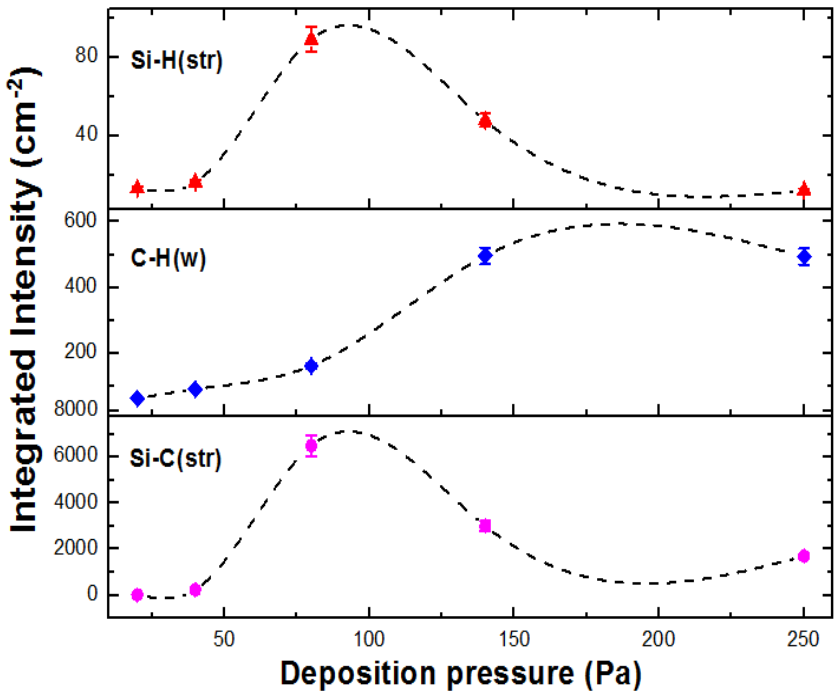

Figure 5.2: From top to bottom: integrated intensities of Si-H(str), C-H(w), and Si-C(str) bonds in SiC films as a function of deposition pressure.

5.2.2 Raman Scattering Spectroscopy Analysis of SiC Films Deposited on c-Si and Glass Substrates

As Si-Si and C-C bonds do not have dipole moment, therefore these bonds cannot be detected in FTIR spectra of the films. Raman scattering spectroscopy is a powerful tool to investigate these phases. Figure 5.3 shows Raman scattering spectra (excitation laser: 325 nm) of SiC films deposited under different deposition pressures. The various observed bands of intrinsic vibrations were appropriately labelled in the figure. The films deposited at 20 and 40 Pa exhibited a sharp peak at 518 cm^{-1} suggesting the presence of Si nano-crystalline phases or clusters in the film structure. At higher pressure, the sharp peak at 518 cm^{-1} disappeared and was replaced by the appearance of a broad peak at 480 cm^{-1}. This peak corresponded to the amorphous Si component suggesting that high deposition pressure was more favourable for the formation of amorphous Si phases in the film structure. The peak corresponds to Si-C bonds (~ 800 cm^{-1}) was weak due to lower cross section of Si-C bond compared to those of Si-Si and C-C bonds (Racine et al., 2001).

The presence of a broad band in the range of 1400-1600 cm^{-1} shown by the spectra of the film prepared at 80 Pa indicates the presence of C-C bonds in the a-C:H clusters within the SiC matrix (Kerdiles et al., 2000). However, this band was not observed in the spectra of the other films.

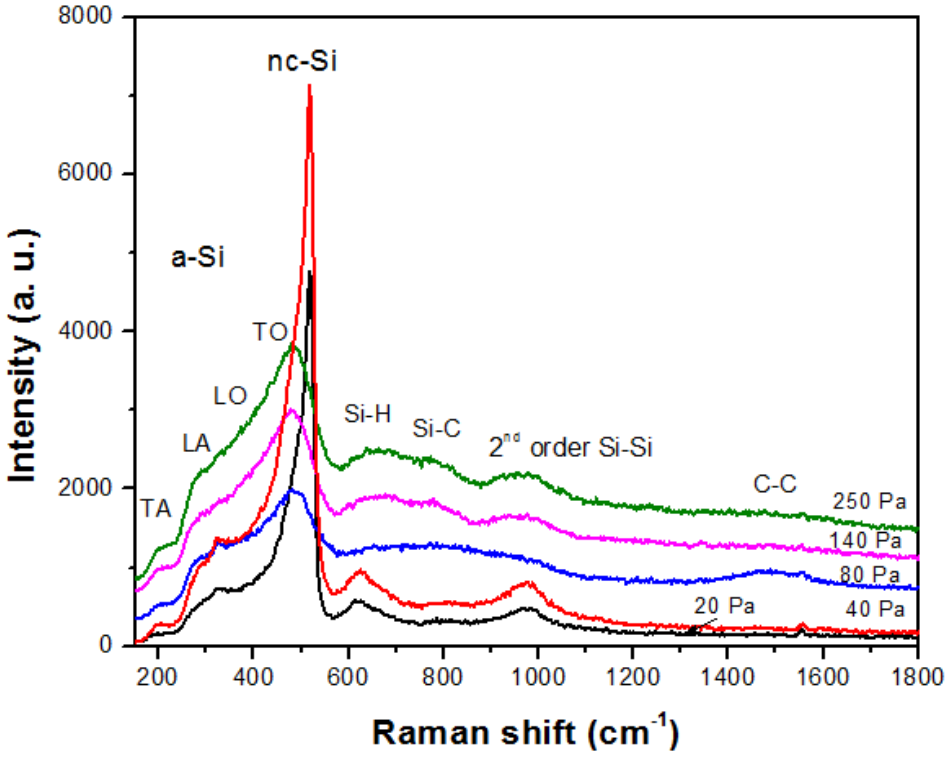

Figure 5.3: Raman scattering spectra with UV excitation (325 nm) from the SiC films deposited on c-Si substrate under different deposition pressures.

Visible Raman scattering (514 nm) was used to further study the a-C:H phases in the film structure and the obtained spectra are shown in Figure 5.4. The films deposited at low pressures below 80 Pa did not show any signature of C-C band, but the films deposited at higher pressures showed a significant appearance of C-C vibrational band. The increase in the slope of the baseline for this band is usually associated with an increase in the hydrogen content in a-C:H films (A. C. Ferrari & Robertson, 2000). Thus, the increase in the gradient of the slope produced by the increase in the deposition pressure as shown in Figure 5.4 showed that the deposition pressure was able to vary the hydrogen content in the a-C:H phases in the film structure. This is consistent with the FTIR analysis where the deposition pressure was shown to increase the hydrocarbon content in the film structure.

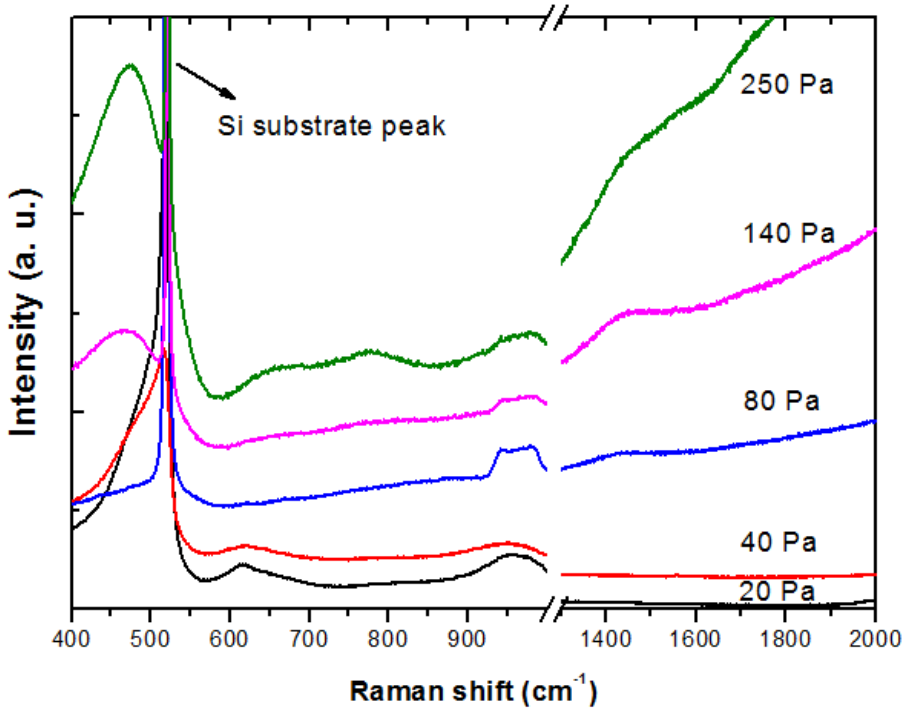

Figure 5.4: Raman scattering spectra with visible excitation (514 nm) from the SiC films deposited on c-Si substrate under various deposition pressures.

The two different observations obtained from the UV and visible Raman scattering of the films deposited at pressure above 80 Pa were contributed by the different penetration depth of UV and visible light into the films. The Raman spectra from the films deposited at lower pressure did not show any difference when these two different excitation wavelengths were used. This indicates that these films had very high absorption coefficient for light in both UV and visible excitation wavelengths. Therefore, the laser beam was mostly absorbed on the upper surface layer of these films and thus, the Raman spectra provide the bonding information of the surface of the film only.

It is generally known that visible Raman spectroscopy is 50-230 times more sensitive to sp^2 sites as visible photons preferentially excite their π states. UV Raman spectroscopy, with its higher photon energy of 3.8 eV, excites both π and σ states and

so is able to probe both sp^2 and sp^3 sites, allowing a direct probe of the sp^3 bonding (A. C. Ferrari & Robertson, 2000). This could be another reason for the different results obtained from the UV and visible excitation Raman spectra for the films deposited at deposition pressures above 80 Pa. This implies that the films prepared at higher pressures above 140 Pa contain C-C bonds predominantly in sp^2 configuration. The higher H content as shown by the increase in the background slope of the Raman spectra in this region for these films may have induced the formation of sp^2-C bonds in the films deposited at higher deposition pressures. However, the film deposited at 80 Pa showed the presence of sp^3 carbon clusters as observed as a broad band in the C-C region in UV Raman spectrum of this film (Figure 5.3).

Figure 5.5 shows the C-C region of visible Raman scattering spectra after baseline subtraction from the films deposited at different pressures. It was observed that the intensity of this band, which is centred at about 1440 cm^{-1} considerably increased with increase in the deposition pressure. Furthermore, the position of this peak was slightly shifted towards higher wavenumbers together with emerging and growing a new component at about 1550 cm^{-1} with the increase in the deposition pressure. This is further indicated an increase in the presence of a-C:H clusters in sp^2 bonding configuration with increase in the deposition pressure.

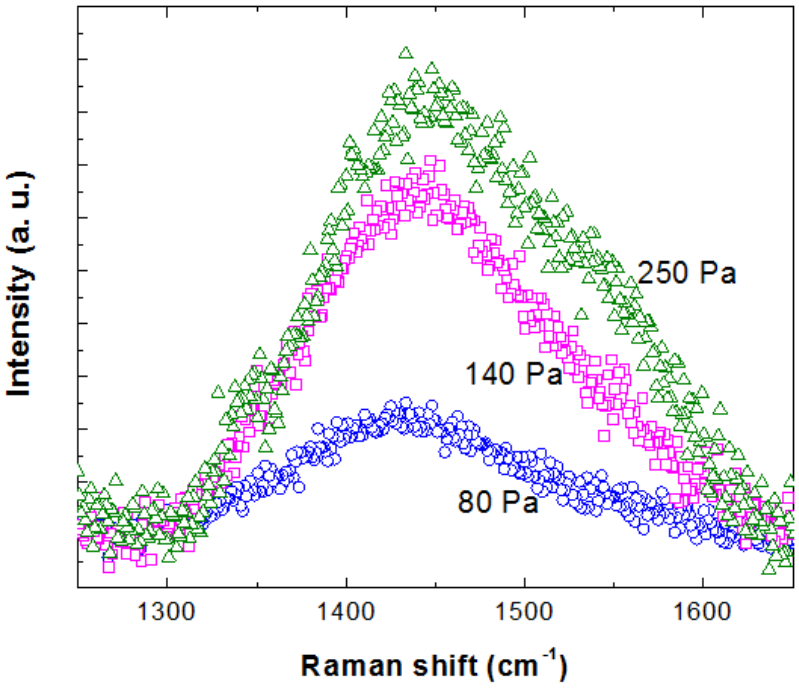

Figure 5.5: Raman scattering spectra with visible excitation wavelength from the SiC films deposited under different deposition pressures in the C-C region.

The results obtained in this part are shown to be partly different from similar works reported by Y. Komura *et al* (Komura, 2008) and T. Wu *et al* (Wu, 2011). In both cases, they reported that the structure of deposited films changed from nc-Si embedded in a-SiC to nc-3C-SiC structure with increasing deposition pressure. However, this work showed that the structure has changed from nc-Si embedded in Si rich a-SiC:H to stoichiometric homogeneous a-SiC to hydrocarbon rich a-SiC:H with increasing deposition pressure. A possible reason for this difference can be contributed by the high hydrogen dilution of the reactive gases in the works reported by Komura *et al* (Komura, 2008) and Wu *et al* (Wu, 2011). This showed that the significant presence of reactive H atoms at the growth surface was very important for the formation of crystalline phases in the a-SiC:H films. Without hydrogen dilution, an increase in deposition pressure reduces the number of reactive hydrogen atoms at the growth surface, resulting in the formation of only amorphous phases in the films.

Raman scattering spectra (excitation wavelength: 514 nm) of the films deposited under various deposition pressures on glass substrate are shown in Figure 5.6. By comparing these spectra with the Raman spectra of those deposited on c-Si, it is seen that the characteristics of the films deposited on c-Si and glass substrates are quite similar. A sharp peak near 520 cm^{-1} together with a broad band centred at ~480 cm^{-1} corresponding to nc-Si grains in the amorphous Si matrix were observed for the films deposited at 20 and 40 Pa. However, only a-Si component was significant for the films deposited at pressures of 80 Pa and above. In the region of signature for C-C bond, a broad band centred at about 1450 cm^{-1} was detected for the films deposited at 80 Pa and above. The intensity of this band increases with increasing deposition pressure. These observations were consistent with what was observed for the films deposited on c-Si substrate. This indicates that the bonding properties present in the film structure were not substrate dependent. This makes it possible to relate the bonding properties to the optical properties of the films as the optical properties are usually obtained from the films deposited on transparent substrates like glass or quartz and bonding properties obtained from FTIR spectra are obtained from films deposited on c-Si substrates.

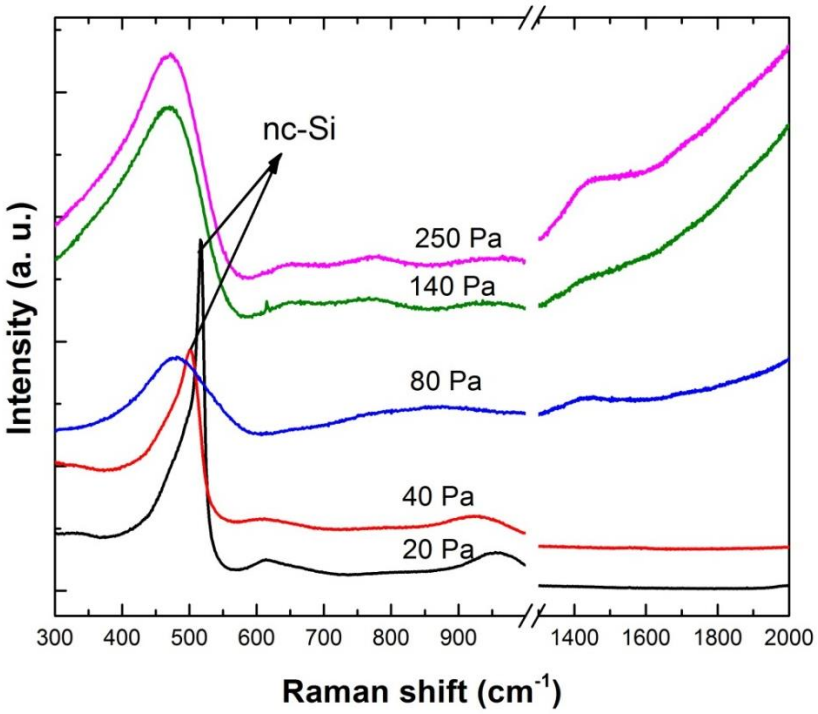

Figure 5.6. Visible Raman scattering spectra of the films deposited under different deposition pressures on glass substrate.

5.2.3 XRD Analysis of SiC Films Deposited on c-Si and Glass Substrates

Figures 5.7 (a) and (b) show XRD patterns of the SiC films deposited under different deposition pressures on c-Si and glass substrates, respectively. The films deposited at 20 and 40 Pa showed crystalline Si peaks located at 28°, 47.5°, and 56.5° corresponding to reflection planes of (111), (220), and (311), respectively. These indicate that nano-crystalline phases were present in these films. However, the films deposited at 80 Pa and above did not show any diffraction peak. Therefore, these films were completely amorphous in structure. It should be noticed that the XRD patterns obtained from the films deposited on glass and c-Si are similar. Nevertheless, in the case of the film deposited at 20 Pa on c-Si substrate, the XRD peak related to Si (311) reflection plane is higher in intensity probably due to contribution from the c-Si

substrate. As indicated in Chapter 4, the c-Si substrate also exhibits an XRD peak at this position.

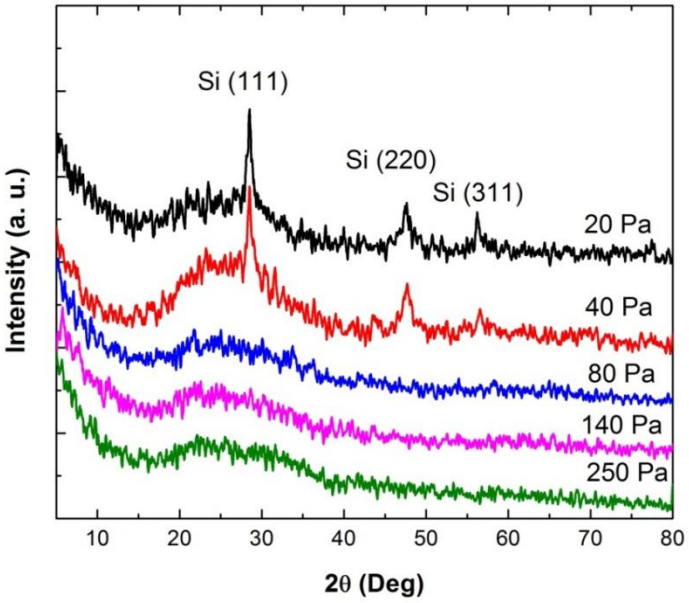

(a)

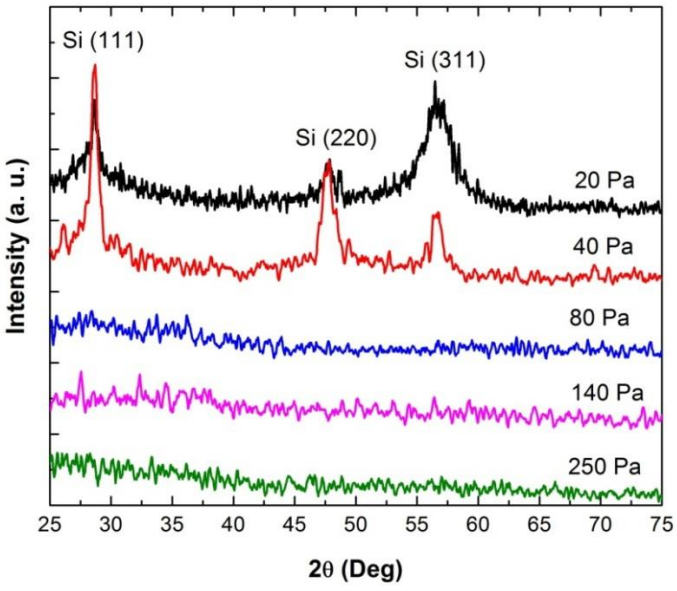

(b)

Figure 5.7: XRD patterns of the films deposited under different deposition pressures on (a) glass and (b) c-Si.

5.2.4 Elemental Composition

Figure 5.8 shows the average relative atomic concentration of silicon, carbon, and oxygen in the films prepared at different deposition pressures. The atomic concentration of carbon in the films prepared at 20 and 40 Pa was about 10%. However, it was increased from ~10% to ~30% when the deposition pressure was increased from 40 to 80 Pa and remained almost constant with further increase in deposition pressure. This indicates that the films deposited under deposition pressures below 80 Pa were Si-rich as demonstrated by the FTIR spectra of these films. These films, however, showed slightly higher oxygen content (~10-12 %), which was almost comparable to carbon content. The oxygen concentration in the films however dropped with increasing deposition pressure, which could be due to the significant increase in C incorporation into the film structure.

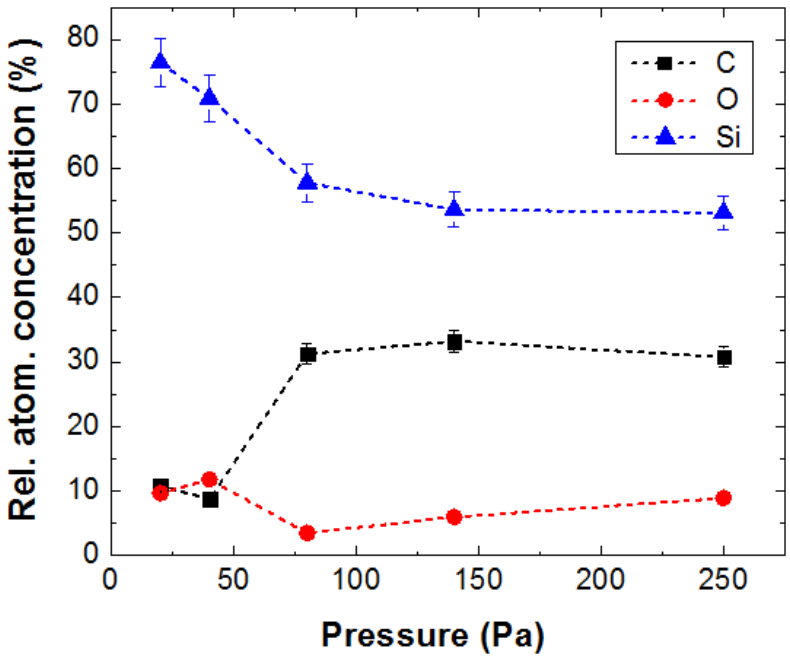

Figure 5.8: The variation of relative atomic concentration of silicon, carbon and oxygen in the films as a function of deposition pressure obtained from AES analysis.

The uniformity of elemental composition within the SiC films deposited under different deposition pressure was investigated by using Auger depth profile as shown in Figure 5.9. It was seen that the carbon incorporation was almost constant throughout the depth of the films deposited at 20 to 80 Pa. However, when deposited at 140 Pa the film demonstrates the presence of two different layers; one with constant carbon content of ~40% and another one with decreasing amount of carbon, which changed from 40% to 20% from the substrate/film interface to the surface of the film. These two layers were shown to have almost similar thicknesses. For the film grown at high pressure of 250 Pa, the first layer with the higher carbon content of ~ 40% was very thin, compared to the layer with decreasing carbon content.

The number of molecules in the chamber increases with increasing deposition pressure. This increases the number of gas phase reactions and produces many radicals. Meanwhile, the rate of impingement of these species on the growth surface increases, which leads to higher etching rate of relatively weak bonds on the surface. Consequently, at higher pressure, although probability of carbon incorporation in the film is higher, they are easily etched away by the abundant radicals produced in the gas phase. Therefore, it was found that 80 Pa is the optimum deposition pressure favourable for the growth of film with stable carbon incorporation during the deposition process.

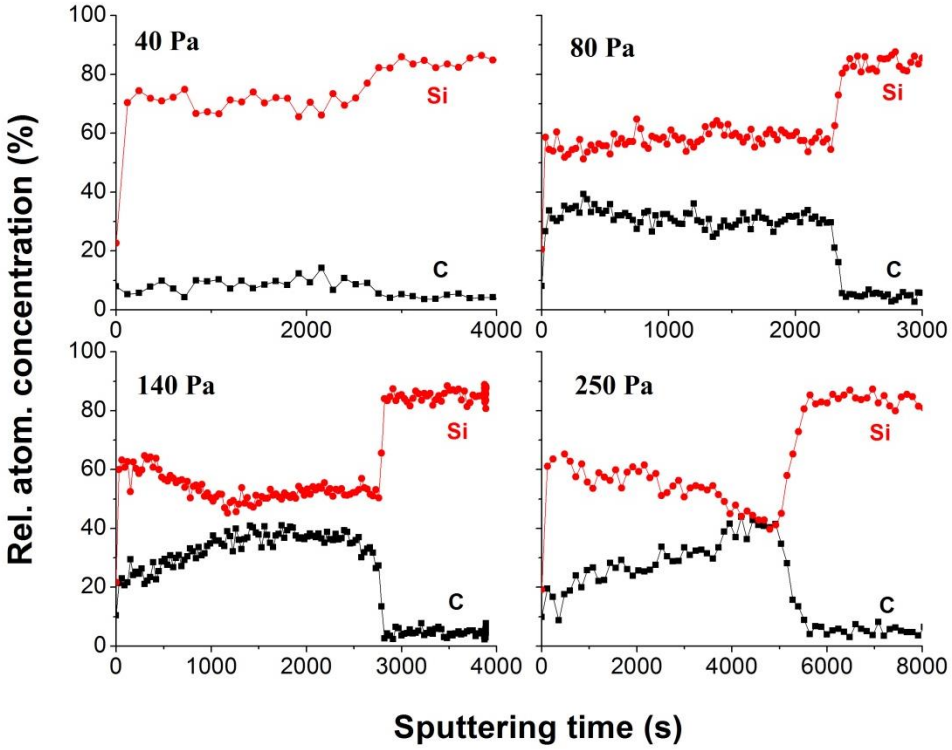

Figure 5.9: Auger depth profile of SiC films deposited under different deposition pressures.

5.2.5 Morphology

The variation in morphology of SiC films deposited at various deposition pressures was studied from surface FESEM images as shown in Figure 5.10. One Si-rich SiC film (40 Pa) was selected as an example for comparison of the morphology with the other a-SiC:H films. The FESEM image of the film containing nc-Si showed a smooth surface morphology with very fine grains, which is characteristic of nano-crystalline films. Other researchers have reported similar morphology from SiC (I. Ferreira, Cabrita, A., Fortunato, E., Martins, R., 2002; Wu, 2011). However, other amorphous SiC films showed formation of larger grains and their size was increased with increasing the deposition pressure. Formation of larger grains at higher pressure can be related to formation of a-C:H and a-Si:H clusters in the films.

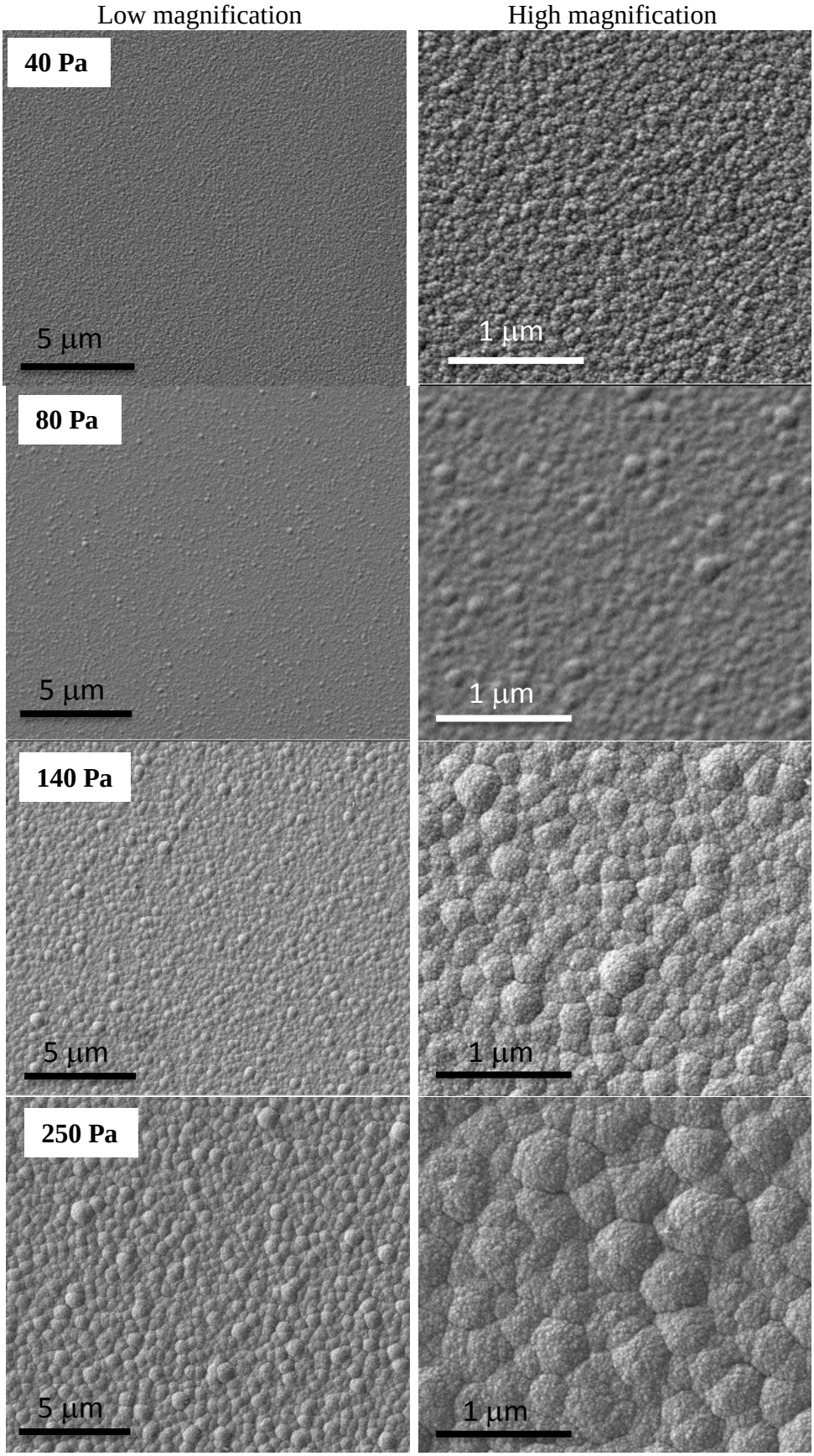

Figure 5.10: FESEM images of the surface of the films deposited at different deposition pressures.

5.2.6 Optical Properties

5.2.6.1 UV-Vis-NIR Spectroscopy

The optical properties of the SiC films deposited under different deposition pressure were studied by UV-Vis-NIR transmission spectra as shown in Figure 5.11 (a). It can be seen that the absorption edge was significantly blue-shifted with increasing deposition pressure from 20 to 80 Pa. However, further increase in the deposition pressure resulted in a red-shift in the absorption edge. The absorption coefficients of the films deposited under different pressures were calculated using equation (3.16) and shown in Figure 5.11 (b). The films prepared at low pressures below 80 Pa (Si-rich SiC films) showed high absorption in the visible region, while the SiC films deposited at higher pressure above 80 Pa were transparent in the wide range of the visible region. It was noticed that there was a turning point for the film deposited at 80 Pa where the transmission in the visible region was the highest.

The energy band gap of the films was calculated using Tauc's plot (Tauc & Abeles, 1972). Si-rich films prepared at 20 and 40 Pa had a band gap of 1.8 and 1.9 eV, respectively. However, an increase in the deposition pressure from 40 to 80 Pa, has remarkably increased the energy band gap up to 2.47 eV. This sharp increase in band gap was shown to be parallel to the sudden increase in Si-C bonds in the film as shown earlier (Figure 5. 2). The increase in the H content in the films deposited at higher pressures may also contribute towards the increase in the energy gap in the films. Further increase in the deposition pressure from 80 to 250 Pa, however, resulted in a slight decrease in energy band gap of the film to 2.2 eV. This may be due to significant increase in sp^2-C bonds in the film structure.

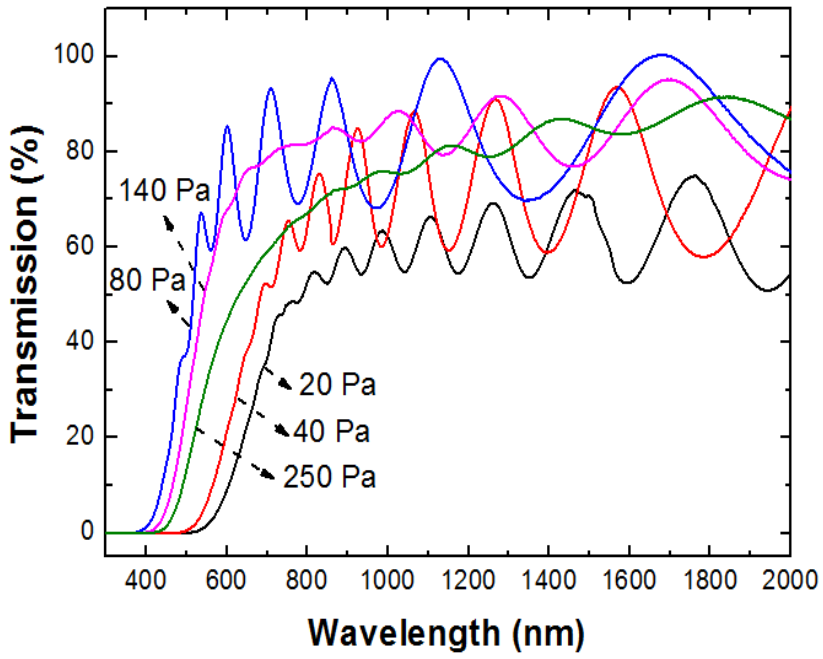

(a)

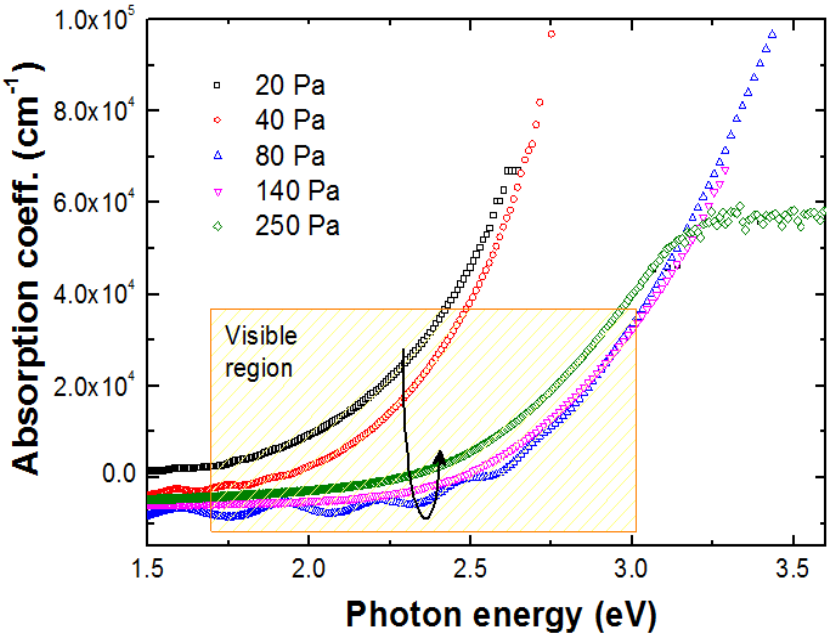

(b)

Figure 5.11: (a) UV-Vis-NIR transmission spectra and (b) Absorption coefficient of the films deposited at different deposition pressures.

The slope of Tauc plot (*B*) represents the disorder parameter where higher value of *B* means lower structural disorder. The Mott formula below shows the different parameters involved in determining the value of *B* (Mott, 1979):

$$B \propto \frac{N(E)^2}{n\Delta E} \tag{5.1}$$

where *n* is the refractive index, *N(E)* is the density of states at the band edge and ΔE is the width of the mobility edge. *B*-parameter of SiC films deposited at various deposition pressures was calculated and shown in Figure 5.12. The *B* value increases to a maximum for the film deposited at 80 Pa and decreases to a minimum at the highest deposition pressure of 250 Pa. The results showed that the Si-rich films deposited at low deposition pressures exhibits relatively high structural disorder which can be due to the existence of nc-Si grains in a-SiC matrix and the presence of compositional disorder due to homonuclear Si-Si bonds in the film structure. However, the film prepared at 80 Pa with the widest optical band gap showed a high *B* value (~ 600 $cm^{-1/2}eV^{-1/2}$), which is larger than the values reported by other researchers for a-SiC:H films (Chew, 2002). High values of *B* have been reported for Si-rich a-SiC:H films and have been attributed to a Si dominated microstructure with mostly sp^3 bonding environment (Chew, 2002). The high *B*-value for film deposited at 80 Pa may indicate that this film has a homogeneous amorphous SiC network dominated by Si microstructures within a dominant sp^3 bonding environment. At pressures above 80 Pa, the *B*-parameter dramatically dropped, indicating that the films were highly disordered. These films as shown by the Raman results consisted of sp^2 carbon phases combined with clusters of a-Si phases clusters. Meanwhile, the Auger depth profile also showed that the elemental composition within the film from the film/substrate interface to the surface was not uniform and could be separated into regions of high and low carbon content.

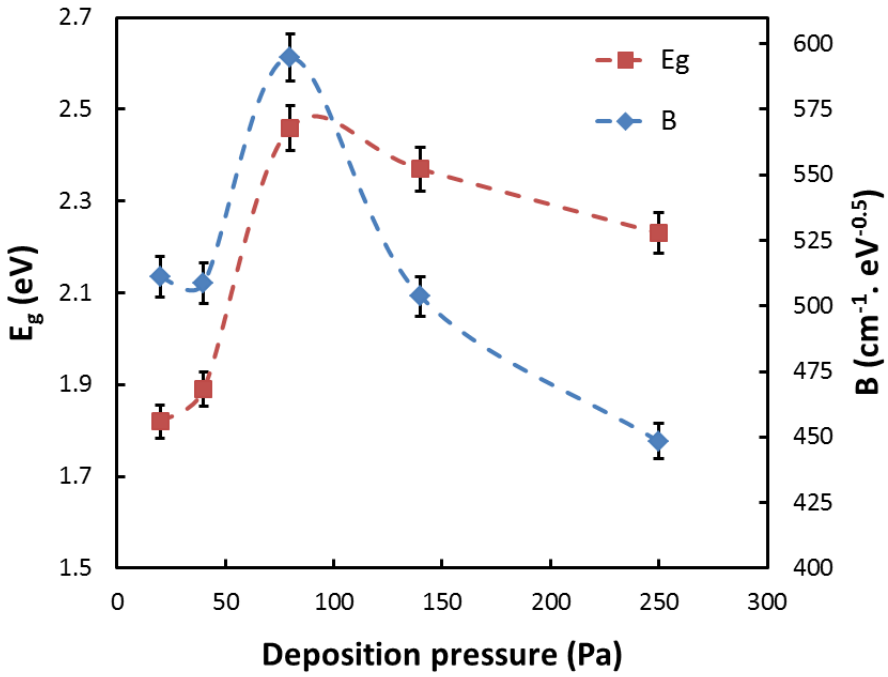

Figure 5.12: Dependence of band gap and disorder parameter (*B*) of SiC films on the deposition pressures.

These results strongly indicate that the key parameter that controlled the energy band gap is the density of Si-C bonds. To further confirm this, the variation of E_g with Si-C bond density is shown in Figure 5.13. This plot shows that E_g had a reverse exponential dependence on Si-C bond density where E_g is shown to increase to a saturation value with increasing Si-C bond density.

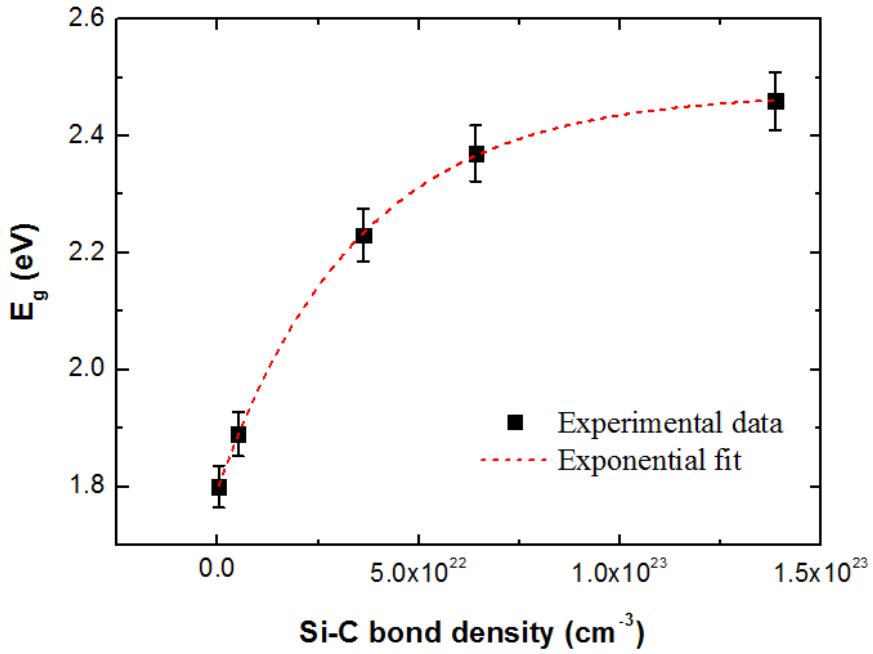

Figure 5.13: Dependence of band gap of the SiC films prepared under different deposition pressures on the Si-C bond density of the films.

Figure 5.14 shows the variation of refractive index of the films deposited under different deposition pressures. The refractive indices of Si-rich a-SiC films (the first two points) were higher (~2.6-2.7) and did not show much variation with the deposition pressure. However, the refractive index of the films is dramatically dropped with further increase in deposition pressure and reached the value of 1.7 at the deposition pressure of 250 Pa.

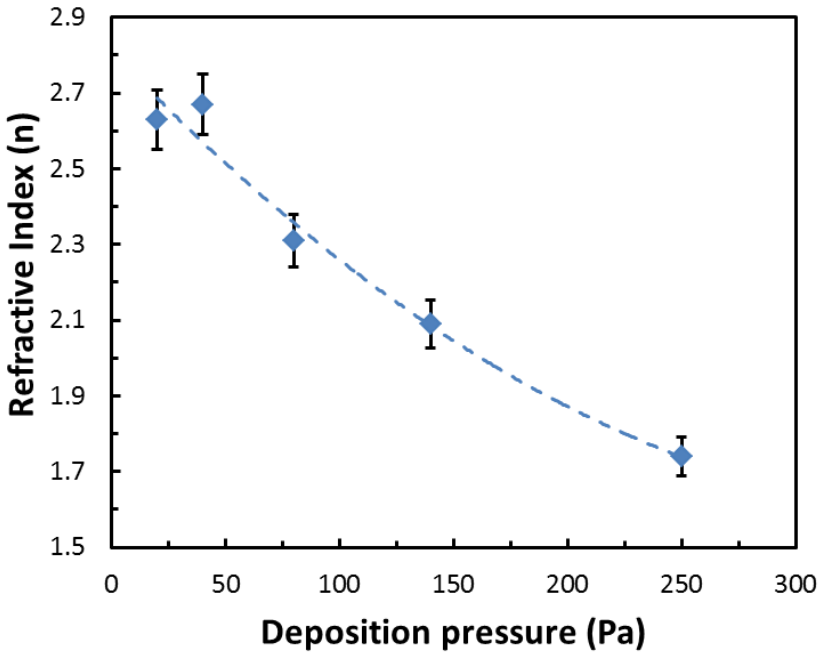

Figure 5.14: Refractive index of SiC films prepared under different deposition pressures.

The abrupt reduction in refractive index and increase in E_g, with increasing deposition pressure from 40 to 80 Pa, could be attributed to the compositional and structural changes of the films from Si-rich a-SiC films to near stoichiometric a-SiC. Incorporation of carbon atoms was high in the films deposited at deposition pressure of 80 Pa and above. However, a slight decrease in E_g was observed (~0.2 eV) with increasing pressure from 80 to 250 Pa. This decrease probably was caused by the increased presence of a-C: H in the form of sp^2 clusters at this pressure as shown in the FTIR and Raman scattering spectra. The presence of these sp^2 carbon clusters, also led to inhomogeneity in the film structure, which was reflected by decrease of the B value in these films

5.2.6.2 Photoluminescence Spectroscopy

Figure 5.15 shows room temperature photoluminescence (PL) spectra of SiC films deposited under various deposition pressures. The films prepared at 20 and 40 Pa exhibited a broad band centred at about 2.1 eV, which is greater than their optical band gap. From structural and compositional characterizations, it was revealed that these films are Si-rich with the presence of nc-Si grains in the amorphous matrix. It has been reported that Si-rich a-SiC films did not produce PL emission at room temperature due to quenching effect (Chew, 2002). Chew et al. have explained that at room temperature, the rate of nonradiative recombination through paramagnetic Si dangling bond states in Si-rich a-SiC films is 10 orders of magnitude higher than that of the band tail radiative recombination. However, they observed PL emission from only C-rich a-SiC films at room temperature. Similarly, in another study of PL properties of a-SiC films, it has been shown that the films with carbon content below 0.55 did not exhibit any PL emission at room temperature (Q. Cheng & et al., 2008). However, higher carbon content resulted in intense PL emission. Nevertheless, broad band room temperature PL has been reported recently from the a-SiC films embedded with nc-Si (G. Ambrosone, Basa, Coscia, & Passacantando, 2012). Reduction in the size of Si nano-crystallites led to enhancement of PL emission and a blue-shift of its position. Therefore, PL band observed in this work for the Si-rich films can be attributed to the existence of nano-crystalline Si phase in the material.

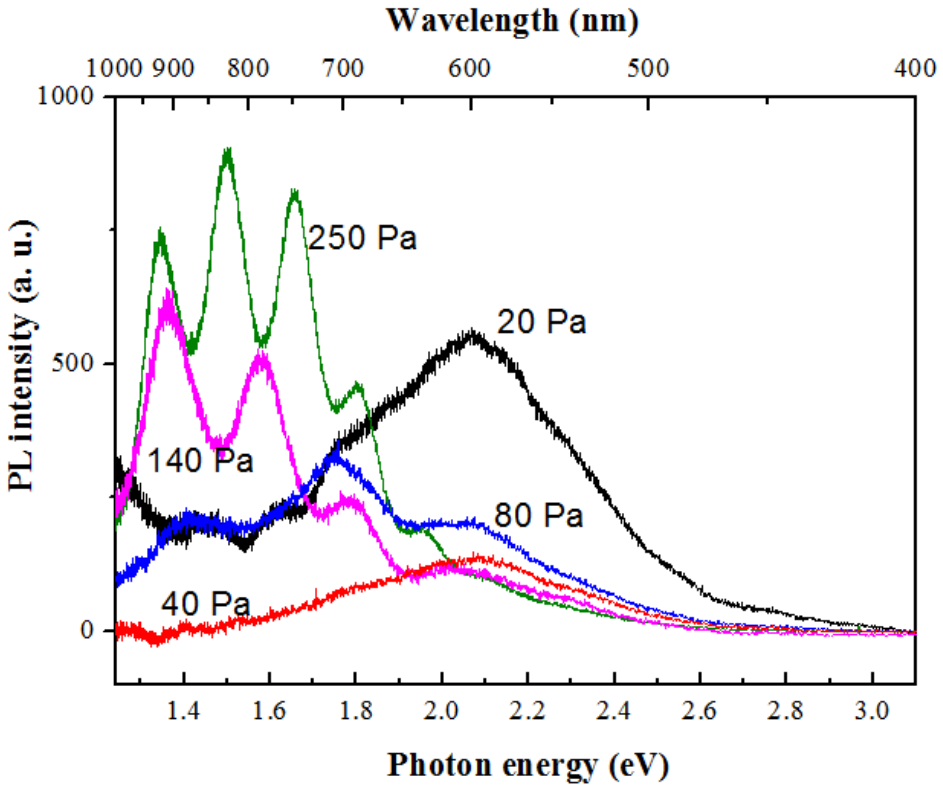

Figure 5.15: Room temperature PL spectra of SiC films deposited under different deposition pressures.

The films deposited under higher deposition pressures exhibited a PL band, with centres shifted to lower energies. Incorporation of carbon in these films in the form of sp^2 clusters in a-SiC matrix, as shown in Raman analysis, resulted in increment of the band tail states into the energy gap. These states acted as centres for radiative recombination producing the PL emission at lower energy from these films. The interference peaks observed in the PL spectra of these films were the result of optical interference of reflected light at the surface of the films and the top surface of the substrate.

5.2.7 Deposition Rate

Figure 5.16 shows the deposition rate of the SiC films versus deposition pressure. A sharp decrease in deposition rate from 0.7 to 0.45 nm/s was observed with the increase in deposition pressure from 20 to 80 Pa. Further increase in pressure led to a sharp increase in the deposition rate from 0.45 to 0.82 nm/s.

At low pressures (< 80 Pa), the probability of dissociating SiH_4 molecules on the hot-wire (HW) as Si and H atoms was high and the concentration of molecules in the chamber was low. This allowed Si and H radicals to have a mean free path comparable to the distance between HW and the substrate. Therefore, they were able to reach the substrate surface directly or after only a few collisions with other molecules. As a result, the number of gas phase reactions that usually lead to creation of C-related radicals was limited and thus, Si-rich films were deposited under this condition. However, bombardment of the growth surface by the H radicals promoted the crystallinity of Si phase in the material as verified from XRD and Raman analysis. By increasing the deposition pressure, the mean free path of Si molecules were reduced and they collided with many more molecules or radicals before reaching the growth sites. This enabled CH_4 molecules to decompose through secondary gas phase reactions while decreasing the deposition rate.

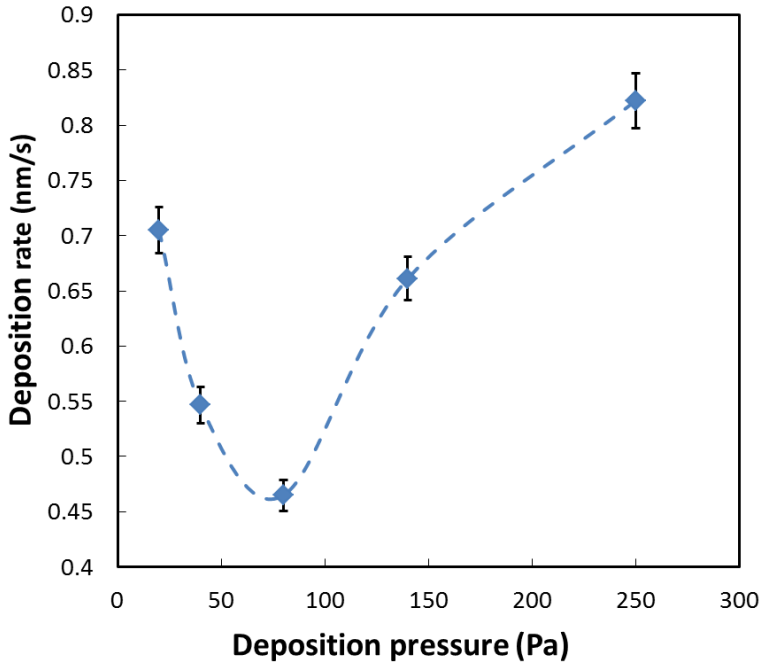

Figure 5.16: Deposition rate of SiC films as a function of deposition pressure.

However, further increase in the deposition pressure (above 80 Pa), resulted in a significant increase in the deposition rate. This increase in deposition rate is attributed to higher incorporation of silicon and carbon into the film, which was made possible by the higher probability of gas phase reactions. Nevertheless, they formed a considerable amount of a-C:H and a-Si:H clusters in a-SiC matrix as confirmed from the Raman and FTIR analysis. This is responsible for degradation of the optical properties of the material such as narrowing the energy band gap.

Figure 5.17 demonstrates a simplified diagram of the deposition mechanism in HWCVD chamber under low and high deposition pressure for comparison. It is seen that at low deposition pressures, the presence of molecules and radicals at low density results in few gas phase reactions. Therefore, Si radicals generated at the HW can easily reach the substrate surface and form a Si-rich film. However, as shown in the figure, under high deposition pressures, many collisions occur in the gas phase that lead to

production of various species such as SiH_n (n=1,2,3), $SiCH_3$, CH_n (n=1,2,3). As a result, more carbon atoms can be incorporated into the film structure.

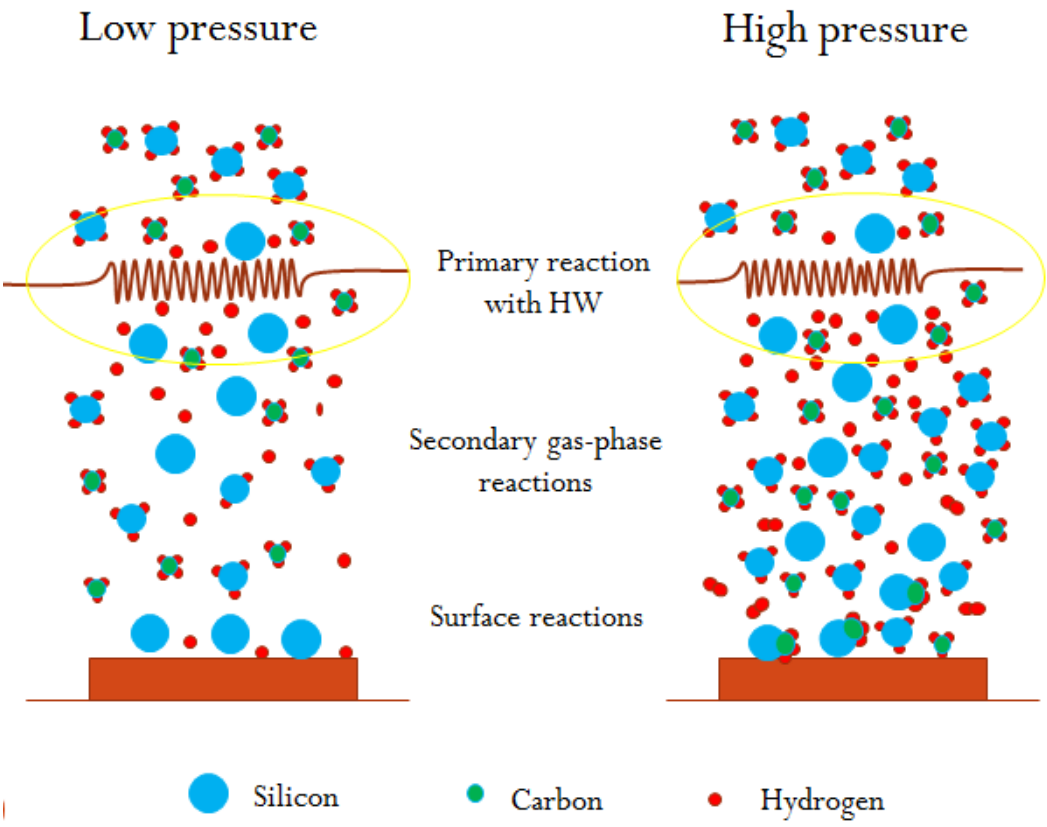

Figure 5.17: Deposition mechanism of SiC from methane and silane gases in HWCVD chamber under low and high deposition pressures.

5.3 Influence of Filament-to-Substrate Distance on the Properties of SiC Films

5.3.1 Introduction

In this section, the influence of the filament-to-substrate distance (d) on the structural, compositional, crystallinity, optical properties and the deposition rate of SiC films were investigated.

5.3.2 FTIR Spectroscopy Analysis of SiC Films Deposited on c-Si Substrate

Figure 5.18 shows the FTIR transmission spectra of the SiC film deposited under different filament-to-substrate distance. Three absorption bands were observed in all the films corresponding to Si-C, Si-H, and C-H stretching vibration mode centred at approximately 800, 2080, and 2900 cm^{-1}, respectively.

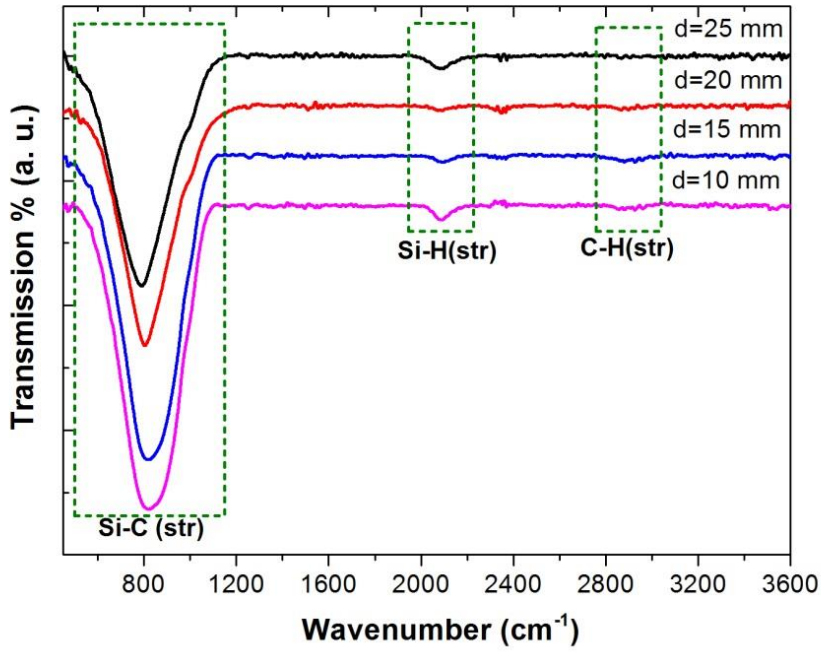

Figure 5.18: FTIR transmission spectra of SiC films deposited under different filament-to-substrate distances (d).

Figure 5.19 shows the Si-C absorption band, which is normalized to the films' thicknesses. It can be seen that the position of Si-C band was progressively shifted from ~ 790 cm^{-1} to ~ 810 cm^{-1} with decrease in d from 25 to 10 mm. In addition, the intensity of Si-C absorption band increased with the decrease in d from 25 mm to 15 mm and slightly decreased with further decrease in d down to 10 mm.

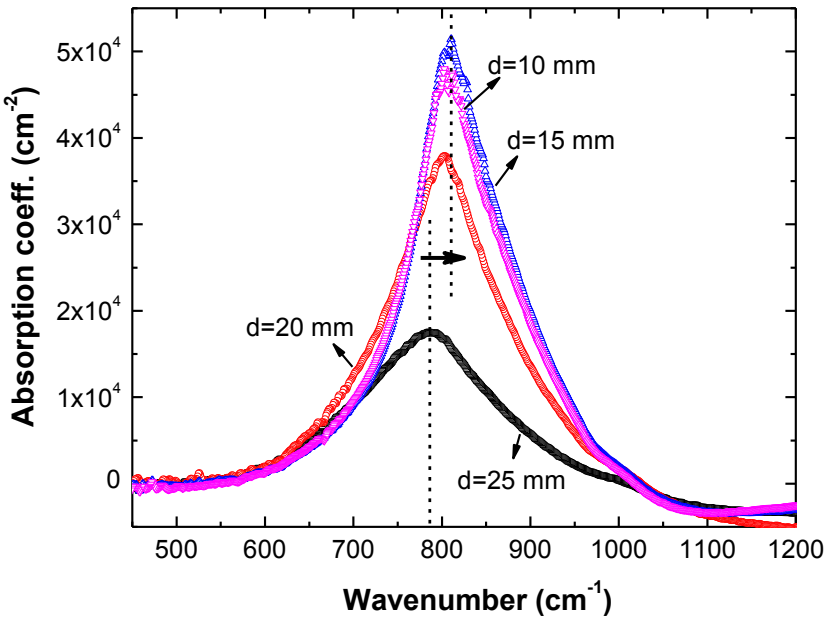

Figure 5.19: Si-C absorption band of SiC films prepared at various filament-to-substrate distances (d).

In order to analyse the FTIR spectra in more detail, the Si-C bands were deconvoluted into consituent peaks, which consisted of one Gaussian and one Lorentzian peak at around 800 cm^{-1} corresponding to Si-C bonds in amorphous and crystalline structures, respectively. Figure 5.20 shows the SiC crystalline volume fraction and Si-C integrated intensity in the films as a function of d. It is seen that the integrated intensity of Si-C peak remarkably increased with decrease in d from 25 to 20 mm and remained almost constant with further decrease in d. However, the SiC crystalline volume fraction increased monotonically from 35% to 65% with decrease in d from 25 to 10 mm. This indicates that at low d, the crystalinity improved correspondingly with distinct increase in Si-C bond density. However, further increase in crystallinity did not result in much change in Si-C bond density. This indicates that the rearrangement of network structure caused by surface reactions and hydrogen etching effect promoted the enhancement in crystallinity, when substrate was closer to

the hot filament. This enhancement in crystalline volume fraction also caused a blueshift of the Lorentzian component of Si-C band. Figure 5.21 demonstrates the linear dependence of peak position of the Lorentzian component of Si-C band with SiC crystalline volume fraction. A blueshift of this peak position has been reported to be attributed to the improvement of SiC crystallinity (Rajagopalan, 2003), however, there has been no reports of similar works providing concrete evidence of this fact.

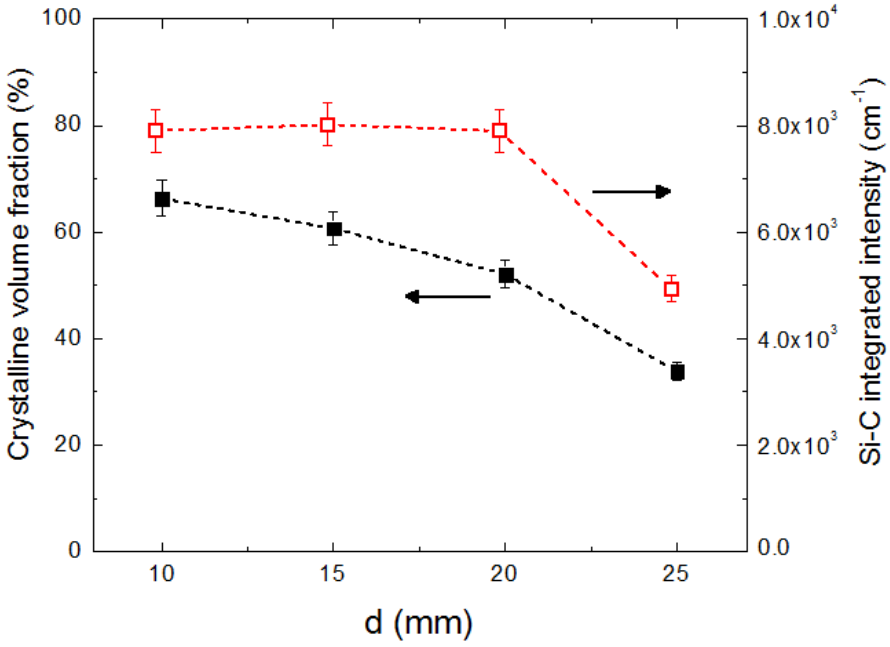

Figure 5.20: The variations of SiC crystalline volume fraction and Si-C integrated intensity in the films as a function of d.

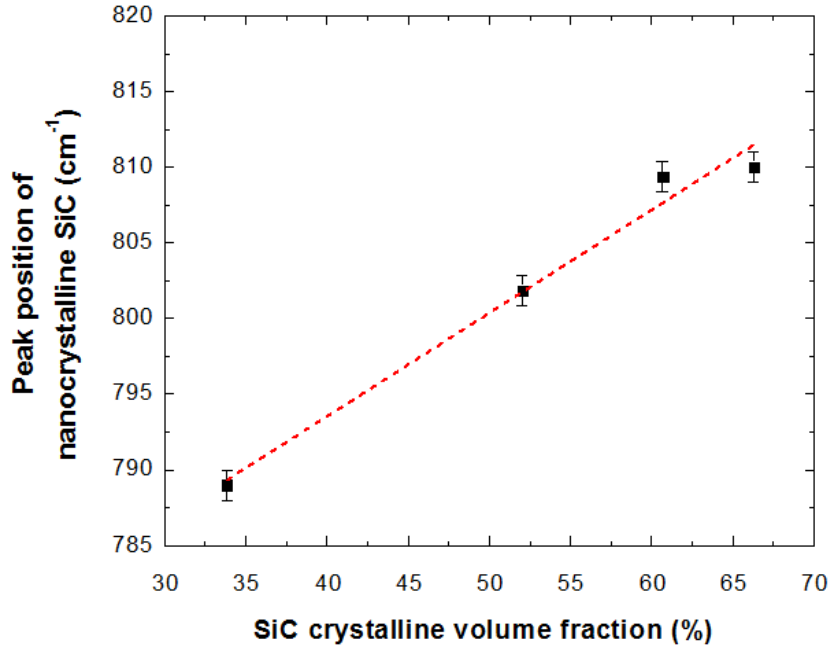

Figure 5.21: Variation of peak posotion of Lorentzian component of Si-C band with SiC crystalline volume fraction.

Figure 5.22 shows the IR absorption band corresponding to Si-H stretching vibrations in the region of 1950-2250 cm^{-1}. Coincidently, the amorphous SiC film which is deposited at the highest d of 25 mm also showed the highest Si-H peak intensity. The intensity of this peak decreases with decreasing d from 25 to 15 mm and increases slightly with further decrease in d to 10 mm. Meanwhile, the position of this band was slightly shifted to higher wavenumber with decrease in d.

The variations of Si-H bond density exhibited the opposite trend with respect to C-H bond density with d as shown in Figure 5.23. This means that there exists an exchange process of H atoms between Si and C atoms. In other words, there is a competition between Si and C atoms to bond with H atoms reaching the growth sites. It was noticed that except for the film prepared at largest d (25 mm), the C-H bond density was always greater than that of Si-H in the films.

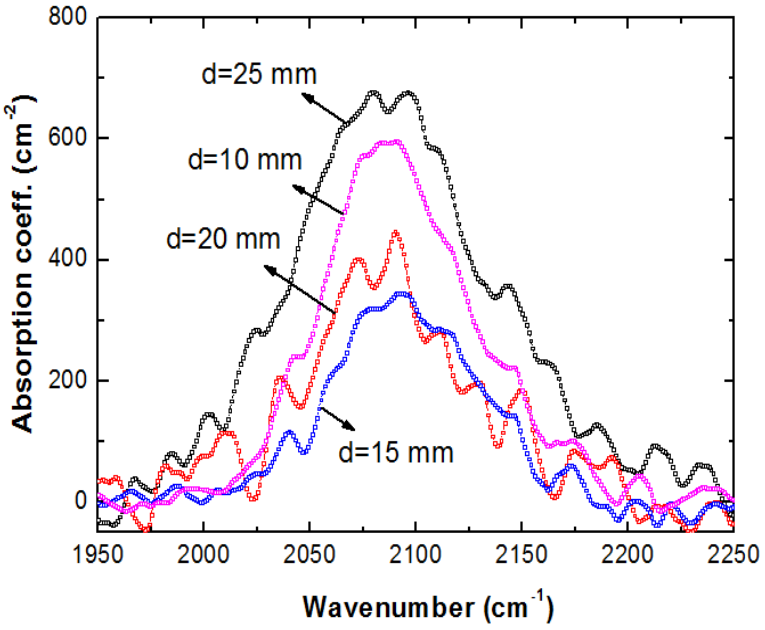

Figure 5.22: The IR absorption band in the region of Si-H stretching vibrations.

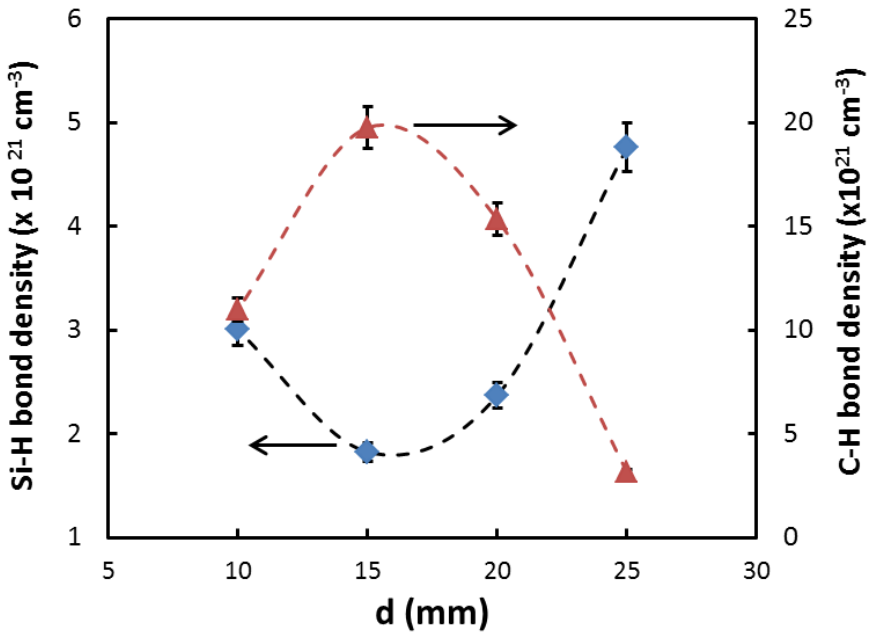

Figure 5.23: Variations of Si-H and C-H bond densities in the SiC films versus filament-to-substrate distance.

5.3.3 Raman Scattering Spectroscopy Analysis of SiC Films Deposited on c-Si and Glass Substrates

To investigate the homonuclear bonding i.e. Si-Si and C-C bonds in the films, the Raman scattering spectra of the films deposited at diffent d is shown in Figure 5.24. It was shown earlier (see section 5.2.2) that the Raman results obtained from UV excitation may not provide enough information on the bonding properties of the films. In this section, only Raman scattering spectra of the films performed with visible light (514 nm) excitation are shown. As can be seen in Figure 5.24, the c-Si peak from the Si substrate is observed from all films indicating that the light penetrated through the film and reached the substrate. Other peaks such as a-Si, 3C-SiC, and C-C were also labelled in the figure. In the region of 600-1000 cm^{-1} corresponding to Si-C bonds (see Figure 5.25), only a broad band centered at 780 cm^{-1} resulted from Si-C in amorphous structure was observed from the film deposited at d of 25 mm. However, with the decrease in d, this broad band was split into two separate bands centred at ~770 cm^{-1} and ~890 cm^{-1} due to TO and LO modes of SiC vibrations in 3C-SiC structure, respectively. This further confirmed earlier observations showing enhancement in SiC crystallinity with decrease in d.

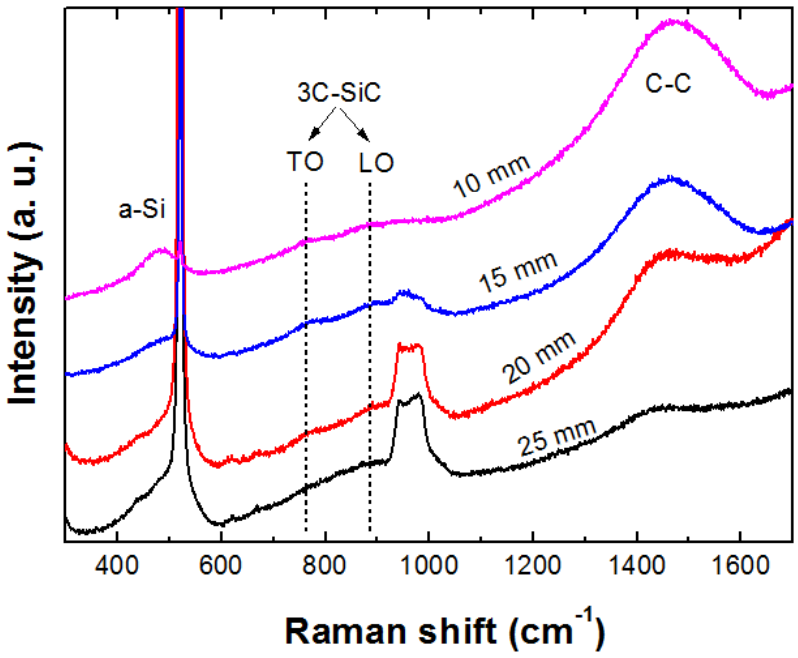

Figure 5.24: Raman scattering spectra of SiC films deposited on c-Si substrate at indicated d.

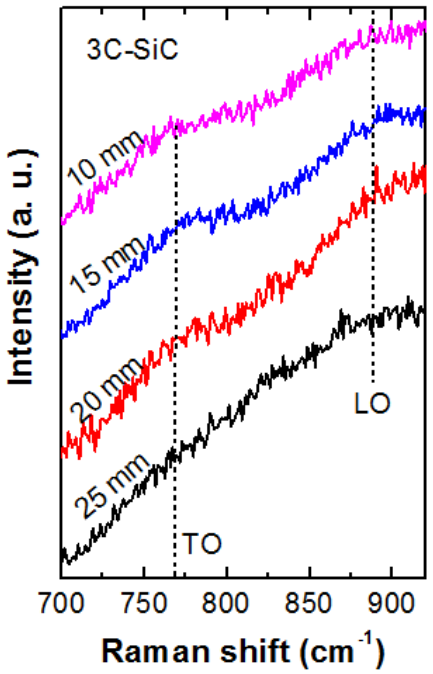

Figure 5.25: Raman scattering spectra of SiC films deposited at different d in the range of Si-C vibrations.

Another significant feature in the Raman spectra was a broad band in the region of 1200-1600 cm^{-1} corresponding to C-C bond in the film structure. The slope of the baseline of this band appears to decrease with increasing d, indicating that the H content in films increases with decreasing d. As d decreases, the Si and H atoms reaching the growth sites become more energetic due to lower probability of collisions with other molecules. The energetic H atoms cousing more active H etching effects thus forming stronger Si-Si, Si-C and C-C bonds in the film structure as the H atoms actively etch away weak Si-H and C-H bonds at the growth sites.

Figure 5.26 shows the Raman spectra in this region after subtracting the baseline from the spectra. It was observed that the position of this band was shifted towards higher wavenumber with decreasing d.

In a-C:H, the G peak is downshifted with increasing band gap and sp^3 content, from 1580 to 1520 cm^{-1} for excitation at 514 nm. In a-C:H this is contributed by the increase in polymeric C network in the film structure. Another cause of downshifting could be due to the presence of excess electron on the more electronegative C atoms linked to Si, resulting in weaker C=C bonds with lower vibrational frequencies (Racine, et al., 2001).

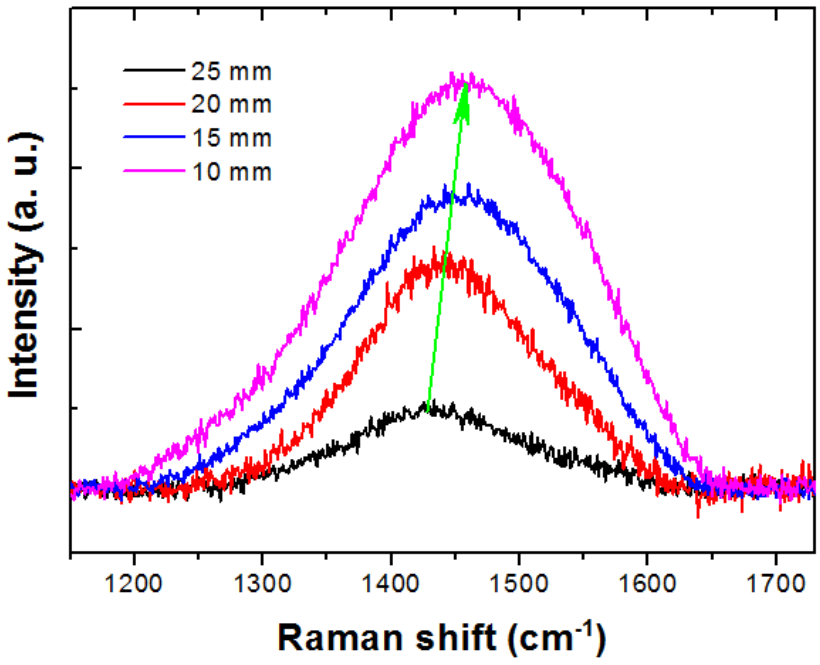

Figure 5.26: Raman scattering spectra of SiC films deposited at different d in the range of C-C vibrations.

The shifting of G peak toward lower frequencies in a-SiC:H has been attributed to incorporation of more Si atoms into the carbon clusters (J. R. Shi et al., 1999; F. Zhao et al., 2009). Thus, the upshifting of this band with decreasing d indicates the fomation of C-C clusters with lower incorporation of Si.

In order to investigate the properties of SiC films deposited under different d on glass substrate, Raman scattering spectra of these films were recorded and shown in Figure 5.27. The Raman spectra of these films exhibit the presence of a-Si, a-SiC, 3C-SiC, and a-C:H phases in the films. Comparing the Raman spectra of the films on glass substrates with those of films on c-Si substrate as shown in Figure 5.24, the structure and phases present in the films deposited on both glass and c-Si substrates were similar. The only difference is the absence of c-Si peak at 520 cm^{-1}, which was due to the substrate and not the film itself.

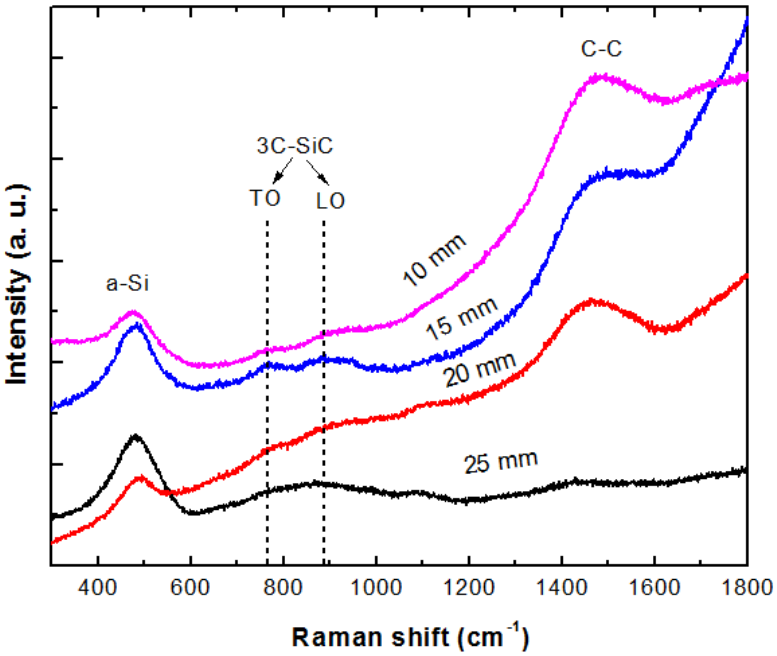

Figure 5.27: Raman scattering spectra of SiC films deposited on glass under different filament-to-substrate distances.

5.3.4 XRD Analysis of SiC Films Deposited on c-Si and Glass Substrates

Figure 5.28 shows the XRD spectra of the SiC films deposited on c-Si substrate at various d. The film prepared at largest d, 25 mm, shows no XRD peak in its spectrum. This indicates that this film is amorphous. However, three XRD peaks related to reflection planes of 3C-SiC emerged for other films as labelled in the Figure. The intensity of the peaks was progressively increased with decrease in d, which indicates improvement of crystallinity with reducing d. This result supports FTIR analysis that also showed enhancement of crystallinity in the films. The SiC mean crystallite size was calculated by employing the Scherrer's formula. The variation of the crystallite size with d is shown in the inset as obtained from the (111), (200) and (311) diffraction peaks.

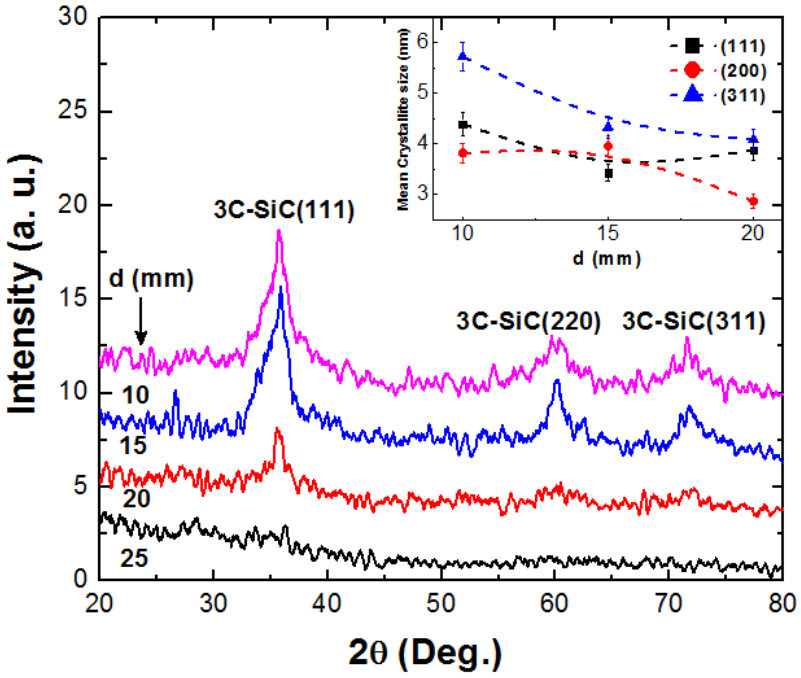

Figure 5.28: XRD pattern of SiC films deposited under various d on c-Si substrate. The inset shows variations of SiC crystallite size estimated from different XRD peaks.

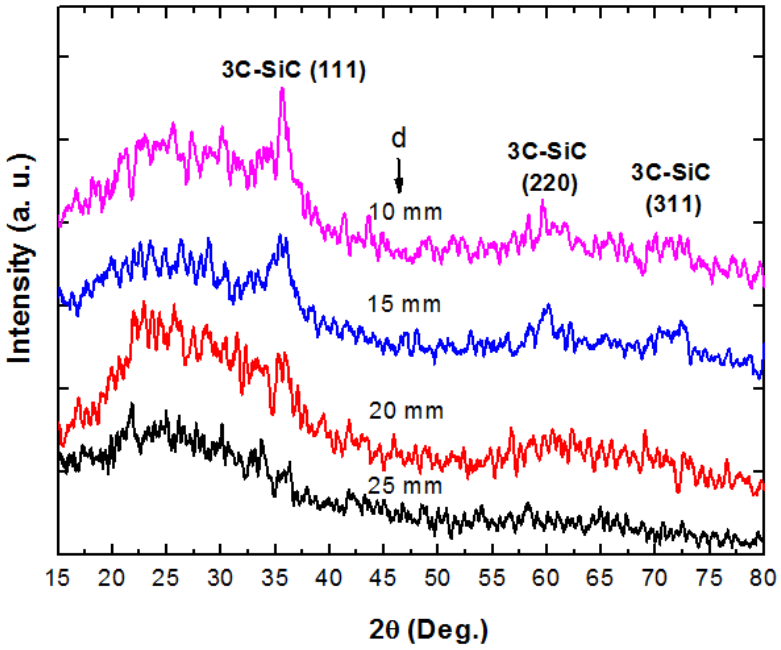

Figure 5.29: XRD patterns of SiC films deposited on glass substrate under various d.

Figure 5.29 demonstrates the XRD patterns of SiC films deposited on glass substrate under various d. The film deposited at 25 mm was completely amorphous. However, the decrease in d from 25 mm to 20 mm resulted in emergence of an small XRD peak at 35.6° corresponding to 3C-SiC(111) plane. Further decrease in d, led to improvement in the crystallinity of SiC films, which was reflected by the appearance of two other XRD peaks at 60° and 71.8° corresponding to 3C-SiC (220) and 3C-SiC (311), respectively. Concurrently, the intensity of XRD peaks progressively increased with the decrease in d.

The results shown in Raman and XRD analysis for the films deposited on c-Si and glass substrates further confirmed that the deposition of SiC films using HWCVD technique under various filament-to-substrate distances was substrate independent. Consequently, the optical properties of these films can be safely correlated to their structural properties.

In this part of this work, the XRD and Raman results further showed that the structural properties - the crystallinity, the presence of crystalline and amorphous Si phase in the film, the hydrogen content and structural order in the carbon phase - were not dependent on the type of the substrate. The substrate temperature and filament temperature in this work were fixed at 300°C and 1900°C, respectively. This is lower than the temperatures reported by Z. Sun et al (Sun, Sun, Wang, & Zheng, 1995) where the SiC growth is observed through HWCVD decomposition of CH_4 mixed with H_2. In another report George et al. used bias enhanced low-pressure hot filament chemical vapour deposition (George, et al., 2002) at substrate temperature of 750°C resulting in growth of SiC from methane gas on Si substrate. The role of bias and low pressure in deposition of SiC film was established. Therefore at low substrate temperature (this work) Si atoms from the c-Si substrate cannot be activated and contribute to the surface

reactions and growth of SiC. Instead, Si-related radicals generated from the dissociation of silane gas are important in the formation of Si-C bonds in the gas phase and/or on the substrate surface.

5.3.5 Elemental Composition

The relative atomic composition and its stability in the SiC films deposited under different filament-to-substrate were studied by Auger depth profile analysis. Figure 5.30 shows the depth profile of the films deposited on c-Si substrate. It was noticed that the silicon and carbon incorporations were almost stable during the deposition. In addition, the carbon content in the SiC films did not significantly changed with d.

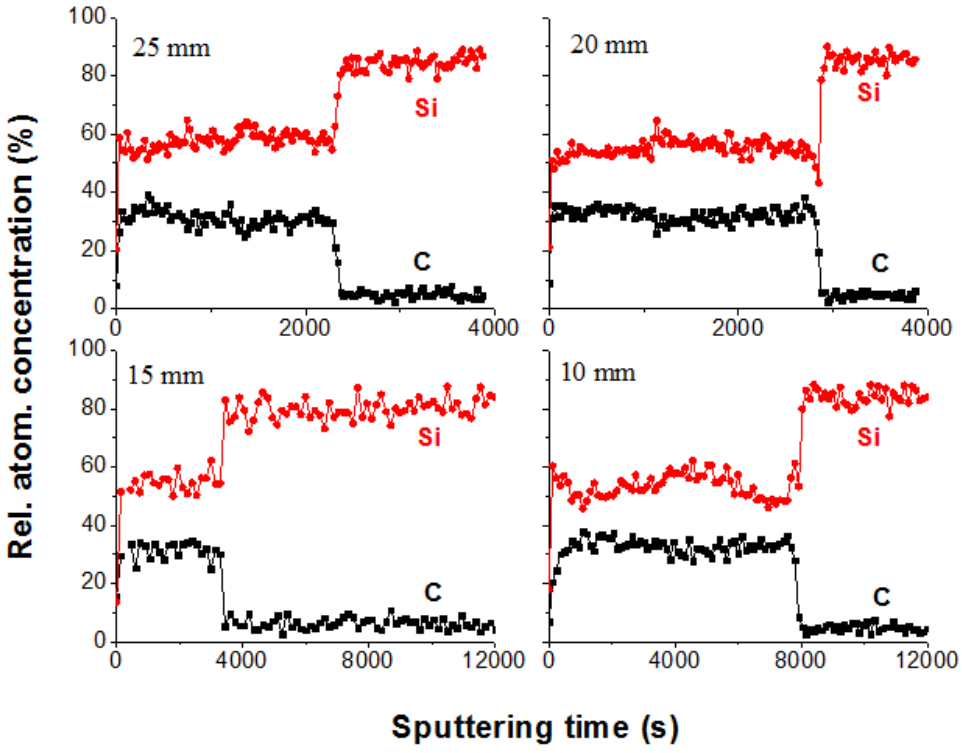

Figure 5.30: Auger depth profile of SiC films deposited at different d.

Figure 5.31 shows the variations of silicon, carbon, and oxygen atomic concentration, determined from AES measurement, as a function of d. It is seen that d had almost no effects on Si, C or O content. Si content was always higher than C content. This is because silane is more actively dissociated by hot filament at this temperature. Carbon incorporation in the films was mostly from gas phase reactions. The oxygen content slightly increased with decrease in d due to oxidation of the film surface as a result of the presence of Si dangling bonds in the films deposited at lower d.

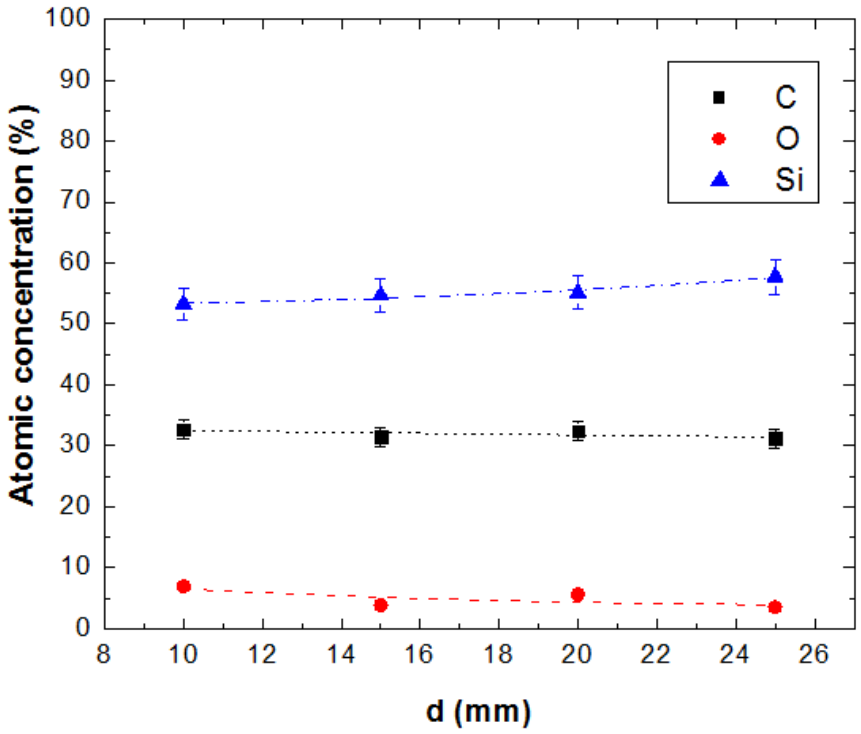

Figure 5.31: Variations of silicon, carbon, and oxygen atomic concentration versus d.

5.3.6 Morphology

Figure 5.32 shows the surface morphology of the films deposited under various d. High and low magnification FESEM images were provided for each film.

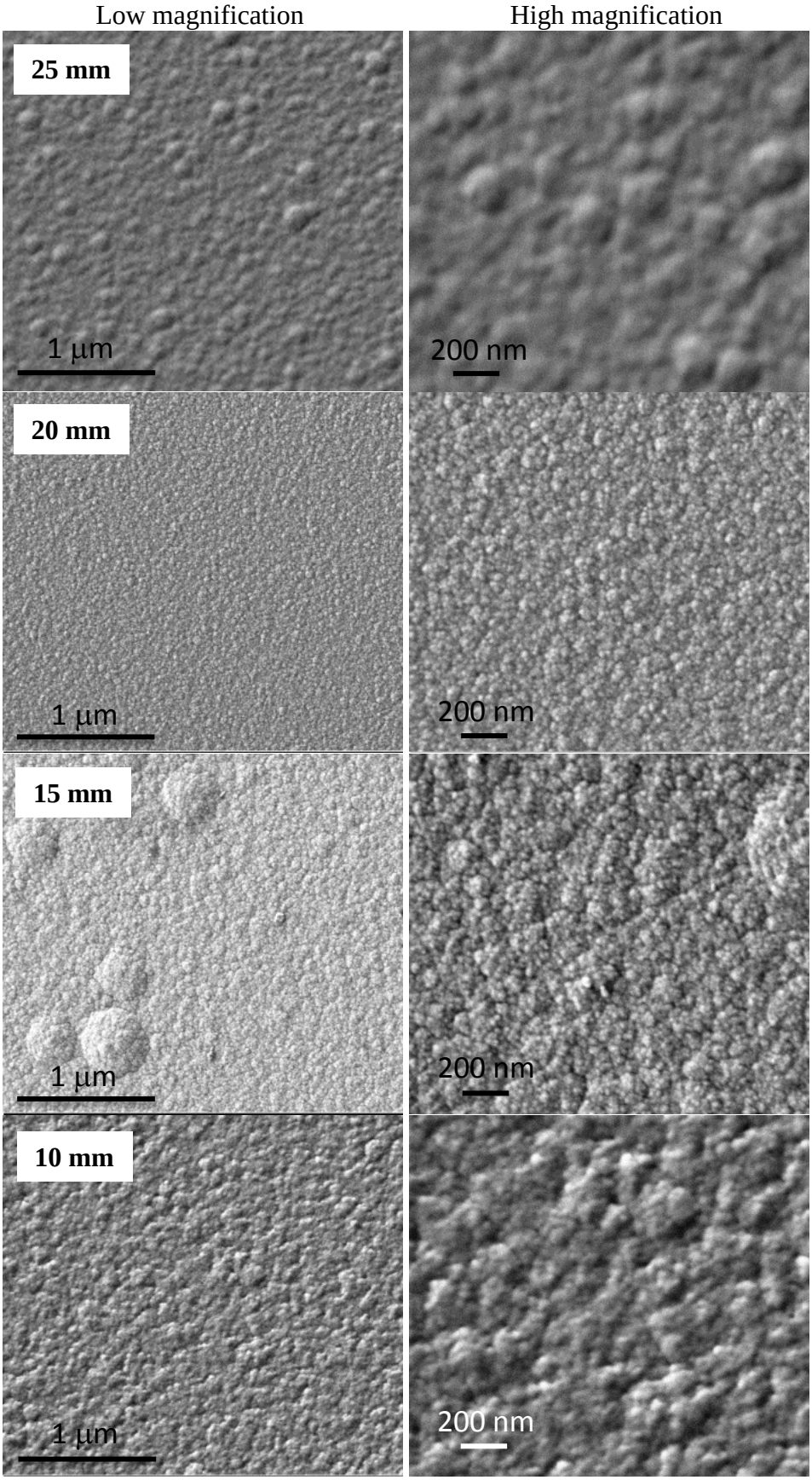

Figure 5.32: FESEM images of the surface of the films deposited at different filament-to-substrate distances.

Amorphous SiC film deposited at d of 25 mm showed large grains with an average diameter of approximately 100-200 nm. However, the film deposited at d of 20 nm, which was shown to be nc-3C-SiC in structure, exhibited a smooth surface with very fine and compact grains. This is a characteristic of the surface morphology of nano-crystalline structures. In spite of improvement in the crystallinity with further decrease in d, the surface compactness of these films is shown to reduce and somewhat produced a porous surface. This could be related to incorporation of hydrogen in the form of a-C:H and a-Si:H phases in the films structure as verified from the FTIR and Raman results. This change in the structure is shown to affect the refractive index of the films.

5.3.7 Optical Properties

5.3.7.1 UV-Vis-NIR Spectroscopy

Figure 5.33 (a) and (b) show the optical transmission spectra and respective Tauc plots of SiC films deposited under different filament-to-substrate distance (d). The variations of energy band gap and refractive index of the films is plotted in Figure 5.34 as a function of d. It is noteworthy that the band gap of the films reached a maximum with decrease in d from 25 to 20 mm. However, further decrease in d led to a redshift in band gap.

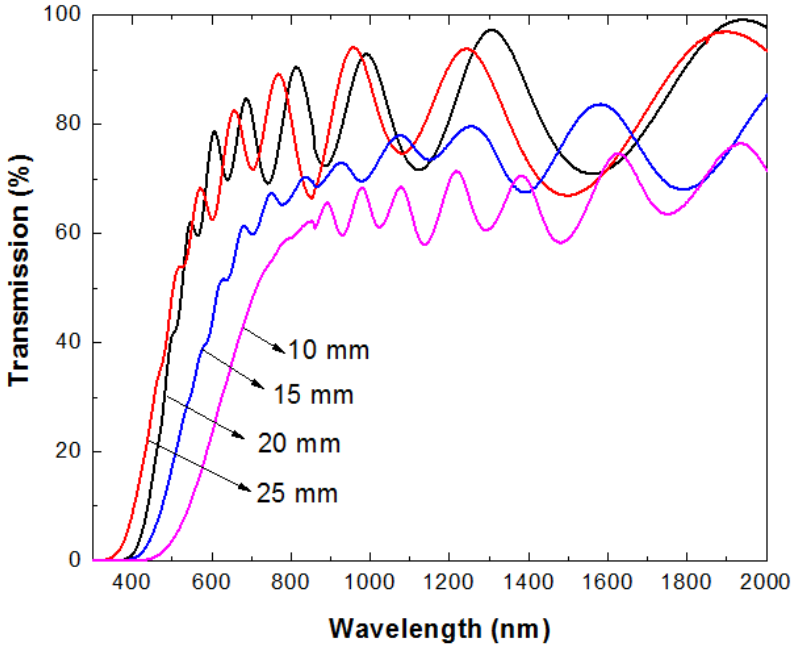

(a)

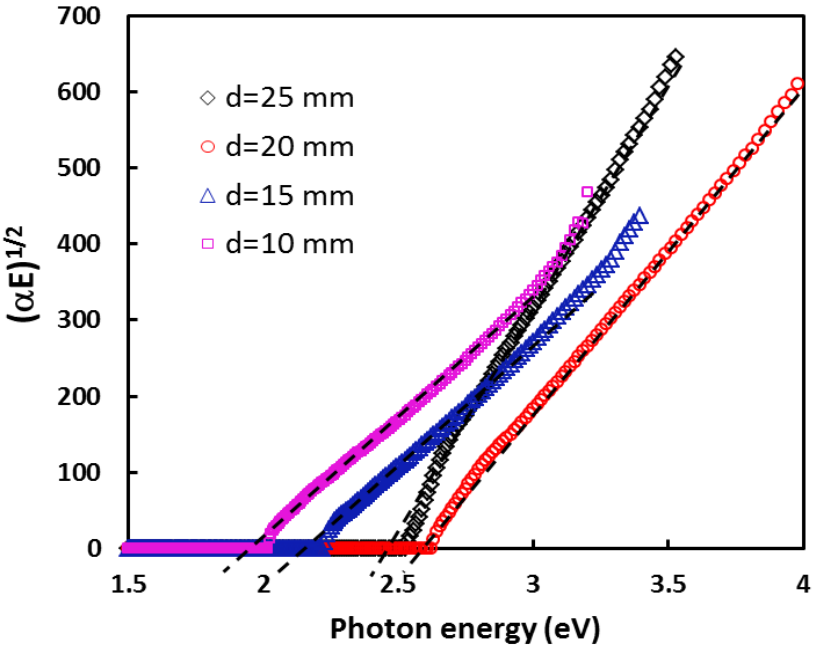

(b)

Figure 5.33: (a) UV-Vis-NIR transmission spectra and (b) Absorption coefficient of the films deposited at different d.

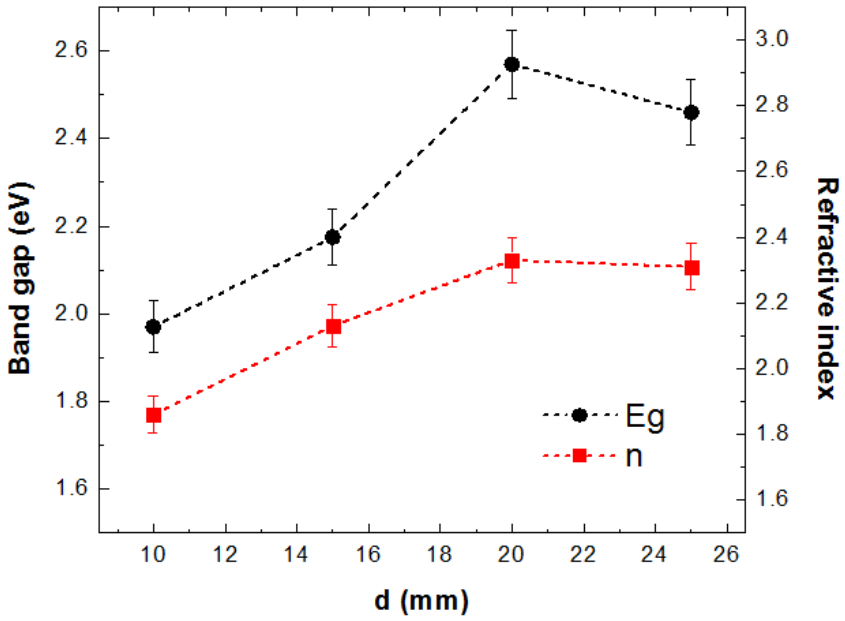

Figure 5.34: Band gap and refractive index of SiC films deposited under different d.

The widening of band gap with the decrease in d originated from significant enhancement of Si-C bond density along with the formation of 3C-SiC nano-crystallite in the film as shown in FTIR and XRD results. Nevertheless, the decrease in energy band gap with further decrease in d did not show any direct dependence on Si-C bond density. The total Si-C bond density in the films did not significantly change with decrease in d from 20 to 10 mm, but the crystallinity of SiC network improved, which was reflected by the enhancement of SiC crystalline volume fraction (see Figure 5.20). Therefore, the narrowing of the energy band gap can be explained by the agglomeration of sp^2 carbon that was observed through Raman spectra. It was found that the C-C band in Raman spectra of these films broadened and shifted to the higher wavenumbers along with the decrease in the energy band gap, which indicates formation of pure a-C:H clusters in the films (M. Park et al., 2001).

Figure 5.35 shows the variation of *B*-parameter and E_{04}-E_g representative of the band tail width of SiC films deposited under various d. It can be clearly seen that these parameters showed opposite trends. This indicates that the film with higher structural order has narrower band tail. This clearly verifies the correlation between structural order and optical properties in SiC alloy. It was noticed that the SiC film with amorphous structure exhibits the highest structural order, which was reflected by the highest *B*-parameter and lowest band tail width. This shows that the formation of nano-crystals produced inhomogeneity in the film that reduced the structural ordering. Furthermore, increase in sp^2 carbon clustering with the decrease in d, as demonstrated in the Raman spectra explains further increase in structural disorder in the film.

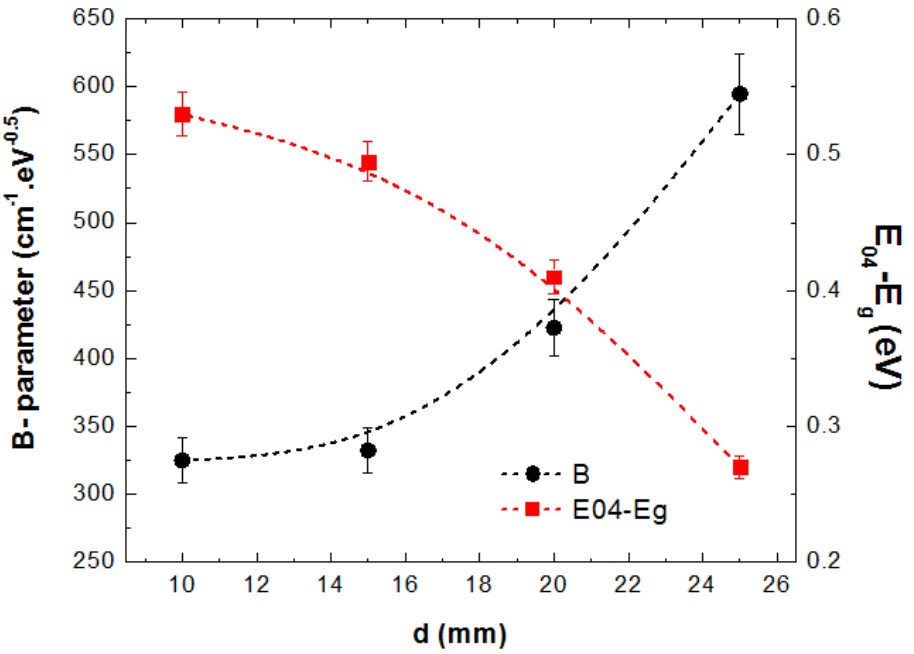

Figure 5.35: Variations of *B*-parameter, the slope of Tauc plot, and E_{04}-E_g, the width of band tail as a function of d. The dashed lines are visual guides.

5.3.7.2 Photoluminescence Spectroscopy

Figure 5.36 shows room temperature PL spectra from SiC films deposited at various d. The positions of the main PL band for all films (E_{PL}) are listed in Table 5.3 and compared with their energy gap. It was observed that E_{PL} was blue-shifted with initial decrease in d from 25 to 20 mm. However, further decrease in d resulted in red-shifting of E_{PL}. This variation is consistent with the trend observed for E_g.

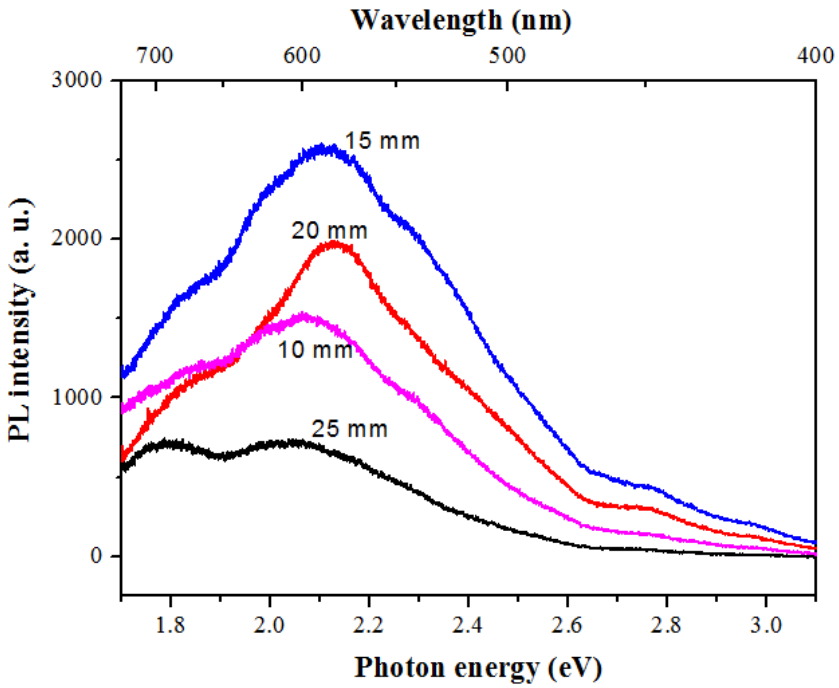

Figure 5.36: Room temperature PL spectra of the SiC films deposited under different filament-to-substrate distances.

As pointed out in section 5.2.6.2, room temperature PL is not usually observed from a-SiC with carbon content below 0.5. However, several researchers have reported PL emission from nano-crystalline SiC embedded in a-SiC (M. B. Yu, Rusli, Yoon, Xu, et al., 2000) or a-SiO_2 (Guo et al., 2001) matrix. However, the values reported for E_{PL} in the previous studies are usually greater than the room temperature optical band gap

energy of the bulk 3C-SiC. For example, Yu et al. have reported a PL energy of 2.6 eV attributed to the quantum size effect in SiC nano-crystallites (M. B. Yu, Rusli, Yoon, Xu, et al., 2000). In another study, visible PL emission with the energy of ~2.5 eV has been observed from SiC nano-crystalline films, which is higher than the their energy band gap (Xu, et al., 2000). Xu et al. have suggested that the origin of this intense photon emission in the SiC nano-crystals is the radiative recombination due to the direct optical transitions. Recently, Yu et al. have observed a PL emission showing a dominant PL band centred at ~2.5 eV originated from radiative recombination in quantized states of SiC nano-crystals and a weaker component at ~ 1.9 eV originated from radiative recombination in the band tail states of amorphous SiC matrix (W. Yu et al., 2011). Therefore, the PL spectra obtained in this work probably were not contributed by the SiC nano-crystals. The radiative recombination resulted from band-to-band transition and this process contributes to the dominant process for the PL emission. However, radiative recombination in the band tail states of amorphous environment is responsible for the peak shoulder detected in the lower energy region.

Table 5.3. PL energy and energy band gap of SiC films deposited under different d.

d (mm) $\pm 1\ mm$	$\boldsymbol{E_{PL}}$ **(eV)** $\pm\ 0.02\ eV$	$\boldsymbol{E_g}$ **(eV)** $\pm 0.01\ eV$
25	2.04	2.46
20	2.14	2.57
15	2.10	2.17
10	2.06	1.97

5.3.8 Deposition Rate

Figure 5.37 shows the deposition rate of SiC films deposited under various d. The deposition rate decreased from ~0.45 nm/s to ~0.25 nm/s with decreasing d from 25 to 20 mm. This reduction in the deposition rate was in agreement with the transition from amorphous to nano-crystalline structure as shown in the XRD results. However, further decrease in d led to a monotonic increase in the deposition rate up to 0.55 nm/s.

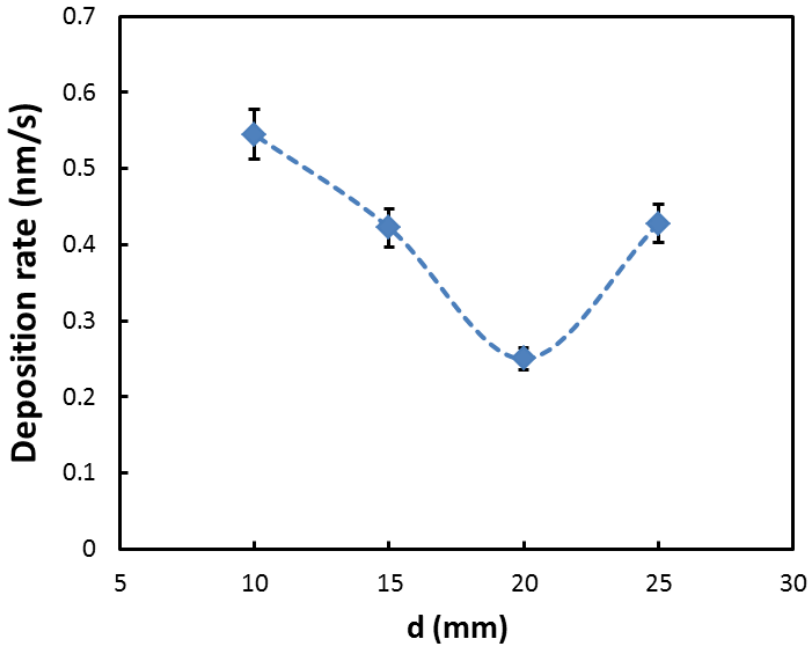

Figure 5.37: Deposition rate of SiC films as a function of d.

The decrease in the deposition rate with decreasing d from 25 to 20 mm is attributed to the increase of the flux of H radicals reaching the film-growing surface. H radicals generated from the SiH_4 decomposition at the HW, usually go through gas phase reactions and thus are converted to other species on the way to the substrate surface. However, the decrease in the distance between filament and the substrate allows H radicals to reach the growth surface directly. These energetic H radicals

promote crystallinity in the film by penetrating the layers below the top surface of the film and was caused the breaking of weak Si-H bonds, thus leading to formation of ordered Si-C network. However, further improvement in crystallinity with decreasing d led to an increase in the deposition rate. Similar enhancement of crystallinity and deposition rate with reduction of d has been reported for nc-Si:H films deposited from pure SiH_4 gas by HWCVD technique (Waman, 2011). They attributed this increase in deposition rate to the enhancement in the diffusion of radicals such as Si-H, $Si-H_2$, or $(Si-H_2)_n$. Nevertheless, in this work, the formation of $C-H_n$ and sp^2 C-C bonds seems to contribute to enhancement of the deposition rate at lower d as shown in IR and Raman results.

Figure 5.38 shows a simple illustration of the deposition mechanism in HWCVD chamber under three different filament-to-substrate distances for comparison. It should be noted that not all radicals species created in the gas phase are shown in the figure. From what has been reported in the literature, in spite of extensive work done in radical measurements from various techniques for Si deposition by HWCVD from SiH_4/H_2 gases (Nakamura & Koshi, 2006; Umemoto, 2002; Zheng & Gallagher, 2006), no direct measurement or theoretical work on chemical reactions and radicals produced in the HWCVD system with SiH_4 and CH_4 gases is available yet. Therefore, the detail of chemical reactions and resulting radicals in the chamber is still unknown. However, from this study, the role of H radicals in the crystallinity of the films was verified in spite of absence of hydrogen dilution of the source gases. These abundant H radicals were generated from the silane decomposition on the hot filament. When the filament is placed far from the substrate, generated radicals on the HW including H radicals are consumed through gas phase reactions. Therefore, the flux of H radicals reaching the substrate surface is fairly low. Under this situation, formation of a significant amount of SiH_n, $SiCH_n$, and CH_n precursors led to deposition of amorphous SiC films with high

hydrogen content and inhomogeneous structure. However, by decreasing the distance between filament and the substrate, availability of high density of H radicals resulted in growth of SiC crystallites in the film structure. Further decrease in d, although enhancing the crystallinity, however, increased the hydrogen incorporation.

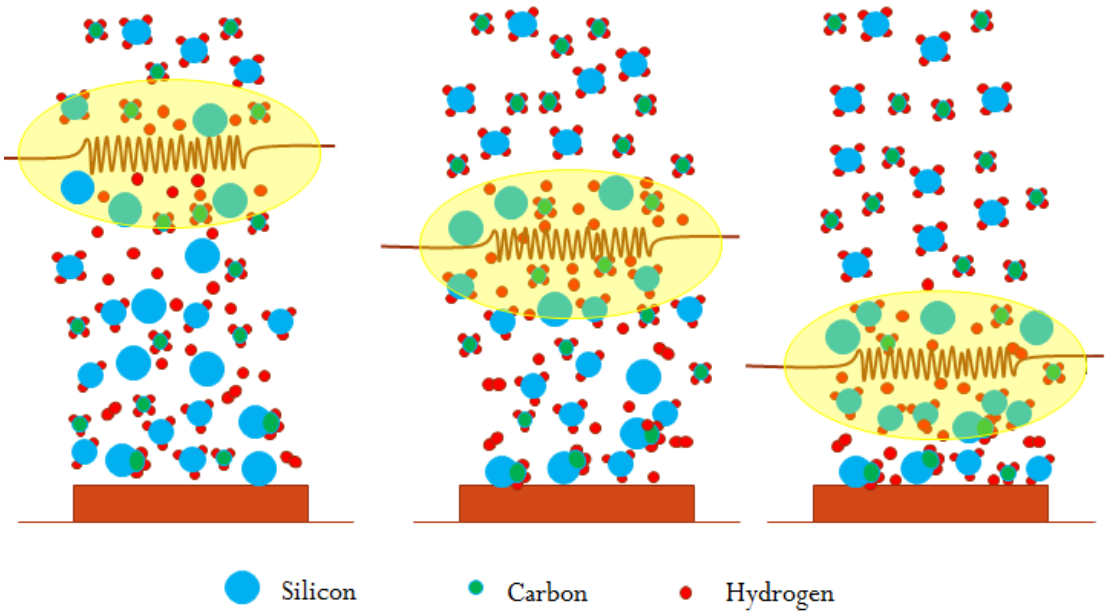

Figure 5.38: Deposition mechanism in the HWCVD chamber under different filament-to-substrate distances.

5.4 Correlation Between Optical Parameters and Structural Properties of SiC Films Deposited by HWCVD

So far, the optical and structural properties of SiC films deposited under different conditions were shown. In addition, the optical parameters were correlated to the structural properties of the films in each set of samples. However, it has been widely reported that the optical properties of SiC films deposited by PECVD are not dependent on deposition conditions and only depend on the carbon content of the SiC films particularly in low carbon content region (G. Ambrosone, et al., 2002; Conde, et al.,

1999; Hartel, 2010; Mastelaro et al., 1996). Nevertheless, in the case of HWCVD SiC films, there is a lack of comprehensive investigation to establish such a correlation. B.P. Swain has correlated the increase of band gap of HWCVD a-SiC:H films to the increase in Si-C bond density. However, the decrease in the size of graphite carbon clusters resulted in saturation of band gap at higher carbon content (B.P. Swain, 2006a). T. Wu et al has reported that the volume fraction of Si-phased in SiC films controls the energy band gap (Wu, 2011). Some other researchers believe that the carbon incorporation in the SiC film plays a key role in regulation of the band gap (A. S. Kumbhar, et al., 1995; Mori, Tabata, & Mizutani, 2006; A. Tabata, Kuroda, M., Mori, M., Mizutani, T., Suzuoki, Y., 2004). However, sometimes the variation of the energy gap or refractive index cannot be explained in terms of the carbon content. For example, in nano-crystalline SiC films the enhancement of energy band gap has been attributed to the improvement of crystallinity (Mao, et al., 2012; A. Tabata & Mori, 2008).

In this work, the deposition of amorphous and nano-crystalline SiC under different deposition conditions by HWCVD method was demonstrated. Although there are many factors affecting energy band gap and refractive index as reported in the literature and this work, most of the previous reports emphasized the influence of carbon content. In order to further establish this influence on the optical properties after establishing that the structural properties of SiC films were not dependent on substrate, the dependence of optical parameters on the carbon content of SiC films prepared in this work at various conditions was studied using optical parameters obtained at various deposition conditions including the parameters obtained in Chapter 4 along with parameters obtained from reported work in the literature.

Figure 5.39 demonstrates the variation of the energy band gap and refractive index of the SiC films deposited under various d as a function of G peak position and

the integrated intensity of the G peak. From this figure, it is seen that the increase in sp^2 carbon clusters also causes a monotonic decrease in the refractive index although an increase in refractive index is expected with improvement of crystallinity. In both graphs, the decreasing trends were observed except for the film prepared under largest d that is amorphous. This film, which is indicated in the figure, did not follow the trend due to different film structure. This indicates that the factors controlling the optical parameters in amorphous SiC films are different for nano-crystalline SiC films.

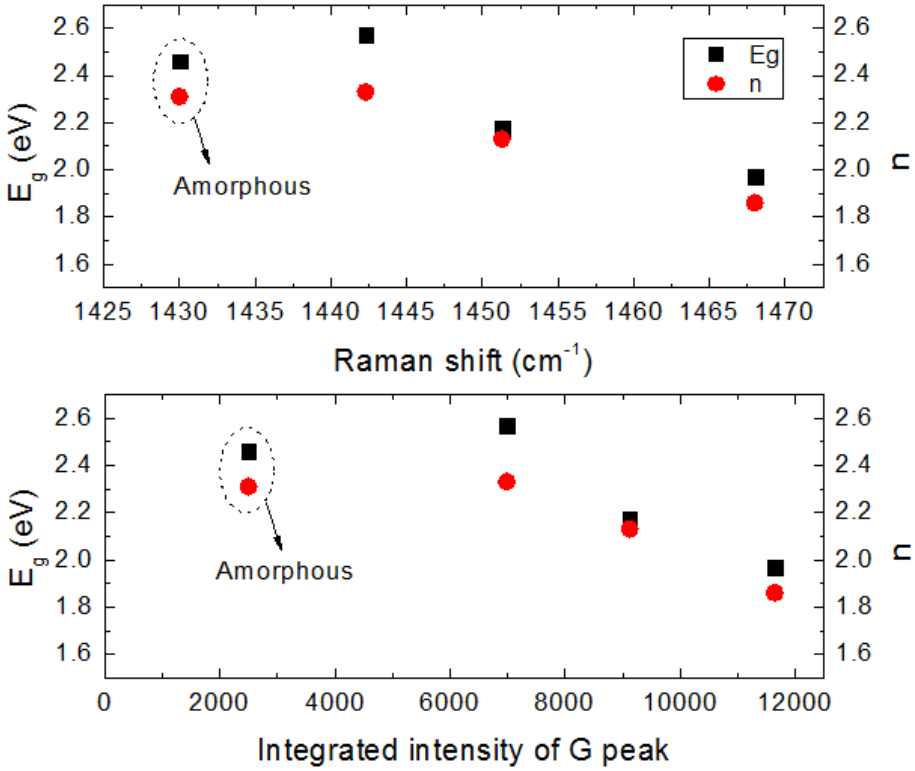

Figure 5.39: Variation of energy band gap and refractive index of the SiC films deposited under different d as a function of G peak position (top graph) and the integrated intensity of G peak (bottom graph).

In order to make a comparison of the present results with what have been reported in the literature from HWCVD deposited SiC films, the data from references are plotted in Figure 5.40 together with present work. This figure shows the variation of energy band gap of SiC films as a function of carbon content in the films. It is worth noting that the data obtained from this work exhibit almost the same trend as previous reports. This indicates that almost linear dependence of E_g on carbon content could be established for HWCVD SiC films.

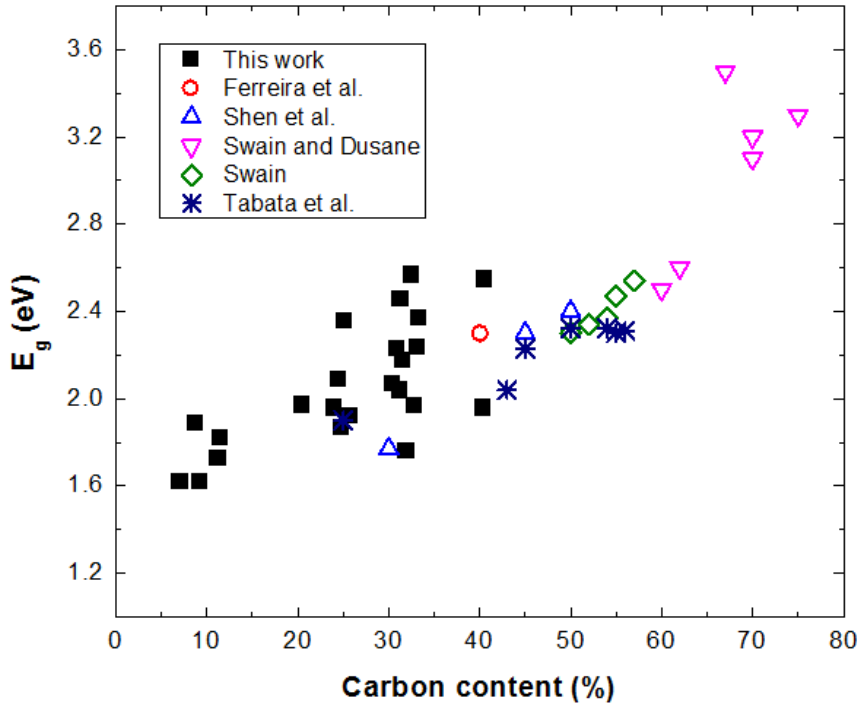

Figure 5.40: Energy band gap of SiC films as a function of carbon content in the films. Full squares show the results obtained in this work. Other symbols are the values from references for comparison as indicated in the figure (I. Ferreira, et al., 2001; Shen, et al., 2012; B.P. Swain, 2006b; Bibhu P. Swain & Dusane, 2006; A. Tabata, Kuroda, M., Mori, M., Mizutani, T., Suzuoki, Y., 2004).

Figure 5.41 illustrates the refractive index of SiC films prepared under different deposition conditions as a function of carbon content in the films. However, since not much reported work is available on the behaviour of the refractive index of HWCVD deposited SiC films as a function of carbon content, this work is compared with the existing reports on refractive index of SiC films deposited by PECVD technique (Akaoglu, Sel, Atilgan, & Katircioglu, 2008; G. Ambrosone, Coscia, U., Ferrero, S., Giorgis, F., Mandracci, P., Pirri, C.F. , 2002; DellaSala, Fiorini, Skumanich, & Amer, 1985; Pascual, Andlijar, Fernhndez, & Bertran, 1995).

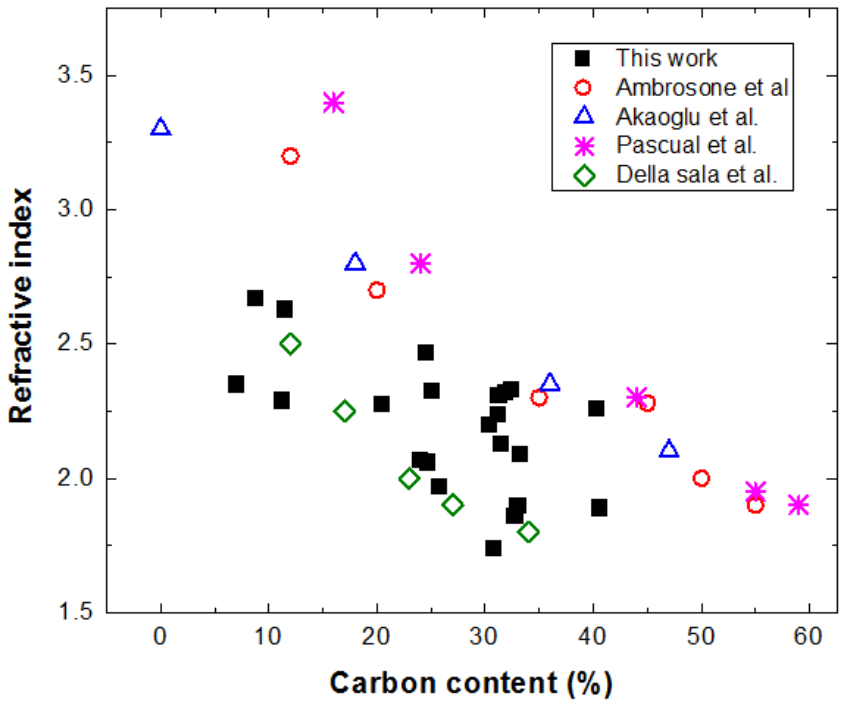

Figure 5.41: Refractive index of SiC films as a function of carbon content in the films. Full squares show the results obtained in this work. Other symbols are the values for PECVD SiC films from references for comparison as indicated in the figure.

From Figure 5.41 it appears that refractive index of SiC films decreases with the increasing carbon content in the films. The data obtained in this work follow the general trend in spite of relatively lower values than PECVD deposited SiC films. This is probably due to the different kinetic mechanism in HWCVD. In HWCVD, because of lower dissociation of CH_4 molecules, usually CH_x radicals are produced and incorporated into the films. Therefore, the presence of many H terminated bonds would result in less dense films. As a result, in this work, SiC films with slightly lower refractive index than PECVD SiC films (in the literature) were obtained. However, refractive index fairly provides an estimation of carbon content in HWCVD SiC films as suggested in early studies (Bullot & Schmidt, 1987).

5.4 Summary

In this chapter, the effects of two important deposition parameters that is deposition pressure and filament-to-substrate distance on the growth rate, structural and optical properties of SiC films were studied. In order to explore the influence of structural properties on the refractive index, optical energy gap and photoluminescence properties of deposited films, the dependence of SiC film deposition in HWCVD on c-Si and glass substrates was also investigated. This is to facilitate the fact that the optical energy gap and refractive index of the films were derived from the optical transmission spectra of the films which can only be measured on films on glass substrates.

The results in this chapter show that deposition pressures and filament-to-substrate distances have strong influence on the growth rate of the SiC films grown by HWCVD system used in this work. The growth rate of SiC films was reduced

significantly at the critical deposition pressure and filament to substrate distance of 80 Pa and 20 mm respectively, where the film structure reached a transition point of structural change from nano-crystalline to a totally amorphous structure. It was also established from the results in this chapter that the formation of a-C:H clusters was responsible for higher deposition rate at high deposition pressures (above 80 Pa) and lower filament-to-substrate distances (below 2.0 cm).

The structural properties of SiC films deposited under various deposition pressures obtained from XRD, Raman and FTIR analysis reveal that the increase in deposition pressure from 40 to 80 Pa has transformed the structure of the film from a structure of Si nano-crystallites embedded in Si-rich amorphous SiC film to a nearly stoichiometric and highly ordered amorphous SiC film structure. Further increase in the deposition pressure resulted in the formation of a multi-phased film structure consisting of a-Si:H, a-C:H, and a-SiC with high structural disorder.

The influence of filament-to-substrate distance (d) on structural properties of SiC films was significant. It was shown that the decrease in d promoted the formation of nano-crystalline SiC phases and a-C:H clusters in the films as verified by the XRD and Raman analysis respectively. The Si-C bond density showed no dependence on the deposition pressure with increasing d from 10 to 20 mm but decreased significantly when the film structure changed to an amorphous film structure with increase in d to 25 mm. From AES measurement it was revealed that the filament-to-substrate distance had no important effect on composition of the films.

The Raman scattering and XRD measurements of the films deposited under various deposition pressures and filament-to-substrate distances were compared for the films deposited on glass and c-Si substrate. The results confirmed that the structure of SiC films grown was not dependent on the substrate used for the films and the problem

of relating the structural properties to the optical energy gap and refractive index obtained only from films deposited on glass substrate can be resolved. To the best of the author's knowledge, most reported work on this aspect did not establish the fact that the structural properties of SiC films grown by HWCVD were independent of substrate prior to relating the structural properties of the films to the optical properties of the films which can only be measured on films deposited on transparent substrates.

Optical characterization and analysis of the films deposited under different deposition pressure showed that the energy gap of the films was largely influenced by the structural changes in the films. It was established that the energy band gap increases exponentially with increasing Si-C bond density. A wide band gap of ~2.5 eV was obtained from a-SiC film deposited at 80 Pa showing that the Si-C bond density was highest for this film. However, an increase in the deposition pressure resulted in a continuous decrease in the refractive index of the films, showing that the decrease in the optical energy gap and refractive index with increasing deposition pressure above 80 Pa were not mainly influenced by the Si-C bond density in the films. This parallel decrease in optical energy gap and refractive index with increase in deposition pressure was attributed to the presence of a-C:H clusters in the film structure. The formation of a-C:H clusters formed defect states in the forbidden gap of the a-SiC structure at high pressures which reduced the optical energy gap of the films. The increase in the H content in a-C:H clusters incorporated in the film structure was responsible for the further decrease in the refractive index with increasing the deposition pressure although the Si-C bond density in the films decreased.

Radiative recombination processes in the films has revealed the role of Si crystallites as radiative recombination centres. The Si-rich SiC films embedded with Si nano-crystallites showed a room temperature PL emission in the visible range.

Amorphous SiC films deposited under high deposition pressure produced PL emission peak at lower energies which originated from radiative recombination in the tail states.

The effects of filament-to-substrate distance on optical energy gap, refractive index and the PL properties of SiC were found to be related to the variation of a-C:H clusters since these properties were not related to the Si-C bond density in the films mainly because the films were mainly nano-crystalline in structure. The increase in the presence of a-C:H clusters at low d led to a decrease in both the optical energy band gap and refractive index as the a-C:H clusters created defect states and increased the H content in the SiC film structure. The increase in the H content was mainly in the a-C:H clusters as reflected by the increase in the slope of C-C bond signature region in the Raman spectra. From the room temperature PL spectra of the films in this series, it was revealed that the main radiative recombination processes were contributed by the band-to-band and band-to-band tail transitions in the amorphous SiC matrix showing that the a-C:H clusters in the film structure played an important role in the PL properties of the films as well.

It was established that the growth mechanism of SiC films by HWCVD is mainly controlled by deposition pressure and filament-to-substrate distance. The deposition pressure determined the rate of gas phase reactions by controlling the density and residence time of the radicals in the deposition chamber. On the other hand, the distance between filament and the substrate governed the flux of energetic H radicals reaching the growth surface and thus had a great effect on the surface reactions. Therefore, these two deposition parameters significantly determined the structural properties of deposited films as well as the deposition rate.

It was shown earlier in this work on the role of Si-C bond density, H content and the a-C:H clusters presence in controlling the refractive index and the optical energy

gap of the films. However, the AES results showed that that the carbon content in the film was the most important overall parameter that controlled the refractive index and optical energy gap of SiC films deposited by the HWCVD in this work. The results in this work showed that increase in the carbon content has increased optical energy band gap of SiC films but showed a reversed trend on the refractive index. The C atoms in the film structure were either bonded to Si atoms forming SiC phases or bonded to C or H atoms forming a-C:H clusters. Therefore, even though the bonding configuration of carbon atoms incorporated in the film structure had control on these optical parameters, the actual carbon content in the film structure played a major role in controlling these two optical parameters as established in this work. This is the first time within the author's knowledge that it is reported that the C content in SiC films deposited by HWCVD is the most important structural parameter that controls the optical energy gap and refractive index of the films.

CHAPTER 6

Conclusions

and

Suggestions For Future

Works

6.1 Conclusions

In this work, a home-built hot-wire chemical vapour deposition system was successfully utilized to grow multi-phased silicon carbide thin films from pure silane and methane gases without hydrogen dilution. In the first part of this work, the SiC films were only grown on crystalline silicon substrates (c-Si) and the influence of precursor gas concentration on chemical bonding, crystallinity and elemental composition properties of the films were studied. The structural properties of the films were analyzed from the Fourier transform infra-red (FTIR), Raman scattering and X-ray diffraction (XRD) spectroscopy measurements. Auger Electron Spectroscopy (AES) depth profiling measurement was done on these films to study the elemental composition distribution within the films. The precursor gas concentration was varied by depositing two series of films where the first series of films consisted of films deposited at different methane (CH_4) flow-rates with the silane (SiH_4) flow-rate fixed at SiH_4 starving condition with flow-rate of 0.5 and 1 standard cubic cm (sccm), and the second series of films deposited at different total gas partial pressures with the SiH_4 to CH_4 flow-rate ratio fixed at 1:20. Two sets of films were deposited for the second series of films where the deposition pressure was fixed equal to the total gas partial pressure and 80 Pa for the first and second set of films respectively. In the second part of this work, the films were deposited simultaneously on both glass and c-Si substrates. The effects of deposition pressure with the SiH_4 to CH_4 flow-rates fixed and substrate to filament distance on the structural and optical properties of films were investigated. The deposition pressure controlled the residence time of precursor molecules in the reactor and the substrate to filament distance determined the energy of the radicals reaching the growth sites and therefore directly influenced surface reactions, which controlled incorporation of atoms into the film structure. Raman scattering and XRD spectroscopy

measurements were done on films deposited on both c-Si and glass substrates and the results were used to show that the structural properties of these films were not substrate dependent. AES depth profiling, FTIR spectroscopy, field emission scanning electron microscopy (FESEM) and photoluminescence (PL) measurements were done only on films on c-Si substrates. These results were used to relate the structural properties to the optical properties of the SiC films and determine the important structural parameters, which can be used to control the optical properties of the films. Finally, the growth mechanism of SiC films deposited by the HWCVD system used in this work was analyzed.

High quality SiC thin films with high deposition rate has been successfully grown using the home-built HWCVD system in Low Dimensional Materials Research Centre, University of Malaya. The highest growth rate of the SiC films achieved in this work, which is close to 1.8 nm/s is higher than the growth rates of SiC films reported in the literature for films grown by HWCVD, PECVD or various sputtering techniques.

The results from this study showed that lower CH_4 gas flow-rate in silane starving condition was more favourable for the formation of SiC films with high density of Si-C bonds. The high density Si-C bond concentration was an important factor contributing to the formation of SiC nano-crystallites deposited at low CH_4 flow rate in this work, where SiC films were deposited by HWCVD without hydrogen dilution. In most reported works on SiC deposition using a similar technique, hydrogen dilution has been established to be necessary for the formation of nano-crystalline phase in SiC films. Thus, it was established here that the formation of SiC crystallites can be manipulated by controlling the CH_4 to SiH_4 flow rate ratio in SiH_4 starving condition where the silane flow-rate did not exceed 1 sccm.

The formation of SiC phases in the film structure was demonstrated to be more favourable at deposition pressure higher than the total gas partial pressure, showing that increase in residence time of the precursor gas molecules in the reaction chamber was an important factor for Si-C bond formation. However, formation of high Si-C bond density at low total gas partial pressure was required to form nano-crystalline SiC phase in the films. In the initial part of this work, it was realized that an optimum total gas partial pressure is required for the formation of SiC nano-crystalline phases in the films. Low total gas partial pressure and longer residence time of the precursor molecules in the reactor were shown to be necessary for the formation of nano-crystalline SiC phases in the film structure. This work also established that nano-crystalline SiC film structure can be grown at much higher CH_4 to SiH_4 flow-rate ratio than those reported by other research groups under similar conditions using HWCVD.

The results in this work showed that at fixed SiH_4 and CH_4 flow-rates, the film structure transformed from a structure of nc-Si phase embedded within an a-SiC phase to a nearly stoichiometric and highly ordered a-SiC at an optimum deposition pressure. Deposition pressure above this optimum pressure was shown to result in the formation of multi-phased film structure consisting of a-Si:H, a-C:H, and a-SiC with high structural disorder.

The influence of filament-to-substrate distance (d) on structural properties of SiC films was significant. It was shown that the decrease in d promoted the formation of nano-crystalline SiC phases and a-C:H clusters in the film structure. The Si-C bond density was not dependent on d when the film structure was nano-crystalline in structure but at large d, the Si-C bond density was shown to decrease significantly and as demonstrated above this consistently led to the formation of an amorphous film structure

Comparison of the Raman scattering spectroscopy and XRD results on the films deposited under various deposition pressure and filament-to-substrate distance on both glass and c-Si substrate verified that the structure of SiC films grown was not dependent on the substrate used for the films. This is an important requirement to correlate the optical energy gap and refractive index of the films, which were measured on films deposited on glass substrates only with the structural properties especially when characterization could only be done on films deposited on c-Si substrates only. To the best of the author's knowledge, most reported work on this aspect did not establish the fact that the structural properties of SiC films grown by HWCVD were independent of substrate prior to relating the structural properties of the films to the optical properties of the films.

Optical energy gap and refractive index of SiC films are important parameters for application of this material in opto-electronic devices. In this work, it was established that these parameters, which were determined from the optical transmission spectra of the films, were strongly affected by the structural changes in the films. The optical energy band gap of the a-SiC films showed significant dependence on the Si-C bond density in the film structure. The largest optical band gap of ~2.5 eV achieved in this work was obtained from a-SiC film with the highest Si-C bond density deposited at the optimum deposition pressure. Increase in deposition pressure above the optimum pressure was demonstrated to produce a parallel decrease in the optical energy gap and refractive index and the presence of a-C:H clusters in the film structure was also shown to be responsible for this trend. The changes in the optical energy gap and refractive index due to the increased presence of a-C:H clusters was shown to have a more dominant effect in nano-crystalline SiC films deposited at different d where the Si-C bond density did not show much variation. The increase in the presence of a-C:H clusters at low d and high deposition pressure led to a decrease in both the optical

energy band gap and refractive index as the a-C:H clusters created defect states and increased the H content in the SiC film structure regardless of the structure of the film, whether it was amorphous or nano-crystalline. The results in this work also revealed that the PL emission from the SiC films was the result of band-to-band transition and radiative recombination processes occurring in the band tail states of the amorphous SiC matrix. Thus it was established that SiC phases and the a-C:H clusters in the film structure played important roles in the PL emission of the films.

The AES results from this work showed that increase in the carbon content increased optical energy band gap of SiC films but showed a reversed trend on the refractive index. This nicely complemented the role of Si-C bond density and a-C:H clusters in controlling both these parameters as explained above since the C atoms in the film structure were either bonded to Si atoms forming SiC phases or bonded to C or H atoms forming a-C:H clusters. Therefore, naturally the amount of carbon atoms incorporated in the film structure can be the main parameter used to control these optical parameters. This is the first time within the author's knowledge that this explanation on how the optical band gap and refractive index of SiC films deposited by HWCVD from the discharge of pure SiH_4 and CH_4 gases without hydrogen dilution is reported.

The deposition mechanisms of the SiC films grown by HWCVD in this work have been established from the analysis on the variation of growth rates, bonding properties and elemental composition of the films with the various growth parameters studied. Generally, the concentration of precursor gases in the chamber and residence time of the precursor gas molecules and growth radicals in the reaction chamber showed strong influence on the growth rate of the films. The concentration of precursor gases in the chamber and residence time was controlled by the CH_4 flow-rate, total gas partial

pressure and the deposition pressure in this work. The deposition parameters were responsible for the increased presence of C and H atoms reaching the growth sites. The H atoms created nucleation sites and the C atoms enhanced the formation of SiC and a-C:H phases in the film structure promoting film growth. The filament temperature used in this work effectively dissociated the SiH_4 gas in the vicinity of the filament but did not contribute much to the number of C atoms reaching the growth sites. The filament to substrate distance on the other hand governed the flux of energetic H radicals reaching the growth surface and thus contributed significantly to the surface reactions, which incorporated atoms into the film structure. Therefore, these two deposition parameters significantly influenced the structural properties of deposited films as well as the deposition rate. Another significant result produced in this work is the transformation of the film structure from amorphous to nano-crystalline phase, which was shown to produce a significant drop in the growth rate. Dominant H etching effect at this critical CH_4 flow-rate with the SiH_4 flow-rate fixed at SiH_4 starving condition and filament-to-substrate distance produced the low growth rate.

6.3 Recommendations For Future Work

The results in this work can be strengthened further if further investigations which are not within the scope of this work are done. A high resolution transmission electron microscopy (HRTEM) analysis can be more conclusive in confirming the presence of the various amorphous and crystalline phases present in the film structure. This measurement is capable of determining the size as well as the polytypes of SiC nano-crystallites present. The energy dispersive X-ray (EDX) analysis equipped with

HRTEM system can also provide a precise record of the elemental composition of the different phases in the film structure.

Better understanding of the gas phase reactions and the main radicals and precursors contributing to the growth of the SiC films can be achieved if in-situ gas-phase diagnostic technique such as mass spectroscopy is available during the film growth process. Consequently, the growth mechanism responsible for the growth of SiC thin film by HWCVD can be clearly understood. As a result, a precise control of the structure of the films under different deposition conditions can be made possible.

Further studies on the effect of other deposition parameters of HWCVD system are recommended. Since the hot filament plays the most important role in the deposition of SiC films by HWCVD, it would be beneficial to study the effect of the use of different filament material, filament geometry and filament layout in relation to the properties of the SiC films, The influence of filament temperature on the film properties is an important area of study to pursue in future studies as dissociation of CH_4 gas can be enhanced by the filament temperature which may result in the formation of other SiC polytypes.

Finally, the application of amorphous and nano-crystalline SiC films as a window layer in silicon solar cells should be investigated and tested in future works. This would further enhance the capability of the home-built HWCVD system used in this work to produce high quality SiC films for this purpose. Additionally, other applications on the SiC material produced by this simple and cost-effective home-built HWCVD system can be tested if mechanical, bio-compatibility and electrical properties of the films are studied. These properties of SiC have generated a lot of interest in

studying the material as a coating material, in medical applications, and electronic devices.

REFERENCES

Akaoglu, B., Sel, K., Atilgan, I., & Katircioglu, B. (2008). Carbon content influence on the optical constants of hydrogenated amorphous silicon carbon alloys. *Optical Materials, 30*, 1257-1267.

Ambrosone, G., Basa, D. K., Coscia, U., & Passacantando, M. (2012). Evolution of structural and optical properties of nanostructured silicon carbon films deposited by plasma enhanced chemical vapour deposition. *Thin Solid Films, 520*(15), 4875-4879.

Ambrosone, G., Coscia, U., Lettieri, S., Maddalena, P., Noce, M. D., Ferrero, S., et al. (2006). Silicon–carbon films deposited at low substrate temperature. *Journal of Non-Crystalline Solids, 352*(9–20), 1371-1375.

Ambrosone, G., Coscia, U., Lettieri, S., Maddalena, P., Privato, C., & Ferrero, S. (2002). Hydrogenated amorphous silicon carbon alloys for solar cells. *Thin Solid Films, 403-404*, 349-353.

Ambrosone, G., Coscia, U., Ferrero, S., Giorgis, F., Mandracci, P., Pirri, C.F. . (2002). Structural and optical properties of hydrogenated amorphous silicon carbon alloys grown by plasma-enhanced chemical vapour deposition at various rf powers. *Philos. Mag. B 82*, 35.

Azis, A. (2012). *Hot-wire plasma enhanced chemical vapour deposition system for preparation of silicon carbide thin films* University of Malaya, Kuala Lumpur.

Bhusari, D. M., & Kshirsagar, S. T. (1993). Effect of radio-frequency power and substrate temperature on properties of hot-plasma-box glow-discharge-deposited hydrogenated amorphous silicon carbon alloys. *Journal of Applied Physics, 73*(4), 1743-1749.

Bullot, J., & Schmidt, M. P. (1987). Physics of Amorphous Silicon–Carbon Alloys. *physica status solidi (b), 143*(2), 345-418.

Chakraborty, K., & Das, D. (2006). Structural studies on the microcrystallization of Si:H network developed by hot-wire CVD. *Solar Energy Materials and Solar Cells, 90*(7–8), 849-863.

Chang, P.-K., Hsu, W.-T., Hsieh, P.-T., Lu, C.-H., Yeh, C.-H., & Houng, M.-P. (2012). Improved stability of amorphous silicon solar cells with p-type nanocrystalline silicon carbide window layer. *Thin Solid Films, 520*(7), 3096-3099.

Chen, T., Huang, Y., Dasgupta, A., Luysberg, M., Houben, L., Yang, D., et al. (2012). Microcrystalline silicon carbide window layers in thin film silicon solar cells. *Solar Energy Materials and Solar Cells, 98*(0), 370-378.

Chen, T., Huang, Y., Yang, D., Carius, R., & Finger, F. (2010). Microcrystalline silicon thin film solar cells with microcrystalline silicon carbide window layers and silicon absorber layers both prepared by Hot-Wire CVD. *physica status solidi (RRL) – Rapid Research Letters, 4*(3-4), 61-63.

Chen, T., Huang, Y., Yang, D., Carius, R., & Finger, F. (2011). Development of microcrystalline silicon carbide window layers by hot-wire CVD and their applications in microcrystalline silicon thin film solar cells. *Thin Solid Films, 519*(14), 4523-4526.

Chen, T., Yang, D., Carius, R., & Finger, F. (2010). Highly Conductive p-Type Silicon Carbon Alloys Deposited by Hot-Wire Chemical Vapor Deposition. *japanese Journal of Applied Physics, 49*, 041303.

Cheng, Q., & et al. (2008). High-rate, low-temperature synthesis of composition controlled hydrogenated amorphous silicon carbide films in low-frequency inductively coupled plasmas. *Journal of Physics D: Applied Physics, 41*(5), 055406.

Cheng, Q., Eugene Tam, Shuyan Xub and Kostya (Ken) Ostrikov. (2010). Si quantum dots embedded in an amorphous SiC matrix: nanophase control by non-equilibrium plasma hydrogenation. *Nanoscale, 2*, 594-600.

Cheng, Q., Xu, S. . (2007). Low-temperature synthesis of homogeneous nanocrystalline cubic silicon carbide films. *Journal of Applied Physics, 102*(5), 056101.

Chevaleevski, O., Myong, S. Y., & Lim, K. S. (2003). Spin defects and transport in hydrogenated nanocrystalline silicon carbide films produced by photo-CVD technique. *Solid State Communications, 128*(9–10), 355-358.

Chew, K., Rusli, Yoon, S. F., Ahn, J., Ligatchev, V., Teo, E. J., Osipowicz, T., Watt, F. (2002). Hydrogenated amorphous silicon carbide deposition using electron cyclotron resonance chemical vapor deposition under high microwave power and strong hydrogen dilution. *Journal of Applied Physics, 92*(5), 2937-2941.

Comninellis, C., & Chen, G. (2009). *Electrochemistry for the Environment*: Springer New York.

Compagnini, G., Foti, G., & Makhtari, A. (1998). Vibrational analysis of compositional disorder in amorphous silicon carbon alloys. *EPL (Europhysics Letters), 41*(2), 225.

Conde, J. P., Chu, V., Silva, M. F. d., Kling, A., Dai, Z., Soares, J. C., et al. (1999). Optoelectronic and structural properties of amorphous silicon–carbon alloys deposited by low-power electron-cyclotron resonance plasma-enhanced chemical-vapor deposition. *Journal of Applied Physics, 85*(6), 3327-3338.

Coscia, U., Ambrosone, G., & Basa, D. K. (2008). Room temperature visible photoluminescence of silicon nanocrystallites embedded in amorphous silicon carbide matrix. *Journal of Applied Physics, 103*(6), 063507.

Dasgupta, A., Ghosh, S., Kshirsagar, S. T., & Ray, S. (1997). Effect of chamber pressure on p-type μc-SiC:H thin films prepared by photo-CVD. *Thin Solid Films, 295*(1-2), 37-42.

Davis, E. A., Piggins, N., & Bayliss, S. C. (1987). Optical properties of amorphous SiN x (:H) films. *Journal of Physics C: Solid State Physics, 20*(27), 4415.

DellaSala, D., Fiorini, P., Skumanich, A., & Amer, N. M. (1985). Gap state spectroscopy in a-$Si_{1-x}C_x$:H alloys *Journal of Non-Crystalline Solids, 77-78*, 853.

Dhanaraj, G., Chen, Y., Chen, H., Cai, D., Zhang, H., & Dudley, M. (2007). Chemical Vapor Deposition of Silicon Carbide Epitaxial Films and Their Defect Characterization. *Journal of Electronic Materials, 36*(4), 332-339.

Doyle, J., Robertson, R., Lin, G. H., He, M. Z., & Gallagher, A. (1988). Production of high-quality amorphous silicon films by evaporative silane surface decomposition. *Journal of Applied Physics, 64*(6), 3215-3223.

Duan, H. L., & Bent, S. F. (2005). The influence of filament material on radical production in hot wire chemical vapor deposition of a-Si:H. *Thin Solid Films, 485*(1–2), 126-134.

Duan, H. L., Zaharias, G. A., & Bent, S. F. (2002). Detecting reactive species in hot wire chemical vapor deposition. *Current Opinion in Solid State and Materials Science, 6*(5), 471-477.

El Khakani, M. A., Guay, D., Chaker, M., & Feng, X. H. (1995). Composition and thermal-annealing-induced short-range ordering changes in amorphous hydrogenated silicon carbide films as investigated by extended x-ray-absorption fine structure and infrared absorption. *Physical Review B, 51*(8), 4903-4914.

Ellison, A., Magnusson, B., Hemmingsson, C., Magnusson, W., Iakimov, T., Storasta, L., et al. (2000). HTCVD growth of semi-insulating 4H-SiC crystals with low defect density. *MRS Online Proceedings Library, 640*, null-null.

Ellison, A., Zhang, J., Peterson, J., Henry, A., Wahab, Q., Bergman, J. P., et al. (1999). High temperature CVD growth of SiC. *Materials Science and Engineering: B, 61–62*(0), 113-120.

Feenstra, K. F., Schropp, R. E. I., & Van der Weg, W. F. (1999). Deposition of amorphous silicon films by hot-wire chemical vapor deposition. *Journal of Applied Physics, 85*(9), 6843-6852.

Feng, S. H., & Chen, J. S. (2002). *Frontiers of Solid State Chemistry: Proceedings of the International Symposium on Solid State Chemistry in China, Changchun, China, 9-12 August, 2002*: World Scientific.

Feng, Z. C. (2004). *SiC Power Materials: Devices and Applications*: Springer.

Feng, Z. C. (2006). Optical properties of cubic SiC grown on Si substrate by chemical vapor deposition. *Microelectronic Engineering, 83*(1), 165-169.

Ferrari, A. C., & Robertson, J. (2000). Interpretation of Raman spectra of disordered and amorphous carbon. *Physical Review B, 61*(20), 14095-14107.

Ferrari, A. C., & Robertson, J. (2004). Raman spectroscopy of amorphous, nanostructured, diamond–like carbon, and nanodiamond. *Phil. Trans. R. Soc. Lond. A, 362*(1824), 2477-2512.

Ferraro, J. R., Nakamoto, K., & Brown, C. W. (2003). Chapter 1 - Basic Theory *Introductory Raman Spectroscopy (Second Edition)* (pp. 1-94). San Diego: Academic Press.

Ferreira, I., Cabrita, A., Fortunato, E., Martins, R. (2002). Composition and structure of silicon-carbide alloys obtained by hot wire and hot wire plasma assisted techniques. *Vacuum, 64*(3-4), 261-266.

Ferreira, I., Costa, M. E. V., Pereira, L., Fortunato, E., Martins, R., Ramos, A. R., et al. (2001). Silicon carbide alloys produced by hot wire, hot wire plasma-assisted and plasma-enhanced CVD techniques. *Applied Surface Science, 184*(1-4), 8-19.

Ferreira, I., Fernandes, B., & Martins, R. (1999). Nanocrystalline silicon carbon doped films prepared by hot wire technique. *Vacuum, 52*(1–2), 147-152.

Finger, F., Astakhov, O., Bronger, T., Carius, R., Chen, T., Dasgupta, A., et al. (2009). Microcrystalline silicon carbide alloys prepared with HWCVD as highly transparent and conductive window layers for thin film solar cells. *Thin Solid Films, 517*(12), 3507-3512.

Fissel, A. (2003). Artificially layered heteropolytypic structures based on SiC polytypes: molecular beam epitaxy, characterization and properties. *Physics Reports, 379*(3–4), 149-255.

Friedrichs, P., Kimoto, T., Ley, L., & Pensl, G. (2011). *Silicon Carbide*: Wiley.

Gallagher, A. (2001). Some physics and chemistry of hot-wire deposition. *Thin Solid Films 395*, 25-28.

George, V. C., Das, A., Roy, M., Dua, A. K., Raj, P., & Zahn, D. R. T. (2002). Bias enhanced deposition of highly oriented β-SiC thin films using low pressure hot filament chemical vapour deposition technique. *Thin Solid Films, 419*(1–2), 114-117.

Gogoi, P., Jha, H. S., & Agarwal, P. (2010). High band gap nanocrystallite embedded amorphous silicon prepared by hotwire chemical vapour deposition. *Thin Solid Films, 518*(23), 6818-6828.

Goh, B. T. (2012). *Layer-by-layer plasma enhanced chemical vapour deposition of nanocrystalline silicon thin films.* University of Malaye, Kuala lumpur.

Griffiths, P., & De Haseth, J. A. (2007). *Fourier Transform Infrared Spectrometry*: John Wiley & Sons.

Guo, Y. P., Zheng, J. C., Wee, A. T. S., Huan, C. H. A., Li, K., Pan, J. S., et al. (2001). Photoluminescence studies of SiC nanocrystals embedded in a SiO2 matrix. *Chemical Physics Letters, 339*(5–6), 319-322.

Guruvenket, S., Azzi, M., Li, D., Szpunar, J. A., Martinu, L., Klemberg-Sapieha, J. E. (2010). Structural, mechanical, tribological, and corrosion properties of a-SiC:H coatings prepared by PECVD. *Surface and Coating Technology, 204*(21-22), 3358-3365.

Harris, G. L. (1995). *Properties of Silicon Carbide*: Inst of Engineering & Technology.

Hartel, A. M., Künle, M., Löper, P., Janz, S., Bett, A. W. (2010). Amorphous Si_xC_{1-x}:H single layers before and after thermal annealing: Correlating optical and structural properties. *Solar Energy Materials and Solar Cells, 94*(11), 1942-1946.

Heintze, M., Zedlitz, R., Wanka, H. N., & Schubert, M. B. (1996). Amorphous and microcrystalline silicon by hot wire chemical vapor deposition. *Journal of Applied Physics, 79*(5), 2699-2706.

Hiromasa, O., Takahiro, H., Tetsuya, M., Hiroaki, K., & Kiyoshi, Y. (2011). Low-temperature synthesis of microcrystalline 3C-SiC film by high-pressure hydrogen-plasma-enhanced chemical transport. *Journal of Physics D: Applied Physics, 44*(23), 235202.

Holt, J. K., Swiatek, M., Goodwin, D. G., Muller, R. P., Goddard Iii, W. A., & Atwater, H. A. (2001). Gas phase and surface kinetic processes in polycrystalline silicon hot-wire chemical vapor deposition. *Thin Solid Films, 395*(1–2), 29-35.

Hori, M., & Goto, T. (2002). Measurement techniques of radicals, their gas phase and surface reactions in reactive plasma processing. *Applied Surface Science, 192*(1–4), 135-160.

Hoshide, Y., Komura, Y., Tabata, A., Kitagawa, A., Kondo, A. (2009). Importance of H_2 gas for growth of hot-wire CVD nanocrystalline 3C-SiC from $SiH_4/CH_4/H_2$. *Thin Solid Films, 517*(12), 3520-3523.

Hoshide, Y., Tabata, A., Kitagawa, A., Kondo, A. (2009). Preparation of n-type nanocrystalline 3C-SiC films by hot-wire CVD using N_2 as doping gas. *Thin Solid Films, 517*(12), 3524-3527.

Hu, Z., et al. (2004). Amorphous silicon carbide films prepared by H_2 diluted silane-methane plasma. *Journal of Crystal Growth, 264*, 7-12.

Huang, S. M., et al. (2002). Ultraviolet and visible Raman spectroscopy characterization of diamond–like carbon film growth by pulsed laser deposition. *Applied Physics A, 74*(4), 519-523.

Itoh, T., Fukunaga, K., Katoh, Y., Fujiwara, T., & Nonomura, S. (2002). Doping of a-SiC_X:H films including μc-Si:H by hot-wire CVD and their application as a wide gap window for heterojunction solar cells. *Solar Energy Materials and Solar Cells, 74*(1-4), 379-385.

Itoh, T., Katoh, Y., Fujiwara, T., Fukunaga, K., Nonomura, S., & Nitta, S. (2001). Preparation of silicon-carbon alloy films by hot-wire CVD and their properties. *Thin Solid Films, 395*(1-2), 240-243.

Jadkar, S. R., Sali, J. V., Funde, A. M., Ali Bakr, N., Vidyasagar, P. B., Hawaldar, R. R., et al. (2007). Deposition of hydrogenated amorphous silicon (a-Si:H) films by hot-wire chemical vapor deposition (HW-CVD) method: Role of substrate temperature. *Solar Energy Materials and Solar Cells, 91*(8), 714-720.

Jadkar, S. R., Sali, J. V., Musale, D. V., Kshirsagar, S. T., & Takwale, M. G. (2002). Influence of silane flow on structural, optical and electrical properties of a-Si:H

thin films deposited by hot wire chemical vapor deposition (HW-CVD) technique. *Solar Energy Materials and Solar Cells, 71*(2), 153-167.

Jha, H. S., Singh, M., Yadav, A., Lalhriatzuala, Deva, D., & Agarwal, P. (2012). Nanocrystalline cubic silicon carbide thin films for the window layer of solar cells deposited by hot wire CVD. 85493D-85493D.

Kaneko, T., Nemoto, D., Horiguchi, A., Miyakawa, N. (2005). FTIR analysis of a-SiC:H films grown by plasma enhanced CVD. *Journal of Crystal Growth, 275*(1–2), e1097-e1101.

Karch, K., Bechstedt, F., Pavone, P., & Strauch, D. (1996). Pressure-dependent properties of SiC polytypes. *Physical Review B, 53*(20), 13400-13413.

Kerdiles, S. (2000). Low temperature deposition of nanocrystalline silicon carbide thin films. *Applied Physics Letters, 76*(17), 2373.

Kerdiles, S., Madelon, R., & Rizk, R. (2001). Spectroscopic ellipsometry analysis of nanocrystalline silicon carbide obtained at low temperature. *Applied Surface Science, 184*(1–4), 150-155.

Kerdiles, S., Rizk, R., Gourbilleau, F., Pérez-Rodríguez, A., Garrido, B., González-Varona, O., et al. (2000). Low temperature direct growth of nanocrystalline silicon carbide films. *Materials Science and Engineering: B, 69–70*(0), 530-535.

Kessels, W. M. M., Hoefnagels, J. P. M., van den Oever, P. J., Barrell, Y., & van de Sanden, M. C. M. (2003). Temperature dependence of the surface reactivity of SiH_3 radicals and the surface silicon hydride composition during amorphous silicon growth. *Surface Science, 547*(3), L865-L870.

King, S. W., French, M., Bielefeld, J., & Lanford, W. A. (2011). Fourier transform infrared spectroscopy investigation of chemical bonding in low-k a-SiC:H thin films. *Journal of Non-Crystalline Solids, 357*(15), 2970-2983.

Klein, S., Dasgupta, A., Finger, F., Carius, R., & Bronger, T. (2008). Electronic properties of low temperature microcrystalline silicon carbide prepared by Hot Wire CVD. *Thin Solid Films, 516*(5), 630-632.

Klein, S., Finger, F., Carius, R., & Stutzmann, M. (2005). Deposition of microcrystalline silicon prepared by hot-wire chemical-vapor deposition: The influence of the deposition parameters on the material properties and solar cell performance. *Journal of Applied Physics, 98*(2), 024905.

Klug, H. P., & Alexander, L. E. (1974). *X-ray diffraction procedures for polycrystalline and amorphous materials*. New York: Wiley.

Komiyama, J., Abe, Y., Suzuki, S., Kita, T., & Nakanishi, H. (2005). Schottky diode characteristics of 3C-SiC grown on a Si substrate by vapor phase epitaxy. *Journal of Crystal Growth, 275*(1–2), e1001-e1006.

Komura, Y., Tabata, A., Narita, T., Kondo, A. (2008). Influence of gas pressure on low-temperature preparation and film properties of nanocrystalline 3C-SiC thin films by HW-CVD using $SiH_4/CH_4/H_2$ system. *Thin Solid Films, 516*(5), 633-636.

Kordina, O., Hallin, C., Ellison, A., Bakin, A. S., Ivanov, I. G., Henry, A., et al. (1996). High temperature chemical vapor deposition of SiC. *Applied Physics Letters, 69*(10), 1456-1458.

Kumbhar, A. A., Dusane, R. O., Bauer, S., & Schröder, B. (1998). Micro-crystalline phase formation in hot wire deposited Si:C:H alloy films from pure methane and silane mixtures. *Journal of Non-Crystalline Solids, 227-230, Part 1*(0), 452-455.

Kumbhar, A. S., Bhusari, D. M., & Kshirsagar, S. T. (1995). Growth of clean amorphous silicon-carbon alloy films by hot-filament assisted chemical vapor deposition technique. *Applied Physics Letters, 66*, 1741.

Lee, M.-S., & Bent, S. F. (2000). Temperature effects in the hot wire chemical vapor deposition of amorphous hydrogenated silicon carbon alloy. *Journal of Applied Physics, 87*(9), 4600-4610.

Lim, K. S., & Shevaleevskiy, O. (2008). Nanocrystalline silicon carbide films for solar photovoltaics: The role of dangling-bond defects. *Pure and Applied Chemistry, 80*(10), 2141.

Mahan, A. H. (2003). Hot wire chemical vapor deposition of Si containing materials for solar cells. *Solar Energy Materials and Solar Cells, 78*(1–4), 299-327.

Mahan, A. H., Carapella, J., Nelson, B. P., Crandall, R. S., & Balberg, I. (1991). Deposition of device quality, low H content amorphous silicon. *Journal of Applied Physics, 69*(9), 6728-6730.

Mahan, A. H., Nelson, B. P., Salamon, S., & Crandall, R. S. (1991). Deposition of device quality, low H content a-Si:H by the hot wire technique. *Journal of Non-Crystalline Solids, 137–138, Part 2*(0), 657-660.

Manifacier, J. C., Gasiot, J., & Fillard, J. P. (1976). A simple method for the determination of the optical constants n, k and the thickness of a weakly absorbing thin film. *Journal of Physics E: Scientific Instruments, 9*(11), 1002.

Mao, H.-Y., Wuu, D.-S., Wu, B.-R., Lo, S.-Y., Hsieh, H.-Y., & Horng, R.-H. (2012). Hot-wire chemical vapor deposition and characterization of p-type nanocrystalline SiC films and their use in Si heterojunction solar cells. *Thin Solid Films, 520*(6), 2110-2114.

Martin, I. T., Teplin, C. W., Doyle, J. R., Branz, H. M., & Stradins, P. (2010). Physics and chemistry of hot-wire chemical vapor deposition from silane: Measuring and modeling the silicon epitaxy deposition rate. *Journal of Applied Physics, 107*(5), 054906.

Mastelaro, V., Flank, A. M., Fantini, M. C. A., Bittencourt, D. R. S., Carreno, M. N. P., & Pereyra, I. (1996). On the structural properties of a-$Si_{1-x}C_x$:H thin films. *Journal of Applied Physics, 79*(3), 1324-1329.

Matsuda, A. (2004). Microcrystalline silicon.: Growth and device application. *Journal of Non-Crystalline Solids, 338–340*(0), 1-12.

Matsumura, H. (1998). Formation of Silicon-Based Thin Films Prepared by Catalytic Chemical Vapor Deposition (Cat-CVD) Method. *Japanese Journal of Applied Physics, 37*, 3175.

Matsumura, H., & Ihara, H. (1988). Catalytic chemical vapor deposition method to prepare high quality hydro-fluorinated amorphous silicon. *Journal of Applied Physics, 64*(11), 6505-6509.

Matsumura, H., Umemoto, H., Izumi, A., & Masuda, A. (2003). Recent progress of Cat-CVD research in Japan—bridging between the first and second Cat-CVD conferences. *Thin Solid Films, 430*(1–2), 7-14.

Matsumura, H., Umemoto, H., & Masuda, A. (2004). Cat-CVD (hot-wire CVD): how different from PECVD in preparing amorphous silicon. *Journal of Non-Crystalline Solids, 338–340*(0), 19-26.

Miyajima, S., Irikawa, J., Yamada, A., & Konagai, M. (2010). High-quality nanocrystalline cubic silicon carbide emitter for crystalline silicon heterojunction solar cells. *Applied Physics Letters, 97*(2), 023504.

Miyajima, S., Yamada, A., & Konagai, M. (2003). Highly conductive microcrystalline silicon carbide films deposited by the hot wire cell method and its application to amorphous silicon solar cells. *Thin Solid Films, 430*(1-2), 274-277.

Miyajima, S., Yamada, A., & Konagai, M. (2007). Characterization of Undoped, N- and P-Type Hydrogenated Nanocrystalline Silicon Carbide Films Deposited by Hot-Wire Chemical Vapor Deposition at Low Temperatures. *Japanese Journal of Applied Physics, 46*, 1415.

Morgan, C. (2006). *Fabrication and Testing of a High Temperature Chemical Vapor Deposition Furnace for the Growth of SiC Thick Epitaxial Films*: University of South Carolina.

Mori, M., Tabata, A., & Mizutani, T. (2006). Properties of hydrogenated amorphous silicon carbide films prepared at various hydrogen gas flow rates by hot-wire chemical vapor deposition. *Thin Solid Films, 501*(1-2), 177-180.

Mott, N. F., Davis, E.A. (1979). *Electronic Process in Non-Crystalline Materials*. Oxford: Clarendon Press.

Muller, R. P., Holt, J. K., Goodwin, D. G., & Goddard, W. A. (2000). Si + SiH_4 Reactions and Implications for Hot-Wire CVD of a-Si:H: Computational Studies. *MRS Online Proceedings Library, 609*, null-null.

Nakamura, S., & Koshi, M. (2006). Elementary processes in silicon hot wire CVD. *Thin Solid Films, 501*(1–2), 26-30.

Ogawa, S., Okabe, M., Ikeda, Y., Itoh, T., Yoshida, N., & Nonomura, S. (2008). Applications of microcrystalline hydrogenated cubic silicon carbide for amorphous silicon thin film solar cells. *Thin Solid Films, 516*(5), 740-742.

Oulachgar, E. H., Aktik, C., Dostie, S., Gujrathi, S., & Scarlete, M. (2007). Characterization of Silicon Carbide Thin Films Obtained Via Sublimation of a

Solid Polymer Source Using Polymer-Source CVD Process. *MRS Online Proceedings Library, 989*, null-null.

Pant, A., Huff, M. C., & Russell, T. W. F. (2001). Reactor and Reaction Model for the Hot-Wire Chemical Vapor Deposition of Silicon from Silane. *Industrial & Engineering Chemistry Research, 40*(5), 1386-1396.

Pant, A., Russell, T. W. F., Huff, M. C., Aparicio, R., & Birkmire, R. W. (2001). Hot-Wire Chemical Vapor Deposition of Silicon from Silane: Effect of Process Conditions. *Industrial & Engineering Chemistry Research, 40*(5), 1377-1385.

Park, M., Teng, C. W., Sakhrani, V., McLaurin, M. B., Kolbas, R. M., Sanwald, R. C., et al. (2001). Optical characterization of wide band gap amorphous semiconductors a-Si:C:H: Effect of hydrogen dilution. *Journal of Applied Physics, 89*, 1130.

Park, Y. S. (1998). *SiC Materials and Devices*: Acad. Press.

Pascarelli, S., Boscherini, F., Mobilio, S., & Evangelisti, F. (1992). Structure of hydrogenated amorphous silicon-carbon alloys as investigated by extended x-ray-absorption fine structure. *Physical Review B, 45*(4), 1650-1654.

Pascual, E., Andlijar, J. L., Fernhndez, J. L., & Bertran, E. (1995). Optical and structural characterization of hydrogenated amorphous silicon carbide thin films prepared by r.f. plasma chemical vapour deposition. *Diamond and Related Materials, 4*, 1205-1209.

Prado, R. J., Fantini, M. C. A., Tabacniks, M. H., Villacorta Cardoso, C. A., Pereyra, I., & Flank, A. M. (2001). Improvements on the local order of amorphous hydrogenated silicon carbide films. *Journal of Non-Crystalline Solids, 283*(1–3), 1-10.

Racine, B., Ferrari, A. C., Morrison, N. A., Hutchings, I., Milne, W. I., & Robertson, J. (2001). Properties of amorphous carbon--silicon alloys deposited by a high plasma density source. *Journal of Applied Physics, 90*(10), 5002-5012.

Rajagopalan, T. (2003). Low temperature deposition of nanocrystalline silicon carbide films by plasma enhanced chemical vapor deposition and their structural and optical characterization. *Journal of Applied Physics, 94*(8), 5252.

Ritikos, R., Siong, C. C., Ab. Gani, S. M., Muhamad, M. R., & Rahman, S. A. (2009). Effect of Annealing on the Optical and Chemical Bonding Properties of Hydrogenated Amorphous Carbon and Hydrogenated Amorphous Carbon Nitride Thin Films. *Japanese Journal of Applied Physics, 48*, 101301.

Rivière, J. P., Zaytouni, M., & Delafond, J. (1996). Characterization and wear behavior of SiC coatings prepared by ion beam assisted deposition. *Surface and Coatings Technology, 84*(1–3), 376-382.

Rovira, P. I., & Alvarez, F. (1997). Chemical (dis)order in a-Si_{1-x} C_x :H for $x<0.6$. *Physical Review B, 55*(7), 4426-4434.

Saddow, S. E. (2012). Chapter 1 - Silicon Carbide Materials for Biomedical Applications *Silicon Carbide Biotechnology* (pp. 1-15). Oxford: Elsevier.

Saleh, R., Munisa, L., & Beyer, W. (2003). Infrared absorption in a-SiC:H alloy prepared by d.c. sputtering. *Thin Solid Films, 426*(1–2), 117-123.

Schrader, B. (Ed.). (1995). *Infrared and Raman spectroscopy*. New York (USA): VCH publishers, inc.

Seo, J. K., Joung, Y.-H., Park, Y., & Choi, W. S. (2011). Substrate temperature effect on the SiC passivation layer synthesized by an RF magnetron sputtering method. *Thin Solid Films, 519*(20), 6654-6657.

Shen, H., Wu, T., Pan, Y., Zhang, L., Cheng, B., & Yue, Z. (2012). Structural and optical properties of nc-3C-SiC films synthesized by hot wire chemical vapor deposition from SiH_4-C_2H_2-H_2 mixture *Thin Solid Films*.

Shi, J. R., et al. (2000). Ultraviolet and visible Raman studies of nitrogenated tetrahedral amorphous carbon films. *Thin Solid Films, 366*(1-2), 169-174.

Shi, J. R., Shi, X., Sun, Z., Liu, E., Yang, H. S., Cheah, L. K., et al. (1999). Structural properties of amorphous silicon-carbon films deposited by the filtered cathodic vacuum arc technique. *Journal of Physics: Condensed Matter, 11*(26), 5111.

Solomon, I. (2001). Amorphous silicon-catbon alloys: a promising but complex and verty diversified series of materials. *Applied Surface Science, 184*, 3-7.

Soni, S. K., Phatak, A., & Dusane, R. O. (2010). High deposition rate device quality a-Si:H films at low substrate temperature by HWCVD technique. *Solar Energy Materials and Solar Cells, 94*(9), 1512-1515.

Sun, Z., Sun, Y., Wang, X., & Zheng, Z. (1995). Epitaxially grown β-SiC on Si in the CH4/H2 system by hot filament chemical vapour deposition. *Materials Science and Engineering: B, 34*(2–3), L13-L16.

Sung, H., Erkens, G., Funken, J., Voss, A., Lemmer, O., & Kreutz, E. W. (1992). The morphology and mechanical properties of Al_2O_3, ZrO_2 and SiC laser-assisted physically vapour deposited films. *Surface and Coatings Technology, 54–55, Part 2*(0), 541-547.

Swain, B. P. (2006a). The analysis of carbon bonding environment in HWCVD deposited a-SiC:H films by XPS and Raman spectroscopy. *Surface and Coating Technology, 201*, 1589-1593.

Swain, B. P. (2006b). Influence of process pressure on HW-CVD deposited a-SiC:H films. *Surface and Coating Technology, 201*, 1132-1137.

Swain, B. P., & Dusane, R. O. (2006). Multiphase structure of hydrogen diluted a-SiC:H deposited by HWCVD. *Materials Chemistry and Physics, 99*(2-3), 240-246.

Swanepoel, R. (1983). Determination of the thickness and optical constants of amorphous silicon. *Journal of Physics E: Scientific Instruments, 16*(12), 1214.

Tabata, A., Hoshide, Y., & Kondo, A. (2010). Highly conductive nitrogen-doped hydrogenated nanocrystalline cubic silicon carbide thin films prepared with a

hot-wire chemical vapor deposition from $SiH_4/CH_4/H_2/N_2$ gas. *Materials Science and Engineering: B, 175*(3), 201-206.

Tabata, A., & Komura, Y. (2007). Preparation of nanocrystalline cubic silicon carbide thin films by hot-wire CVD at various filament-to-substrate distances. *Surface and Coating Technology, 201*(22-23), 8986-8990.

Tabata, A., Komura, Y., Hoshide, Y., Narita, T., & Kondo, A. (2008). Properties of Nanocrystalline Cubic Silicon Carbide Thin Films Prepared by Hot-Wire Chemical Vapor Deposition Using $SiH_4/CH_4/H_2$ at Various Substrate Temperatures. *Japanese Journal of Applied Physics, 47*, 561.

Tabata, A., Komura, Y., Kanaya, M., Narita, T., Kondo, A., & Misutani, T. (2006, May 2006). *Preparation of Nanocrystalline Silicon Carbide Thin Films by Hot-Wire Chemical Vapor Deposition at Various Filament Temperature.* Paper presented at the Photovoltaic Energy Conversion, Conference Record of the 2006 IEEE 4th World Conference on.

Tabata, A., Komura, Y., Narita, T., & Kondo, A. (2009). Growth of silicon carbide thin films by hot-wire chemical vapor deposition from $SiH_4/CH_4/H_2$. *Thin Solid Films, 517*(12), 3516-3519.

Tabata, A., Kuno, Y., Suzuoki, Y., Mizutani, T. (1997). Properties of hydrogenated amorphous silicon carbide films prepared by a separately excited plasma CVD method. *Journal of Physics D: Applied Physics, 30*(2), 194-201.

Tabata, A., Kuroda, M., Mori, M., Mizutani, T., Suzuoki, Y. (2004). Band gap control of hydrogenated amorphous silicon carbide films prepared by hot-wire chemical vapor deposition. *Journal of Non-Crystalline Solids, 338-340*, 521-524.

Tabata, A., & Mori, M. (2008). Structural changes of hot-wire CVD silicon carbide thin films induced by gas flow rates. *Thin Solid Films, 516*(5), 626-629.

Tang, H., Tan, S., Huang, Z., Dong, S., & Jiang, D. (2005). Surface morphology of α-SiC coatings deposited by RF magnetron sputtering. *Surface and Coatings Technology, 197*(2–3), 161-167.

Tauc, J., & Abeles, F. (1972). *Optical Properties of Solids*. North-Holland. Amsterdam.

Tersoff, J. (1994). Chemical order in amorphous silicon carbide. *Physical Review B, 49*(23), 16349-16352.

Toal, S. J., Reehal, H. S., Barradas, N. P., & Jeynes, C. (1999). Growth of microcrystalline β-SiC films on silicon by ECR plasma CVD. *Applied Surface Science, 138–139*(0), 424-428.

Umemoto, H., Ohara, K., Morita, D., Nozaki, Y., Masuda, A., Matsumura, H. . (2002). Direct detection of H atoms in the catalytic chemical vapor deposition of the SiH_4/H_2 system. *Journal of Applied Physics, 91*, 1650.

van Veenendaal, P. A. T. T., & Schropp, R. E. I. (2002). Processes in silicon deposition by hot-wire chemical vapor deposition. *Current Opinion in Solid State and Materials Science, 6*(5), 465-470.

Vasin, A. V., Kolesnik, S. P., Konchits, A. A., Rusavsky, A. V., Lysenko, V. S., Nazarov, A. N., Ishikawa, Y., Koshka, Y. (2008). Structure, paramagnetic defects and light-emission of carbon-rich a-SiC:H films. *Journal of Applied Physics, 103*(12), 123710-123717.

Waman, V. S., Kamble, M. M., Pramod, M. R., Gore, S. P., Funde, A. M., Hawaldar, R. R., Amalnerkar, D. P., Sathe, V. G., Gosavi, S. W., Jadkar, S. R. (2011). Influence of the deposition parameters on the microstructure and opto-electrical properties of hydrogenated nanocrystalline silicon films by HW-CVD. *Journal of Non-Crystalline Solids, 357*(21), 3616-3622.

Wang, R., Ma, R., & Zupan, M. (2006). Modeling of Chemical Vapor Deposition of Large-Area Silicon Carbide Thin Film. *Crystal Growth & Design, 6*(11), 2592-2597.

Wiesmann, H., Ghosh, A. K., McMahon, T., & Strongin, M. (1979). a-Si : H produced by high-temperature thermal decomposition of silane. *Journal of Applied Physics, 50*(5), 3752-3754.

Will, J., Hoppe, A., Müller, F. A., Raya, C. T., Fernández, J. M., & Greil, P. (2010). Bioactivation of biomorphous silicon carbide bone implants. *Acta Biomaterialia, 6*(12), 4488-4494.

Willander, M., Friesel, M., Wahab, Q.-u., & Straumal, B. (2006). Silicon carbide and diamond for high temperature device applications. *Journal of Materials Science: Materials in Electronics, 17*(1), 1-25.

Wu, T., Shen, H., Cheng, B., Pan, Y., Liu, B., Shen, J. (2011). Formation of α-$Si_{1-x}C_x$:H and nc-SiC films grown by HWCVD under different process pressure. *Applied Surface Science, 258*(3), 999-1003.

Xu, S. J., Yu, M. B., Rusli, Yoon, S. F., & Che, C. M. (2000). Time-resolved photoluminescence spectra of strong visible light-emitting SiC nanocrystalline films on Si deposited by electron-cyclotron-resonance chemical-vapor deposition. *Applied Physics Letters, 76*(18), 2550-2552.

Yeop Myong, S., Kew Lee, H., Yoon, E., & Su Lim, K. (2002). Highly conductive boron-doped nanocrystalline silicon-carbide film prepared by low-hydrogen-dilution photo-CVD method using ethylene as a carbon source. *Journal of Non-Crystalline Solids, 298*(2–3), 131-136.

Yoshida, S., Ito, T., Hiraki, A., Saito, H., Fujita, S., Ishitani, Y., et al. (2007). Fundamental Properties of Wide Bandgap Semiconductors. In K. Takahashi, A. Yoshikawa & A. Sandhu (Eds.), *Wide Bandgap Semiconductors* (pp. 25-96): Springer Berlin Heidelberg.

Yu, M. B., Rusli, Yoon, S. F., Chen, Z. M., Ahn, J., Zhang, Q., et al. (2000). Deposition of nanocrystalline cubic silicon carbide films using the hot-filament chemical-vapor-deposition method. *Journal of Applied Physics, 87*(11), 8155-8158.

Yu, M. B., Rusli, Yoon, S. F., Xu, S. J., Chew, K., Cui, J., et al. (2000). Hydrogenated nanocrystalline silicon carbide films synthesized by ECR-CVD and its intense visible photoluminescence at room temperature. *Thin Solid Films, 377–378*(0), 177-181.

Yu, W., Lu, W., Han, L., Fu, G. (2004). Structural and optical properties of hydrogenated amorphous silicon carbide films by helicon wave plasma-enhanced chemical vapour deposition. *Journal of Physics D: Applied Physics, 37*, 3304-3308.

Yu, W., Wang, X., Geng, C., Lve, X., Lu, W., & Fu, G. (2011). Decay processes of photoluminescence in a nanocrystalline SiC thin film. *Applied Surface Science, 258*(5), 1733-1737.

Yu, W., Wang, X., Lu, W., Wang, S., Bian, Y., Fu, G. (2010). Effects of substrate temperature on microstructural and photoluminescent properties of nanocrystalline silicon carbide films. *Physica B: Condensed Matter, 405*(6), 1624-1627.

Zhang, S., Li, L., & Kumar, A. (2009). *Materials Characterization Techniques*: Talor & Francis Group, CRC Press.

Zhao, F., Li, H. X., Ji, L., Mo, Y. F., Quan, W. L., Zhou, H. D., et al. (2009). Structural, mechanical and tribological characterizations of a-C : H : Si films prepared by a hybrid PECVD and sputtering technique. *Journal of Physics D: Applied Physics, 42*(16), 165407.

Zhao, Q., Li, J. C., Zhou, H., Wang, H., Wang, B., & Yan, H. (2004). Parameters determining crystallinity in [beta]-SiC thin films prepared by catalytic chemical vapor deposition. *Journal of Crystal Growth, 260*(1-2), 176-180.

Zheng, W., & Gallagher, A. (2006). Hot wire radicals and reactions. *Thin Solid Films, 501*(1-2), 21-25.

LIST OF PUBLICATIONS

ISI-Indexed Journal Publications

1. F. Shariatmadar Tehrani, M.R. Badaruddin, R.G. Rahbari, M.R. Muhamad, S.A. Rahman, **Low-pressure synthesis and characterization of multiphase SiC by HWCVD using CH_4/SiH_4**, Vacuum 86 (2012) 1150-1154.

2. F. Shariatmadar Tehrani, B.T. Goh, M.R. Muhamad, S.A. Rahman, **Pressure dependent structural and optical properties of silicon carbide thin films deposited by hot wire chemical vapor deposition from pure silane and methane gases**, Journal of Materials Science: Materials in Electronics 24 (2013) 1361-1368.

Non-ISI Indexed Journal Publications

1. F. Shariatmadar Tehrani, R. Ritikos, B.T. Goh, M.R. Muhamad and S.A. Rahman, **Effect of methane flow rate on the properties of HWCVD silicon carbide thin films,** Solid State Science and Technology 19 (2011) 26-31.

Conference Presentations

1. Fatemeh Shariatmadartehrani, Muhamad rasat Muhamad,and Saadah Abd Rahman, **Structural and optical properties of high deposition rate silicon carbide prepared by Hot Wire CVD,** The 5th International conference of Thin Films 2010, Harbin, China-Poster presentation.

2. Fatemeh Shariatmadar Tehrani, Saadah Abdul Rahman, **Influence of filament-to-substrate distance on properties of silicon carbide thin films deposited by HWCVD technique**, 4th International Conference of Solid State Science and Technology (ICSSST 2012) December 18 – 20, 2012, Melaka, Malaysia – Oral presentation.

Submitted for Publication

1. F. Shariatmadar Tehrani, B.T. Goh, R. Ritikos, M. R. Muhamad, S. A. Rahman, **Transformation from amorphous to nano-crystalline SiC thin films prepared by HWCVD technique without hydrogen dilution**, Submitted to Journal of Material Science-Poland on Aug 2012, Status: under review.

APPENDIX A

Measurable and Calculated Values Obtained from Samples Studied in This Work

Table A.1: Si-C bond density, deposition rate, and energy gap of the SiC films deposited by HWCVD technique at various methane flow rate and two constant silane flow rate.

CH_4 (sccm) ± 0.1	SiH_4 (sccm) ± 0.01	N_{Si-C} (cm^{-3}) $\pm 0.1\times10^{23}$	Deposition rate (nm/s) ±0.01	E_g (eV) ±0.02
10.0	0.50	2.0×10^{23}	0.09	2.00
30.0	0.50	7.1×10^{22}	0.29	2.36
50.0	0.50	7.9×10^{22}	0.31	1.98
75.0	0.50	8.3×10^{22}	0.47	2.08
100.0	0.50	1.0×10^{23}	0.40	2.16
10.0	1.00	1.8×10^{23}	0.35	1.60
20.0	1.00	8.4×10^{22}	0.65	1.96
40.0	1.00	5.6×10^{22}	0.78	1.94
70.0	1.00	5.9×10^{22}	0.80	2.02
100.0	1.00	3.4×10^{22}	0.92	1.88

Table A.2: Si-C bond density, deposition rate, and energy gap of the SiC films deposited by HWCVD technique at various total gas partial pressures.

Sample ID	CH_4 (sccm) ± 0.1	SiH_4 (sccm) ± 0.01	Deposition pressure (Pa) ± 1	N_{Si-C} (cm^{-3}) $\pm 0.1\times10^{23}$	Deposition rate (nm/s) ± 0.01	E_g (eV) ± 0.02
VP-1	10.0	0.50	12	4.2×10^{22}	0.33	2.54
VP-2	20.0	1.00	20	3.3×10^{20}	0.82	1.86
VP-3	30.0	1.50	27	4.6×10^{20}	0.81	1.72
VP-4	40.0	2.00	33	3.5×10^{20}	1.13	1.62
VP-5	50.0	2.50	38	7.2×10^{20}	1.73	1.68
FP-1	10.0	0.50	80	1.8×10^{23}	0.15	2.10
FP-2	20.0	1.00	80	9.5×10^{22}	0.56	1.96
FP-3	30.0	1.50	80	1.9×10^{22}	0.61	1.92
FP-4	40.0	2.00	80	1.7×10^{22}	0.82	1.88
FP-5	50.0	2.50	80	1.2×10^{22}	1.14	1.84

Table A.3: Si-C bond density, deposition rate, and energy gap of the SiC films deposited by HWCVD technique at various deposition pressures.

CH_4 (sccm) ± 0.1	SiH_4 (sccm) ± 0.01	Deposition pressure (Pa) ± 1	N_{Si-C} (cm^{-3}) ± 0.1×10^{23}	Deposition rate (nm/s) ± 0.01	E_g (eV) ± 0.02
20.0	1.00	20	2.9×10^{20}	0.70	1.82
20.0	1.00	40	5.1×10^{21}	0.55	1.90
20.0	1.00	80	1.4×10^{23}	0.47	2.46
20.0	1.00	140	6.4×10^{22}	0.66	2.38
20.0	1.00	250	3.6×10^{22}	0.82	2.22

Table A.4: Si-C bond density, deposition rate, and energy gap of the SiC films deposited by HWCVD technique at various filament-to-substrate distances.

CH_4 (sccm) ± 0.1	SiH_4 (sccm) ± 0.01	Filament-to-substrate distance (mm) ± 1	N_{Si-C} (cm^{-3}) ±0.1×10^{23}	Deposition rate (nm/s) ± 0.01	E_g (eV) ± 0.02
20.0	1.00	10	1.7×10^{23}	0.54	1.98
20.0	1.00	15	1.7×10^{23}	0.42	2.16
20.0	1.00	20	1.6×10^{23}	0.25	2.58
20.0	1.00	25	1.1×10^{23}	0.43	2.46